NASA/TM–2018-220114
NESC-RP-17-01264

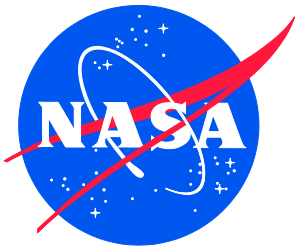

Re-Architecting the NASA Wire Derating Approach for Space Flight Applications

Steven L. Rickman/NESC, Kenneth L. Johnson/NESC
Langley Research Center, Hampton, Virginia

Elham Maghsoudi
Jet Propulsion Laboratory, Pasadena, California

George A. Slenski
Analytical Mechanics Associates, Hampton, Virginia

Benjamin I. Furst
Jet Propulsion Laboratory, Pasadena, California

Daniel J. Wentzel
White Sands Test Facility, Las Cruces, New Mexico

Anthony Bautista, Emma J. Nelson
Jet Propulsion Laboratory, Pasadena, California

November 2018

NASA STI Program . . . in Profile

Since its founding, NASA has been dedicated to the advancement of aeronautics and space science. The NASA scientific and technical information (STI) program plays a key part in helping NASA maintain this important role.

The NASA STI program operates under the auspices of the Agency Chief Information Officer. It collects, organizes, provides for archiving, and disseminates NASA's STI. The NASA STI program provides access to the NTRS Registered and its public interface, the NASA Technical Reports Server, thus providing one of the largest collections of aeronautical and space science STI in the world. Results are published in both non-NASA channels and by NASA in the NASA STI Report Series, which includes the following report types:

- TECHNICAL PUBLICATION. Reports of completed research or a major significant phase of research that present the results of NASA Programs and include extensive data or theoretical analysis. Includes compilations of significant scientific and technical data and information deemed to be of continuing reference value. NASA counter-part of peer-reviewed formal professional papers but has less stringent limitations on manuscript length and extent of graphic presentations.

- TECHNICAL MEMORANDUM. Scientific and technical findings that are preliminary or of specialized interest, e.g., quick release reports, working papers, and bibliographies that contain minimal annotation. Does not contain extensive analysis.

- CONTRACTOR REPORT. Scientific and technical findings by NASA-sponsored contractors and grantees.

- CONFERENCE PUBLICATION. Collected papers from scientific and technical conferences, symposia, seminars, or other meetings sponsored or co-sponsored by NASA.

- SPECIAL PUBLICATION. Scientific, technical, or historical information from NASA programs, projects, and missions, often concerned with subjects having substantial public interest.

- TECHNICAL TRANSLATION. English-language translations of foreign scientific and technical material pertinent to NASA's mission.

Specialized services also include organizing and publishing research results, distributing specialized research announcements and feeds, providing information desk and personal search support, and enabling data exchange services.

For more information about the NASA STI program, see the following:

- Access the NASA STI program home page at *http://www.sti.nasa.gov*

- E-mail your question to help@sti.nasa.gov

- Phone the NASA STI Information Desk at 757-864-9658

- Write to:
  NASA STI Information Desk
  Mail Stop 148
  NASA Langley Research Center
  Hampton, VA 23681-2199

NASA/TM–2018-220114
NESC-RP-17-01264

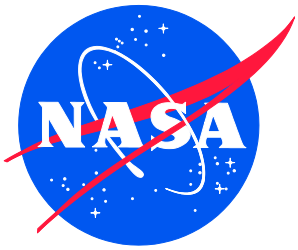

Re-Architecting the NASA Wire Derating Approach for Space Flight Applications

Steven L. Rickman/NESC, Kenneth L. Johnson/NESC
Langley Research Center, Hampton, Virginia

Elham Maghsoudi
Jet Propulsion Laboratory, Pasadena, California

George A. Slenski
Analytical Mechanics Associates, Hampton, Virginia

Benjamin I. Furst
Jet Propulsion Laboratory, Pasadena, California

Daniel J. Wentzel
White Sands Test Facility, Las Cruces, New Mexico

Anthony Bautista, Emma J. Nelson
Jet Propulsion Laboratory, Pasadena, California

National Aeronautics and
Space Administration

Langley Research Center
Hampton, Virginia 23681-2199

November 2018

Acknowledgments

Statistical analysis software suites Design Expert® and Statgraphics® used in analyses performed at Marshall Space Flight Center (MSFC) are hosted by their Safety and Mission Assurance by contractor Bastion Technologies, Inc. Their sponsorship of these licenses is much appreciated. The team would like to acknowledge the help of NASA Langley statistician Dr. Kathryn Ballard for her assistance in best-subsets regression and identifying the best regression models.

Mr. Kenneth G. Toro, a statistician at LaRC, is acknowledged for his peer review of the test planning and statistical analysis content of this report.

Mr. Eric Sunada, JPL; Mr. Carl ("Jack") Ercol, APL; Mr. Daniel H. Nguyen, GSFC; and Mr. David Gilmore, The Aerospace Corporation are acknowledged for their peer review of the thermal analysis.

The assessment team also thanks JSC/Mr. Lanny Plaisance, NESC/Mr. Steven Gentz, NESC/Mr. Dan Murri, NESC/Mr. Jon Holladay, NESC/Mr. Michael Meyer, and NESC/ Mr. Robert Beil for their peer review and comments on the final report.

Available from:

NASA STI Program / Mail Stop 148
NASA Langley Research Center
Hampton, VA 23681-2199
Fax: 757-864-6500

NASA Engineering and Safety Center
Technical Assessment Report

Re-Architecting the NASA Wire Derating Approach for Space Flight Applications

October 25, 2018

Report Approval and Revision History

NOTE: This document was approved at the October 25, 2018, NRB. This document was submitted to the NESC Director on November 13, 2018, for configuration control.

Approved:	*Original Signature on File*	11/13/18
	NESC Director	Date

Version	Description of Revision	Office of Primary Responsibility	Effective Date
1.0	Initial Release	Steve Rickman, NASA Technical Fellow for Passive Thermal, JSC	10/25/18

Table of Contents

Technical Assessment Report

List of Figures

List of Tables

Technical Assessment Report

1.0 Notification and Authorization

Mr. Steve Rickman, NASA Technical Fellow for Passive Thermal, proposed a pathfinder study to develop an apparatus for wire and wire bundle thermal testing to measure their performance, and to support development of thermal analytical models. Development of such capability would enable wire and wire bundle amperage capacity (i.e., "ampacity").

Key stakeholders that will benefit from this work are the NASA community, including Space Launch System (SLS), Commercial Crew Program (CCP), and commercial partners; the satellite/robotics community; and others.

Additional stakeholders include the Department of Defense (DOD), and the commercial and defense aviation industry. This work will also have broad application for civilian uses, so residential and industrial electricians, electronics systems installers, electronics systems designers, and others will likely benefit.

2.0 Signature Page

Submitted by:

Team Signature Page on File – 11/14/18

Mr. Steven L. Rickman Date

Significant Contributors:

Mr. Kenneth L. Johnson Date

Dr. Elham Maghsoudi Date

Mr. George A. Slenski Date

Mr. Benjamin I. Furst Date

Mr. Daniel J. Wentzel Date

Mr. Anthony Bautista Date

Ms. Emma J. Nelson Date

Signatories declare the findings, observations, and NESC recommendations compiled in the report are factually based from data extracted from program/project documents, contractor reports, and open literature, and/or generated from independently conducted tests, analyses, and inspections.

3.0 Team List

Name	Discipline	Organization
Core Team		
Steven L. Rickman	NESC Lead, Passive Thermal	NESC (JSC)
Christopher J. Iannello	NESC Deputy Lead, Electrical Power	NESC (KSC)
Ben Furst	Thermal Engineer	JPL
Elham Maghsoudi	Thermal Engineer	JPL
Subha Comandur	Cable Harness Engineering	JPL
Kenneth Johnson	Design of Experiments, Statistics	NESC NSET (MSFC)
Daniel Wentzel	Design of Experiments, Statistics	NSET Member (WSTF)
Antonietta Conte	Properties Testing (Research Scholar)	JPL
Emma Nelson	Uncertainty Analysis	JPL
Anthony Bautista	Testing and Instrumentation (Intern)	JPL
George Slenski	Electrical Systems and Harnessing	LaRC/AMA
Consultants		
Thomas Evans	Electrical Power Systems	GSFC/AS&D, Inc.
Eric Sunada	Senior Thermal Engineer	JPL
Mark Lysek	Instrumentation	JPL
Business Management		
Stephanie Hamrick	Program Analyst	LaRC/MTSO
Assessment Support		
Linda Burgess	Planning and Control Analyst	LaRC/AMA
Kylene Kramer	Project Coordinator	LaRC/AMA
Erin Moran	Technical Editor	LaRC/AMA

3.1 Acknowledgements

Statistical analysis software suites Design Expert® and Statgraphics® used in analyses performed at Marshall Space Flight Center (MSFC) are hosted by their Safety and Mission Assurance by contractor Bastion Technologies, Inc. Their sponsorship of these licenses is much appreciated. The team would like to acknowledge the help of NASA Langley statistician Dr. Kathryn Ballard for her assistance in best-subsets regression and identifying the best regression models.

Mr. Kenneth G. Toro, a statistician at LaRC, is acknowledged for his peer review of the test planning and statistical analysis content of this report.

Mr. Eric Sunada, JPL; Mr. Carl ("Jack") Ercol, APL; Mr. Daniel H. Nguyen, GSFC; and Mr. David Gilmore, The Aerospace Corporation are acknowledged for their peer review of the thermal analysis.

The assessment team also thanks JSC/Mr. Lanny Plaisance, NESC/Mr. Steven Gentz, NESC/Mr. Dan Murri, NESC/Mr. Jon Holladay, NESC/Mr. Michael Meyer, and NESC/ Mr. Robert Beil for their peer review and comments on the final report.

4.0 Executive Summary

Design of wiring for aerospace vehicles relies on an understanding of "ampacity," which refers to the current carrying capacity of wires, individually or in wire bundles. Designers rely on aerospace standards (e.g., JPL D-8208 and AS50881) to derate allowable current flow to prevent exceeding wire temperature limits due to resistive heat dissipation within the wires or wire bundles. These standards often add considerable design margin [ref. 2] and are based on empirical data. Commercial providers are taking an aggressive approach to wire sizing, which challenges the conventional wisdom of the established standards. NASA designs may also benefit from this work.

The goal of this study was to assess the feasibility of developing physics-based and regression thermal models of single wires and wire bundles. If feasible, and ultimately developed and validated, these models could be used in place of relying on empirical data-based standards to derate allowable current flow, to prevent exceeding wire temperature limits due to resistive heat dissipation within the wires or wire bundles.

In the present effort, a preliminary a physics-based thermal model of single wires and wire bundles was successfully developed and demonstrated. A test facility was also developed for accurately measuring the thermal profile of single wires and wire bundles. The thermal model wire temperature predictions were validated based on comparing results with the experimental testing completed. The wire bundle test facility collected wire conductor temperature data under vacuum and atmospheric conditions and varying environmental temperatures and currents for the two most common wire types used on spacecraft. Test results also correlated well with published wire bundle derating standards, JPL D-8208, and AS50881. A preliminary regression model was also developed and correlated with the same standards.

The results of the present study strongly support further model development and validation testing, which will allow the model to provide significant insight into wire bundle current carrying capacity design and to replace published wire derating standards.

Based on limited testing and analysis conducted during this pathfinder phase, the assessment team concluded:

- Both the response surface model and physics-based thermal model developed during this assessment correlate with the pathfinder test data and AS50881.
- For the limited scope of the pathfinder study, modern AS22759 wire constructions (e.g., Teflon™-Kapton®- Teflon™ (TKT) and cross-linked ethylene tetrafluoroethylene (XL-ETFE) showed good agreement with the models developed and wire current rating curves per AS50881.
- Wire insulation to wire insulation contact conductance required to correlate bundle wire models during this assessment differ from the values obtained during the previous assessment and is believed to be due to the different bundle construction used during the previous study.
- Uncertainty in temperature measurements for a resistance-based temperature measurement is inversely proportional to the parameters temperature coefficient of resistivity α, current I, resistance per unit length-at a reference temperature R_{L0}, and wire length L, and directly proportional to voltage.

- The measured values of the qualified (i.e., certified to a wire specification) wire constructions used in this assessment were within specification requirements yet were different from the nominal specification values given for resistance at room temperature, conductor diameter, and overall finished wire diameter. An accurate measurement of the conductor resistance and temperature coefficient, conductor diameter, and overall finished wire diameter is required to develop thermal models that correlate well to laboratory measured single wire and wire bundle temperatures.

As a result of the assessment, the NESC team recommends that wire resistance change, due to thermal aging, should be considered in any future work. Additionally, testing and analysis for other wires types, gauges, and configurations should be conducted with and without convection to further improve the physics-based and response surface models. The benefits of the oil bath testing to determine key thermal modeling parameters (e.g., the temperature coefficient of resistivity and resistance per unit length at a reference temperature) were clear and these measurements should continue to be made to support all future wire testing and analysis. Finally, NASA should consider adoption of a wire derating standard that applies to all programs and includes bounding variabilities.

5.0 Assessment Plan

The proposed work aimed to extend the testing and analysis work performed under the previous study [ref. 1]. The ultimate goal is to replace NASA wire derating tables with an analytical model that:

1. addresses single wires and bundles;
2. provides nominal loading and overcurrent protective device settings;
3. can address user conditions, including various ambient temperature and pressure conditions, bundle sizes, mixed wire gauges, and varying construction materials/techniques (e.g., varying outer coating emissivity);
4. has comparable or improved accuracy as compared to current methods; and
5. is widely available and can be easily used with no unusual software requirements and readily provided to NASA partners and the Society for Automotive Engineers (SAE) with open rights.

6.0 Problem Description

Design of wiring for aerospace vehicles relies on an understanding of "ampacity," which refers to the current carrying capacity of insulated wires, individually or in wire bundles. Designers rely on standards to derate allowable current flow to prevent exceeding wire temperature limits due to resistive heat dissipation within the wires or wire bundles. These standards often add considerable margin and are based on empirical data. Commercial space providers are taking an aggressive approach to wire sizing, which challenges the conventional wisdom of the established standards.

There is a clear need for an analytical and computational approach for determining wire bundle current rating with respect to the wiring configuration and surrounding environment. Thermal modeling of wire bundles correlated to lab testing can allow for more accurate representation of wiring systems compared to using current rating curves and derating factors. Accurate thermal modeling of wire bundles has the potential to improve the safety, reliability, and optimization of aerospace wiring power and signal distribution systems.

NASA does not have an Agency standard for defining wire and cable current ratings and derating guidance. There are individual standards that address limited wire rating from GSFC, MSFC, JSC, and JPL. Other NASA Centers may or may not have specific guidance related to wire current ratings. Most standards and technical memos reference MIL-W-5088, which has been replaced by AS50881, which is primarily for military aircraft. Programs such as CCP specifically call out wire current ratings as a critical requirement for human-rated systems (i.e., CCT-REQ-1130 and CCT-STD-1140).

Wire and wire bundle testing were performed during a previous NESC assessment [ref. 1] resulting in data to inform thermal models developed as a predictive tool to aid in ampacity determination. Two wire bundle configurations were tested during this assessment, one comprised of 22 American Wire Gauge (AWG) wire, and the other comprised primarily of 22 AWG wire with a small fraction of wires 20 AWG. The test results and the associated model development provided encouraging results as the physics-based thermal models could be

correlated to the test data. This suggested that models, with further development, may be refined to ultimately supplant the long held practice of using published wire derating standards.

Thermal design of electrical wiring systems has been historically based on free air single wire current rating curves. The curves are used to determine the temperature rise in a wire bundle using current, ambient temperature, and conductor size. Derating factors such as altitude, power loading, number of wires in a bundle, and surrounding temperature are also used to determine the maximum current rating of a given wiring system. These ampacity derating curves were initially developed by the Navy Research Laboratory (NRL) in 1947 [ref. 2]. Current rating curves were further refined in the 1960s, 1970s, and 1980s by aircraft original equipment manufacturers (OEMs) and government agencies, and were published in MIL-W-5088 [ref. 3] (a.k.a., M5088) Wire insulations used to generate the MIL-W-5088 current rating curves were based on thick-walled insulations which are different than the thin wall insulations used today. In the 1980s MIL-W-5088 was converted to the SAE document AS50881 [ref. 4], and the ampacity curves are given in multiple tables and figures in the document. Laboratory testing has shown the curves are conservative since they were based on data from multiple aircraft companies, and worst-case values were typically used when determining conductor temperatures and various ambient temperatures and current levels [ref. 5]. In some cases, the curves can under report conductor temperatures given specific bundle configurations and harness jacketing. Proximity to other bundles and structure can further skew installed wiring temperatures compared to values obtained from the current rating curves and derating factors. The published curves do not take into consideration proximity to other wire harnesses or structure, mixed wire sizes, different wire jacket emittances, or a variety of currents on individual conductors. NASA programs have used the AS50881 [ref. 4] ampacity curves as guidance even though the curves only provide wire bundle derating up to 100,000 ft by providing additional derating curves for vacuum environments (e.g., JPL D-8208 [ref. 6]). NASA also conducted testing documented in the 88-220 Eagle Engineering Report [ref. 25]. The 88-220 is the basis for NASA wire standards for the International Space Station (ISS), MPCV, SLS, and CCP. The results were used in ISS Program SSP30312 Electrical, Electronic, and Electromechanical (EEE) and Mechanical Parts Management and Implementation Plan for Space Station and NASA Technical Memorandum 102179 [refs. 26 and 28].

NASA programs typically specify a “smart short” current value for wire gauges and bundles. A “smart short” is the single wire maximum fault current-carrying capacity the wire can carry in its operating environment without causing the insulation temperature to exceed its rating. Ideally, the “smart short” current will have margin to the value given in the present AS50881 ampacity curves. The “smart short” value informs the selection of protective device interrupt rating due to the interplay of numerous wire harness design variables.

This study is a follow-on to NESC-RP-14-00949 [ref. 1], which employed a thermal vacuum chamber to evaluate the thermal rises in wire harnesses employed in a commercial spacecraft. A basic thermal model was developed to predict wire conductor temperatures under various current loads and environmental conditions as documented in references 13 and 17. The outcome of the testing and the associated model development provided encouraging results as the physics-based thermal model correlated with the test data. A considerable number of lessons learned from the first evaluation were employed in this follow-on effort. It was found detailed characterization of the selected wire insulation needs to be added to the model to accurately predict temperature in a wire harness. This included measuring resistance of the conductors at room temperature,

conductor and insulation diameters, and the increase in resistance as a function of temperature. It was also determined that a more thermally stable test fixture was needed to refine the model. For this follow-on study, an isothermal temperature controlled chamber was designed to remove the thermal influence of the chamber walls. As in the previous study, a 10-ft (~3 meters) wire/wire bundle was selected to mitigate end effects and placed in the shroud using an "S" pattern. Baffles were included in the chamber to minimize heating influences from the zigzag pattern of the wire/wire bundle. The wire/wire bundle was suspended in the shroud using low conductance standoffs. Wire construction types and wire sizes were selected based on JPL recommendations and on common wire types used in modern aerospace applications. The selected wire constructions were all silver-plated copper conductor insulated TKT and XL-ETFE insulations. Wire sizes were 20 and 26 AWG (a.k.a, gauge) along with some limited 22-gauge XL-ETFE wire testing. Modeling and testing was initially conducted using single wires, and then bundles consisting of 32 wires each size and insulation type.

7.0 Technical Activities

7.1 Design and Analysis of Test Facility

7.1.1 Overview

A test facility was developed to measure the temperature of a single wire and wire bundle carrying varying levels of electrical current in a controlled thermal environment. The facility was designed to simulate an infinitely long wire carrying a fixed current in a uniform thermal environment at steady state conditions. This was done for three reasons: (1) to match the conditions of and validate the numerical thermal wire bundle model detailed in this report; (2) to simulate the hottest possible (worst-case) thermal conditions of a wire carrying a specified current; and (3) to be consistent with prior derating standard test programs. Special effort was taken to ensure stable environmental conditions and accurate measurements.

7.1.2 System Design and Operation

The test facility consisted of a wire bundle test article suspended in a temperature-controlled shroud, which was in turn contained in a pressure-controlled (vacuum) chamber. A power supply was used to control the amount of current flowing through the wire, while thermocouples were used to measure the wire bundle temperature. See Appendix B for details on the thermocouple attachment method. The shroud temperature and chamber pressure were also monitored. A general schematic of the system is shown in Figure 7.1.2-1. Additional details of each subsystem are given in Appendix B. Table 7.1.2-1 shows the general operating characteristics of the test facility.

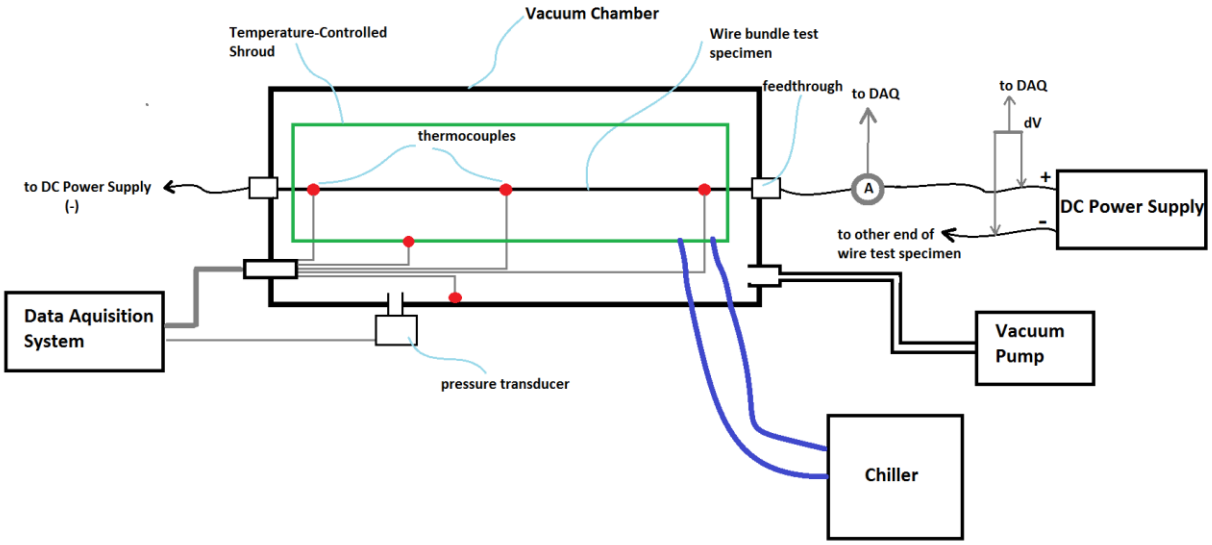

Figure 7.1.2-1. Schematic of the Wire Harness Thermal Test Facility

Table 7.1.2-1. Operating Characteristics of the Test Facility

Maximum vacuum level	1e-7 Torr
Shroud Internal Dimensions	0.51 m x 0.84 m x 0.10 m (20 in x 33 in x 4 in)
Shroud Temperature Range	(-50°C) to (+80°C)
Max ΔT Across Shroud	< 5°C
Max Allowable Wire Heat Dissipation	~350 W
Wire Bundle Shrouded Length	2.5 m (8.3 ft)*

*Wire bundle lengths were approximately 10 ft, but the length within the shroud was closer to 8.3 ft.

7.1.2.1 Temperature-Controlled Shroud

Wire and wire bundle derating standards assume a constant environment temperature. To simulate this, a custom aluminum shroud designed and fabricated to regulate the environmental temperature surrounding each wire test article during testing. The shroud consisted of an aluminum box with aluminum tubing brazed onto the exterior (Figure 7.1.2.1-1).

To control the box temperature, fluid from a temperature-controlled chiller was routed through the box tubing. Each wire test article was suspended in the box in a zigzag pattern using Teflon™ stand-offs. Aluminum baffles were welded into the box to ensure the zig zagging test article was always surrounded by the temperature-controlled shroud (to minimize heat transfer between different wire segments—see Figure 7.1.2.1-2). Teflon™ clamps at the wire feedthroughs were used to keep the wire test articles in place during testing and used to insulate the wire bundles from the shroud. The interior of the box was painted black to produce a uniform and known high emissivity surface. The exterior of the box was covered using a single layer of aluminized Mylar™ to thermally isolate the shroud from its surroundings. There were 15 thermocouples mounted to the exterior of the shroud to monitor its temperature. The interior of the box measured 0.51 m x 0.84 m x 0.10 m (20 in x 33 in x 4 in) and the shrouded length of the wire was approximately 2.5 m (8.3 ft). The shroud/chiller combination was capable of

maintaining a temperature between -50°C and +80°C with a maximum ΔT across the shroud of 2.5°C for vacuum conditions and 5°C for atmospheric pressure conditions.

Figure 7.1.2.1-1. Temperature-Controlled Shroud with Thermocouples

Figure 7.1.2.1-2. Interior of the Temperature-Controlled Shroud with a Wire Bundle Installed

a. Shroud Design Requirements

The most important requirement considered for the shroud design was to maintain the operating temperature as low as -50°C and as high as +80°C for a wire bundle at a constant temperature of 200°C. The shroud was sized to ensure that it can accommodate a ~10-ft (~3.3 m) wire harness and fit inside the vacuum chamber. Sufficiently long test articles are required to negate the effects of heat loss through the wire terminations.

b. Thermal Model

Thermal Desktop® was used to build a thermal model for the shroud and evaluate the shroud operation prior to fabrication. The shroud operation depended on the chiller performance. An ultra-low temperature (ULT) recirculating chiller from FTS Systems was used for the test. The initial heat dissipation was estimated to be less than 1000 watts. The RC211 model operating temperature range is between -50°C to +80°C. However, for 1000 watts heat rejection, the coolant temperature does not get lower than -50°C, which is aligned with the shroud design temperature range requirements.

To design the cooling lines attached to the shroud two inner diameters of tubing were considered: 3/8 and 1/4 inch. Pressure drop was calculated in the tubing for a total of 8 turns on the shroud, and fit on the chiller pump curve for FC77 working fluid as shown in Figure 7.1.2.1-3. The chiller operates at 2 gallons per minute (GPM) for a 1/4-inch diameter tubing, and 4 GPM for a 3/8-inch diameter tubing. Table 7.1.2.1-1 shows FC77 properties.

Table 7.1.2.1-1. FC77 Properties

Chiller working fluid	Thermal Conductivity $(w/m \cdot K)$	Specific Heat $(J/kg \cdot K)$	Density (kg/m^3)	Viscosity$(Pa \cdot s)$
FC77	0.058	1046	1780	0.001032

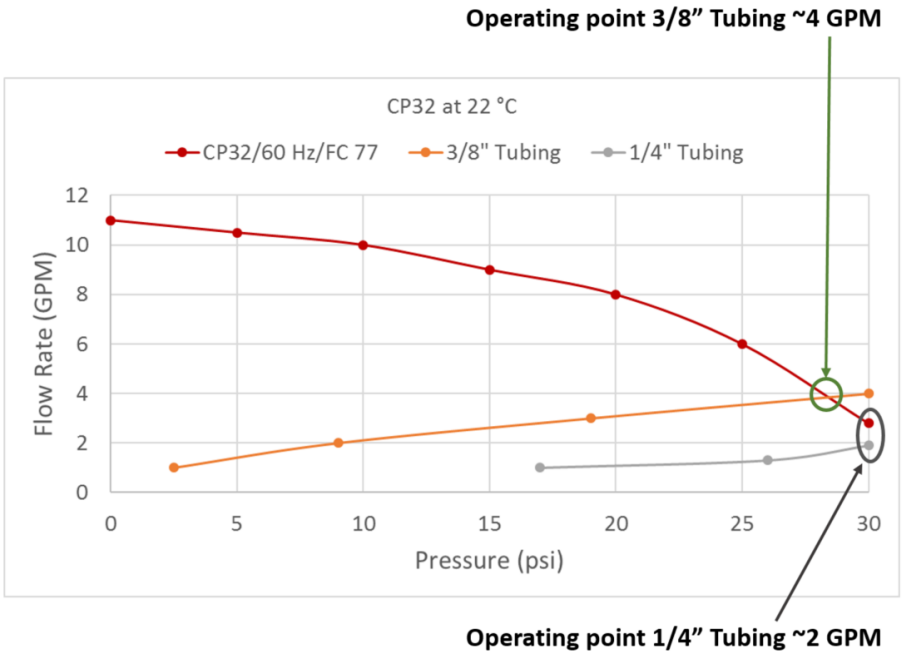

Figure 7.1.2.1-3. Chiller Pump Curve vs Pressure Curve (FC77)

A preliminary single plate shroud model was built using Thermal Desktop®. The shroud single plate has a length of 33 inches, width of 20 inches and thickness of 1/4 inch. Aluminum and copper plate, and tubing of 1/4 inch and 3/8 inch diameter were modeled. The thermal conductivity of copper and aluminum are 390 W/m-K, and 168 W/m-K, respectively. The shroud box included two plates with tubing attached. A total of 500 watts of heat, equivalent to half of the maximum considered total heat dissipation from the wire at 200°C was applied to the

single plate shroud model. Only tubing convection and conduction were considered for the single plate shroud modeled and radiation was not taken into account.

Figure 7.1.2.1-4 shows the temperature profile for the aluminum and copper single plate model with cooling tubes of 3/8-inch diameter. For both material temperatures, the gradient on the plate does not exceed 1°C. The copper plate shows a smaller temperature gradient.

Table 7.1.2.1-2 summarizes the results for all single plate shroud designs. Higher flow rate (i.e., 4 GPM) shows smaller temperature gradient on the plate. Overall, copper shroud indicated smaller temperature gradient across the plate.

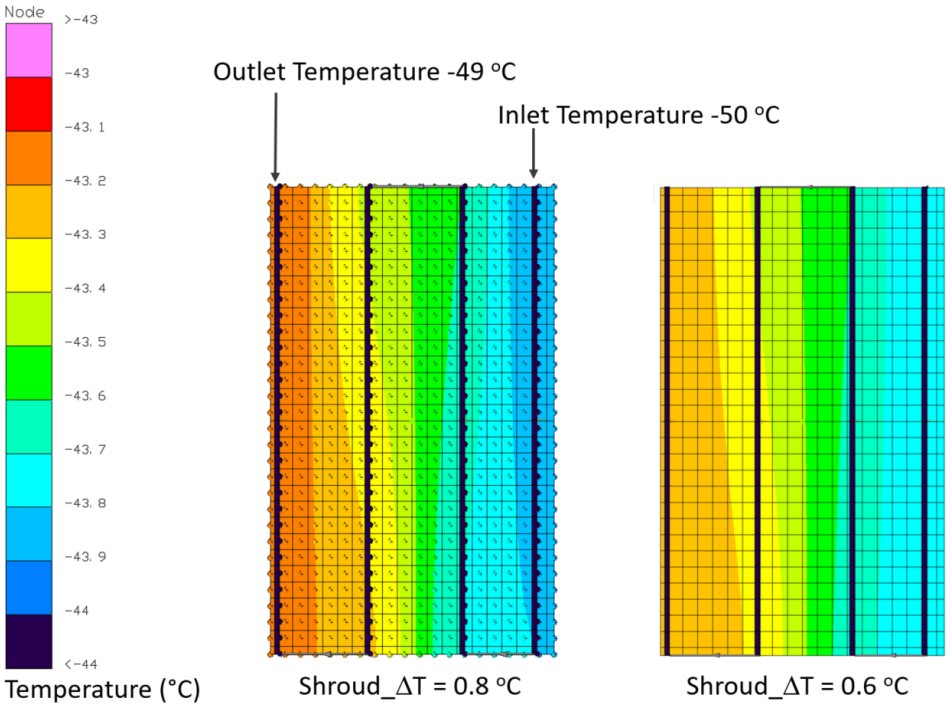

Figure 7.1.2.1-4. Single Plate Shroud Model 3/8-inch Tubing – Left, Aluminum, Right, Copper

Table 7.1.2.1-2. Single Plate Shroud Design

Tubing ID [in]	Material	Flowrate [GPM]	Inlet Temp [°C]	Outlet Temp [°C]	Maximum Plate Temp [°C]	Minimum Plate Temp [°C]	Plate ΔT [°C]
1/4	Aluminum	2	-50	-47.88	-42.21	-43.74	1.5
3/8	Aluminum	4	-50	-48.99	-43.12	-43.89	0.8
3/8	Copper	4	-50	-48.99	-43.21	-43.8	0.6

A full shroud model including the baffles and a wire dissipating heat at 200°C was built in Thermal Desktop®. The model was first checked without the wire. In this case, as shown in Figure 7.1.2.1-5, 500 watts of heat was applied to each top and bottom plates. The predicted temperature gradient on the shroud remained below 2°C.

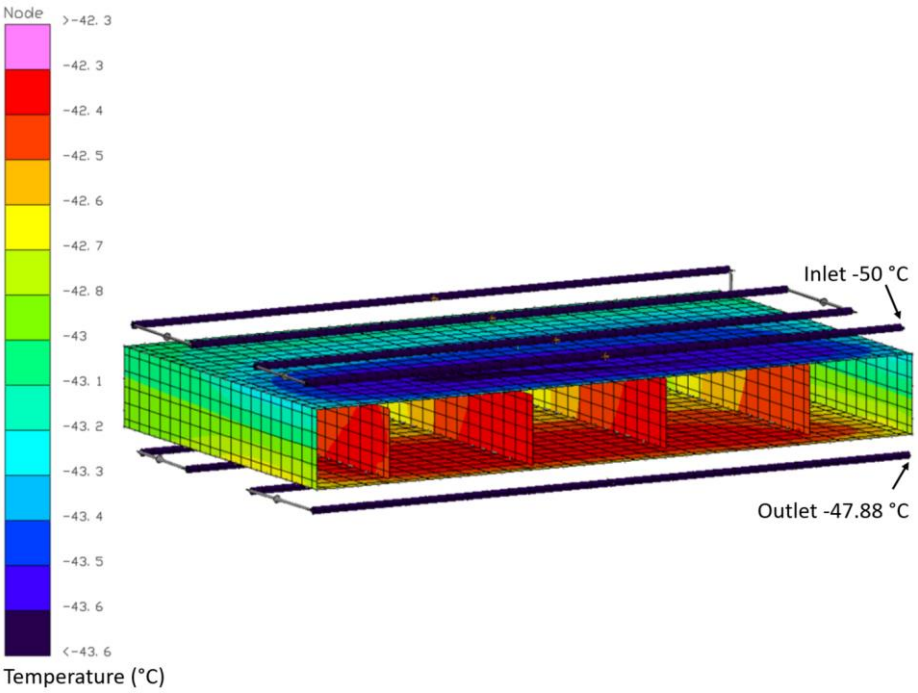

Figure 7.1.2.1-5. Full Aluminum Shroud Model including Baffles without Wire – Radiation, Conduction, and Convection were taken into account

Figure 7.1.2.1-6 shows the full shroud model including the wire radiating at 200°C. A wire bundle diameter was selected to represent a bundle with one hundred 20 AWG wires. Figure 7.1.2.1-7 shows the temperature profile in full shroud thermal model for aluminum and copper. The copper shroud shows a smaller temperature gradient (2°C) on the shroud than aluminum (4°C).

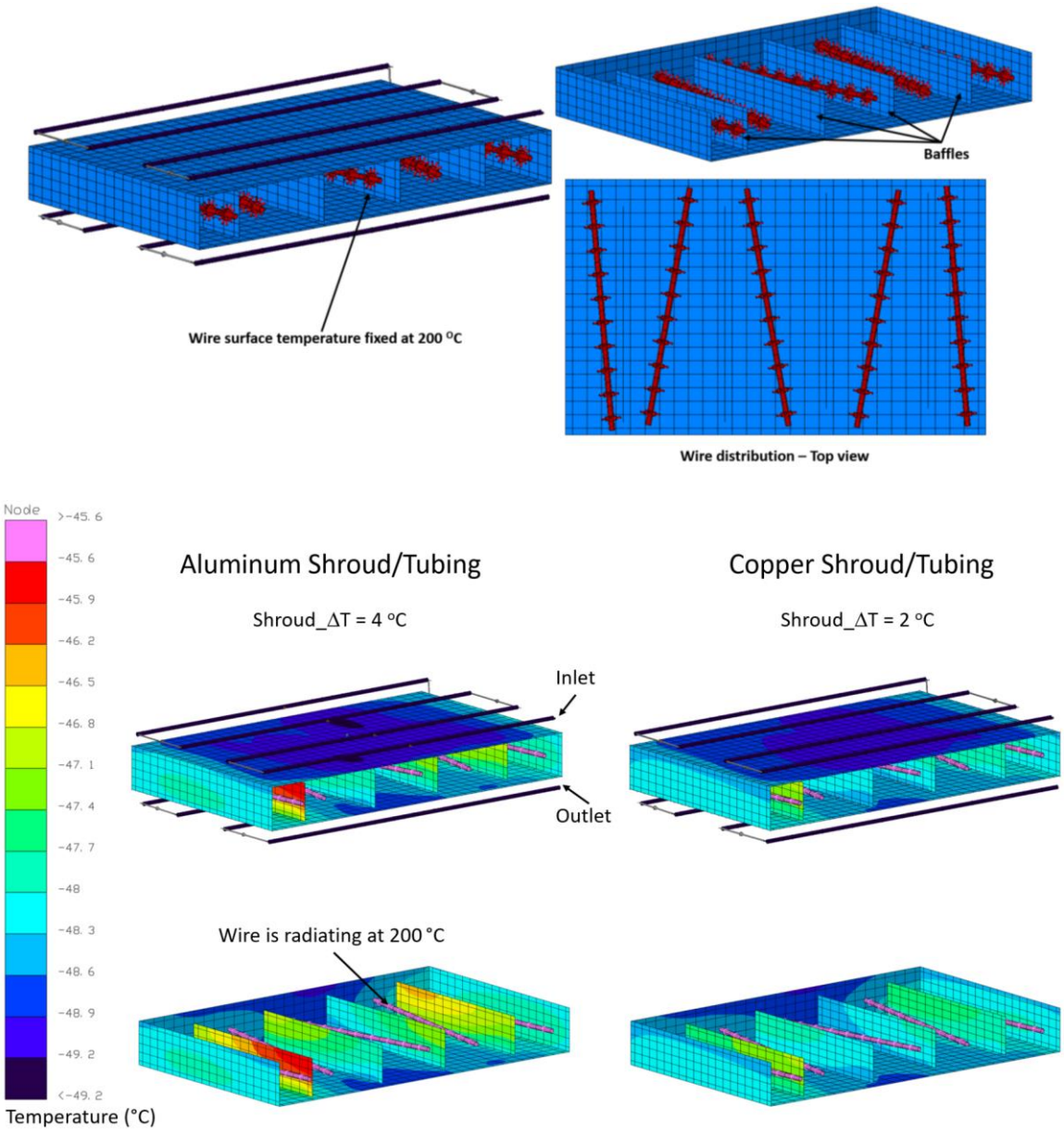

Figure 7.1.2.1-6. Temperature Profile – Full Shroud Thermal Model – Left, Aluminum; Right, Copper

c. Nominal Shroud Design and Fabrication Considerations

Thermal analysis obtained a maximum ΔT of 4°C on an aluminum shroud with four tubes each on the top and bottom plates. The 3/8-inch diameter tubing showed higher thermal performance than the 1/4-inch diameter tubing. Having the shroud box and tubing made of aluminum makes the brazing process faster, less costly, and easier to fabricate. Table 7.1.2.1-3 summarizes the nominal specifications for the shroud design chosen for construction. Figure 7.1.2.1-7 shows the drawing of the shroud design.

Table 7.1.2.1-3. Single Plate Shroud Design Analysis Parameters

Shroud Dimensions	33 × 20 × 4 inches
Shroud Thickness	1/4 inch
Tubing Diameter	3/8 inch
Maximum Allowable Heat Load	1,000 watts
Minimum Allowable Temperature	-7°C
Maximum Expected ΔT	4°C
Material	Aluminum

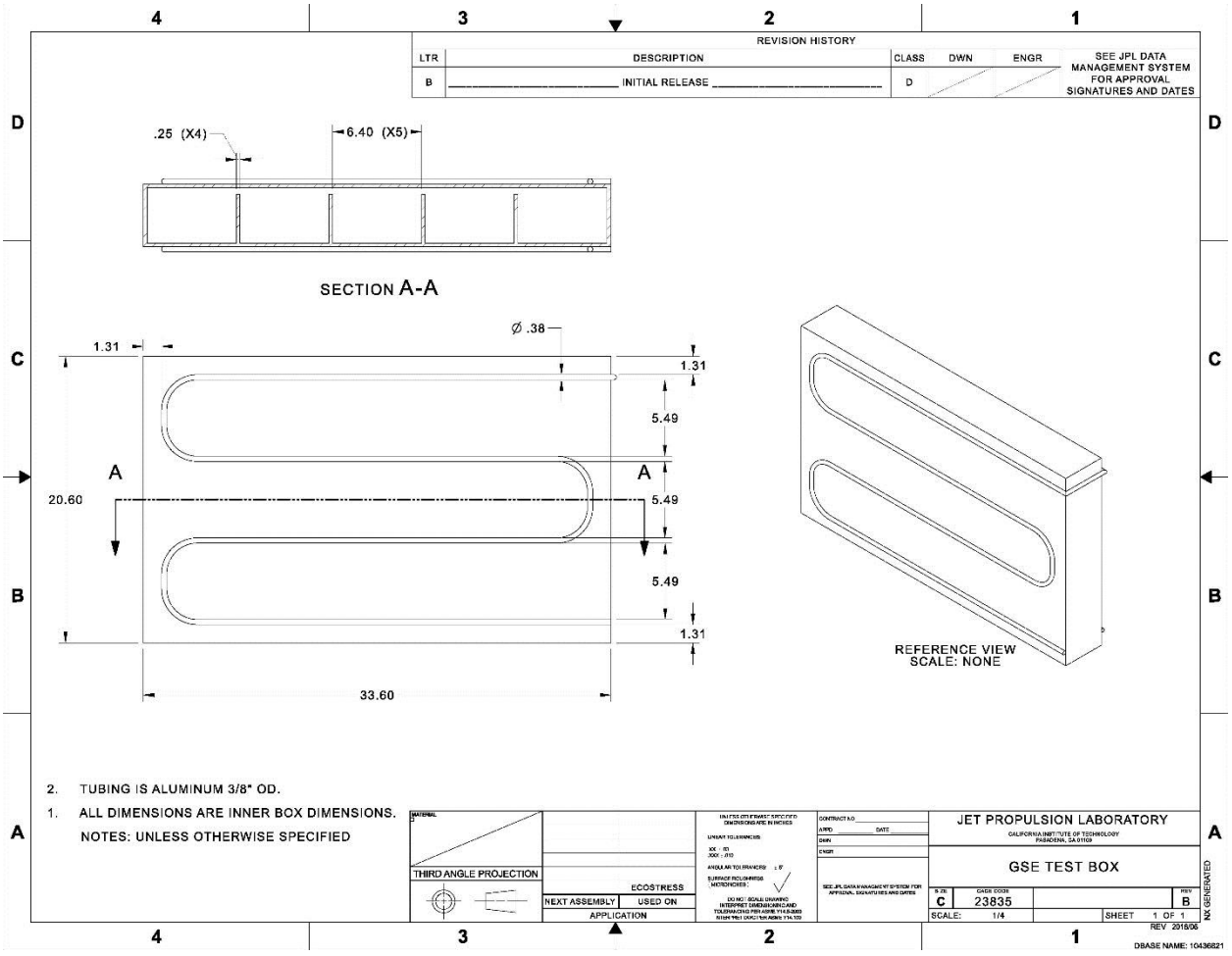

Figure 7.1.2.1-7. Shroud Computer-Aided Design (CAD) File

d. Paint and Bake-out

The shroud was painted black to provide a consistently high infrared emissivity surface. On the interior surface, the shroud was coated with two layers of high temperature engine paint [ref. 8]. The paint is designed to withstand temperatures from 704 to 1093°C, well beyond the temperature range planned for the test program.

After painting was completed, the shroud and witness sample were dried for 24 hours. To avoid outgassing at high temperatures inside the vacuum chamber, the painted shroud was baked out.

The shroud and a painted witness sample were placed in a furnace at 200°C as shown in Figure 7.1.2.1-8. A thermocouple was attached to the shroud to ensure it reached the target temperature, and the shroud and furnace temperature were monitored during the bake-out. Table 7.1.2.1-4 shows the bake-out details.

Figure 7.1.2.1-8. Shroud Spray Painting and Bake-out

Table 7.1.2.1-4. Shroud Bake-Out Details

Bake-out Temperature [℃]	Bake-out Duration	Cool-down Duration
100	1 hr and 35 minutes	3 hrs
200	3 hrs	1 day

When bake-out was completed, a reflectometer was used to measure the emissivity of the witness sample. The reflectometer was set to the infrared range (i.e., 3 to 35μm). The accuracy of the reflectometer is ±3% full scale. Two painted samples were used for measurements. Prior to measurement, the reflectometer was calibrated using a gold and MLS-855B sample with specified emissivity. Figure 7.1.2.1-9 shows the measured emissivities on the painted sample surface.

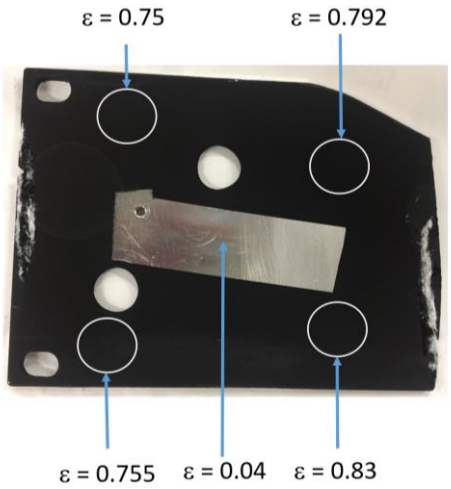

Figure 7.1.2.1-9. Measured Emissivity on a Witness Sample Processed with the Shroud

7.1.2.2 Pressure-Controlled Chamber

To control the environmental pressure surrounding the test article, the shroud was placed inside of a pressure-controlled vacuum chamber (Figure 7.1.2.2-1). The vacuum chamber was capable of maintaining pressures from 1e-7 Torr (1.3e-10 atm) to ~760 Torr (~1 atm). During the test campaign, only two pressure conditions were used: vacuum (<1e-5 Torr) and atmospheric (~760 Torr). During the vacuum condition, the chamber was sealed and the vacuum pump was activated. During the atmospheric condition, the chamber was filled with nitrogen gas and vented to the atmosphere via a port on the chamber top.

Figure 7.1.2.2-1. Pressure-Controlled (Vacuum) Chamber

7.1.2.3 Measurement System

A data acquisition system (DAQ) was set up to measure the critical parameters of the test and supporting hardware. The following variables were measured during testing:

- the temperature of the wire conductor in the bundle (see Section 7.2 for mounting details)
    - 2 wire temperatures were measured in the bundles—one centrally located and the other on a bundle exterior surface wire
- the current passing through the wire bundle
- the voltage across the wire bundle
- the temperature of the shroud (in 15 locations for single-wire, and 14 locations for the 32-wire bundles)
- the pressure inside the vacuum chamber (during vacuum conditions)
- the air temperature within the shroud
- the temperature of the vacuum chamber
- the temperature of the ambient room air

A schematic of the measurement system is shown in Figure 7.1.2.3-1. All temperatures were measured with type E thermocouples. Estimated measurement errors are shown in Table 7.1.2.3-1. These estimates include the accumulated error from the measurement instrument and the DAQ system. For the wire bundle temperature measurements, additional analyses were performed to understand the influence of the mounted thermocouple on the wire bundle temperature (see Appendix A).

Wire conductor temperatures were monitored using a thermocouples soldered directly to the conductor using a high melting point solder (composition: SN95SB5; 240 ºC melting point). Thermocouples were mounted in the center (lengthwise) of the test article to ensure that any end effects were minimized. For single wire test articles, one thermocouple was mounted to the wire conductor. For the 32-wire bundle articles, two thermocouples were mounted on two separate wires: a central wire (i.e., internal) and an exterior wire (i.e., bundle surface) (see Section 7.2).

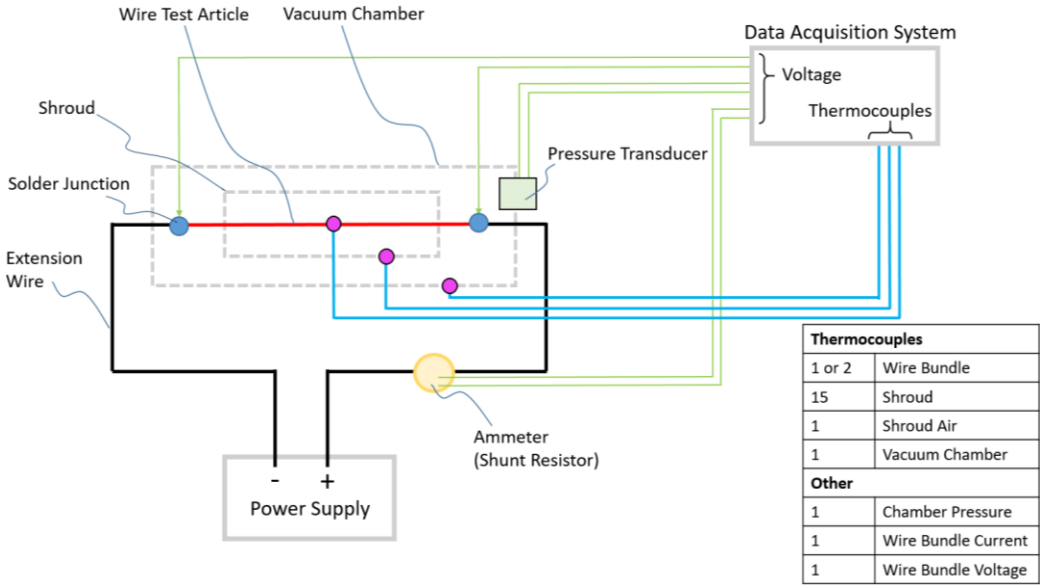

Figure 7.1.2.3-1. Schematic of the Measurement System

Table 7.1.2.3-1. Estimated Measurement System Errors

Measured Parameter	**Max Error**
Temperature	± 2°C
Chamber Pressure	15 % of reading at vacuum
Wire Bundle Current	± 0.1A
Wire Bundle Voltage Drop	± 4 mV

7.2 Description of Test Articles

The primary[1] test campaign focused on two gauges of wire (20 AWG and 26 AWG), two insulation types TKT and XL-ETFE and two bundle configurations (single wire and a 32-wire bundle). TKT and XL-ETFE insulation are the primary insulation types used on modern aerospace systems. Test articles were fabricated at JPL using flight grade wire. The general procedure for fabricating a test article was to cut the wire, form the bundle, and mount the thermocouple on the appropriate wire(s). The bundle was spot tied, if necessary, and installed into the shroud for testing. Table 7.2-1 shows the details regarding the wiring used for the test articles.

[1] Late in the test program, 22 AWG XL-ETFE wire was added.

Table 7.2-1. Details of Wire Used in Testing

Wire #	Wire PN	Insulation	Conductor Base Metal, AWG	Plating	Wire Supplier
1	M22759/33-20-9	XL-ETFE	Hi-Strength Stranded Cu Alloy, 20 AWG	Silver	WireMasters
2	M22759/33-26-9	XL-ETFE	Hi-Strength Stranded Cu Alloy, 26 AWG	Silver	WireMasters
3	M22759/33-20-9	XL-ETFE	Hi-Strength Stranded Cu Alloy, 20 AWG	Silver	A.E. Petsche
4	M22759/33-26-9	XL-ETFE	Hi-Strength Stranded Cu Alloy, 26 AWG	Silver	A.E. Petsche
5	AS22759/181-20-9	TKT	Hi-Strength Stranded Cu Alloy, 20 AWG	Silver	CarlisleIT/Thermax
6	AS22759/181-26-9	TKT	Ultra-Hi-Strength Stranded Cu Alloy, 26 AWG	Silver	CarlisleIT/Thermax

7.2.1 Test Procedures

The goal of each test was to measure the amount of electrical current that would raise the wire test article temperature to steady state temperatures to 200°C with the given environmental conditions. To achieve this state, the following procedures were followed: (1) the vacuum chamber was set to the specified test pressure using vacuum pumps as necessary; (2) the shroud was set to specified test temperature using the chiller; (3) the wire temperature was gradually increased to about 200°C by step-wise increases in the current; (4) the wire was held at 200°C for at least a period of 1 hour to ensure steady state conditions were reached; and (5) once the wire was verified to be at steady state (less than 0.1°C/hour), the test was ended.

7.3 General Remarks on Testing

The test campaign was conducted without any significant issues. Testing generally went as expected with all subsystems working properly. The wire temperature measurement system (thermocouple soldered to conductor) worked well and was cross-checked using the resistance wire thermometry approach whereby wire temperature is inferred via the wire resistance. The current supply system provided stable current with typical fluctuations of approximately 1 mA. The shroud was able to maintain isothermality within 5°C at atmospheric pressure, and 2.5°C at vacuum conditions for the largest bundles with the coldest shroud temperatures. Typically, isothermality was much better than these ranges. The vacuum chamber was typically able to hold pressure between 1e-5 and 1e-7 Torr for the vacuum cases.

Data from a typical test is shown in Figure 7.3-1. From 0 to 2 hours, vacuum was applied to the chamber and the shroud was cooled to the set temperature of -50°C. At about 1.8 hours, 1A was applied to the wire bundle. At about 5.8 hours the central bundle temperature was elevated to

200°C by increasing the current to 2.3A. The current was adjusted real time to maintain the target temperature of 200°C. At about 7.7 hours, the test ended where the wire current was set to zero, and the shroud chiller and vacuum pump were turned off. The system was left to reach thermal equilibrium under residual vacuum.

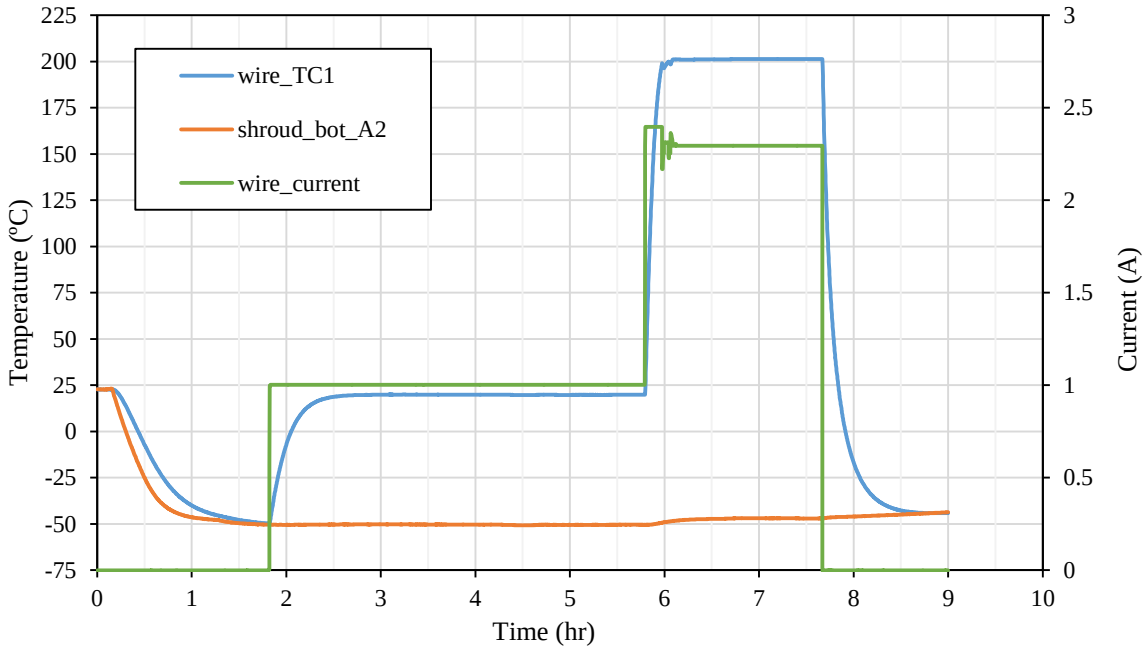

Figure 7.3-1. Representative Test Data Taken from Run #5 (26 AWG/XL-ETFE Insulation/32-wire Bundle/Vacuum)

7.4 Test Design and Procedures

This section outlines the analysis and negotiations involved in designing the test matrix. A design of experiments (DOE) approach was used to construct an analyzable dataset that would efficiently uncover the most important relationships between input factors and response outputs.

The DOE methodology began with the following team generated primary problem statement:

- *How far can we increase loading on a power transmission wire without destroying the wire insulation?*

Secondary problems included:

- *Given simulation models written to characterize the physics, how well do these models match test?*
- *A table or calculator relating AWG to maximum current rating in various space mission environments is needed.*

Key response metrics required to solve these problems included steady-state wire temperatures at a particular current input. Analysis of historical data [ref. 9] showed this to be a useful predictor. Figure 7.4-1 shows that current (blue stepped trace) drives wire temperature (multiple colored traces marked T2 to T11 in the legend). Wire temperature stabilizes after a brief transition period after the current is increased.

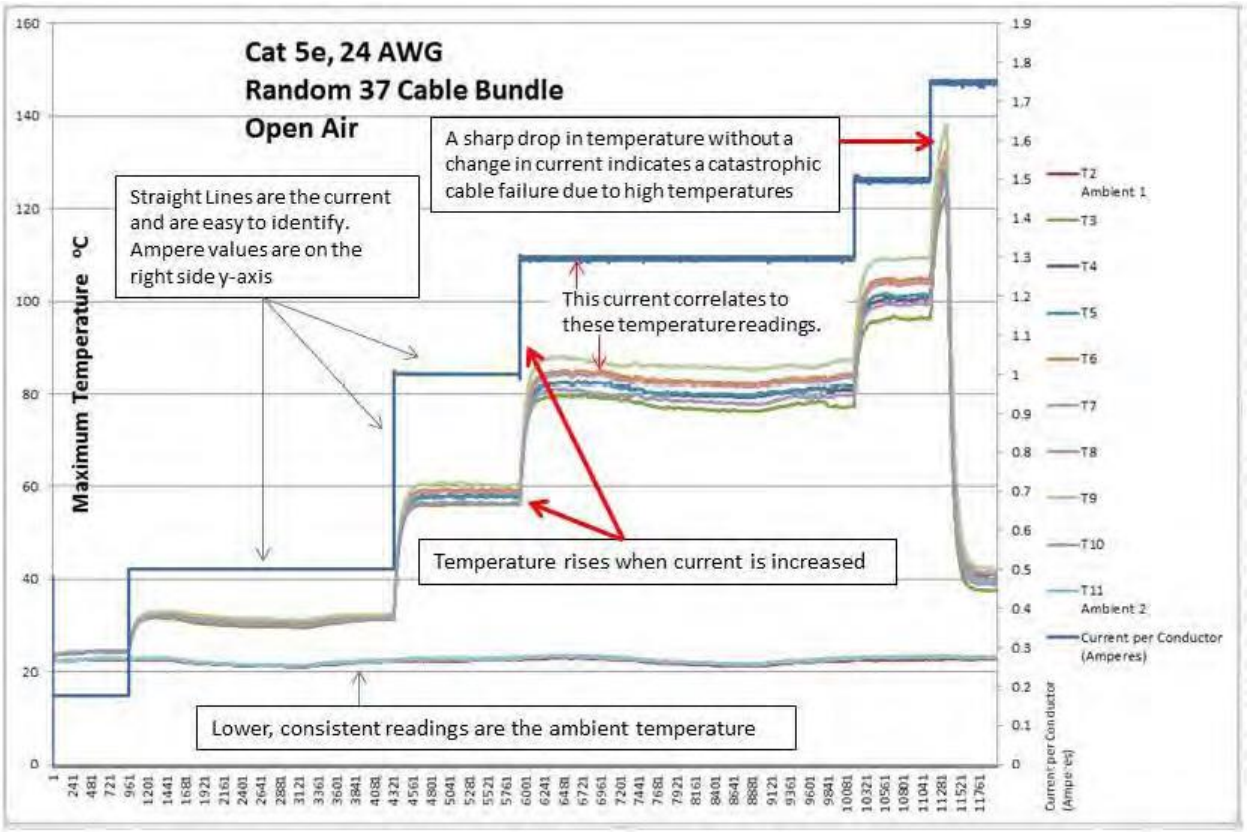

Figure 7.4-1. Historical data graph showing relationships between input factors and response variables. © 2015 UL LLC © 2015 SPI: The Plastics Industry Trade Association 20150930.

However, wire temperature is not stable during times of steady current. Much of the variation can be explained by variations in the ambient temperature, which trace is the light green line around 23°C in the lower plot in Figure 7.4-2. Controlling for this effect resulted in a more reasonable steady-state remainder, as can be seen in the upper plot.

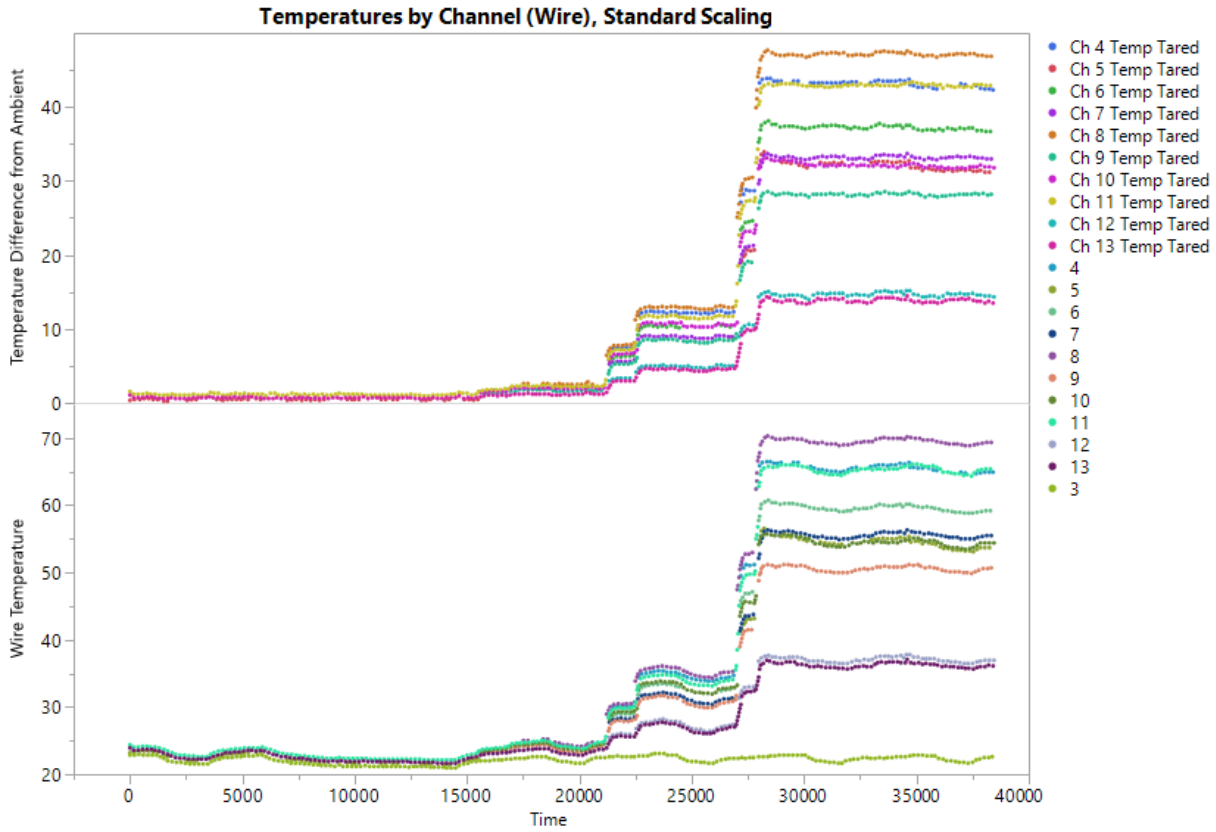

Figure 7.4-2. Comparison of data without controlling for ambient temperature (bottom) and after doing so (top). Data from [ref. 9]; 2015 UL LLC © 2015 SPI: The Plastics Industry Trade Association 20150930.

These two figures indicate variability in wire temperature between individual wires increased with increasing temperature. Part, or most, of this effect is likely due to differing locations of the wires in the cable in this historical data. However, some might also be due to an increase in instrument variability, or increasingly variable test environment convection currents at higher temperatures. If unexplained random variations (e.g., not related to any of the input factors, including wire location in a bundle) were higher at higher temperatures, then this was characterized and accounted for in the analysis.

Input factors were chosen through negotiation on the team guided by the problem statement tempered by constraints. Number of wires per bundle, AWG, insulation type, environmental pressure, and environmental temperature were identified as key factors of interest. Other factors were discussed, but postponed for future investigation due to constraints.

Constraints to testing included cost, schedule, state of knowledge, and difficulty in achieving test conditions. Cost was bounded by the budget, which limited number of tests, size of test chamber, and number of test articles, among other considerations. Schedule constraints primarily affected number and duration of tests, but also had an effect on what materials could be tested due to lead time.

The state of knowledge of the problem, while mature, required that some cost, schedule and personnel resources needed to be consumed in determining some material properties values required for modeling assumptions through test as discussed in other report sections.

Difficulty in achieving test conditions required considerable thought. Ideally, in most cases, test runs should be run in a random order. This prevents uncontrolled and generally unrecognized "rogue variables" from biasing test data and analysis results. For instance, if the resistance of a wire increases over a number of tests and all tests in a vacuum are run before all the tests at 1 atm, then the current required to reach 200 ºC insulation temperature will be artificially deflated for the 1 atm tests. If the tests are run in random order, then the change in the current metric will be distributed randomly among the data rather than biasing findings. In this example case, any effect of resistivity increase was expected to be small, but there are many other biasing effects that can and do occur in real testing. Randomization can be "cheap insurance" against biases induced by rogue variables [ref. 10].

It was recognized from nearly the beginnings of DOE methods development that it is not always "cheap" to randomize. Well-understood test planning and accompanying analysis methods are available to handle such constraints. Here, complete randomization would have required wires to be changed for each run, a time-consuming and expensive undertaking. Instead, it was planned to leave the same wire or bundle in the chamber for a series of three tests before changing, saving 2/3 of the associated effort, time and cost compared to full randomization.

There is a cost to doing this. It also cuts the effective number of associated samples by 2/3. It would be incorrect to claim that in 27 test runs that wires were also changed 27 times (counting original insertion as one) when in fact there were only 9 changes. Since confidence in analysis results is firmly related to sample size, restricting randomization like this can have considerable consequence.

To deal with this, "split-plot" test planning and analysis tools were used [refs. 11, 12]. These advanced yet standard techniques handle the different number of effective samples, known in the literature as plots, correctly. Standard commercial software suites JMP® and Design Expert® were used for design and analysis.

Choosing factor levels. Engineering analysis is an effort to recognize the signal due to the signal of an effect over test, instrument, environmental and other noises – a signal-to-noise ratio (S/N). Statistical significance is nothing more than a measure of how likely the S/N of the signal seen is due to random chance: 0.05 (5%) significance means there is only a 1/20 chance the effect could be due to random noise. Here, a signal would be the difference in temperature response values between, say, a 32-wire bundle vs. a single wire.

In this testing, different ways were used to bolster signals. A relatively large sample size – 27 test runs – is the most obvious. Because of the small plot sizes, wires-per-bundle, insulation type and wire gauge (i.e., AWG) values that provided large signal differences were chosen. Had the test been run using only single and twisted-pair wires, the difference may have been too small to see in only eight top-level plots (usually called whole plots), so a 32-wire bundle was chosen as the case to contrast with a single wire.

This is an extension of the fact that running tests at the extremes of the ranges of quantitative factors allows the clearest estimate of the difference between those extremes. For this reason, testing was performed during the basic series at only 20 and 26 AWG. Running 12 tests at each case allows comparison of the mean of 12 observations at smaller gauge vs. 12 at larger, thus giving a more highly-significant, lower-uncertainty estimate of the difference than if measurements were scattered across several wire diameters. Values at intermediate wire diameters can be estimated by exercising the linear regression model relating AWG to response

metrics easily, assuming a linear response. The team decided this was good enough for this first phase. If necessary, it could be refined or validated by analyses or in a subsequent phase. Similar thinking was applied to environmental pressure and temperature, with one change. Because the effect of chamber temperature on wire temperature was known by analysis of other data [ref. 9] to result in a curved graph, and environmental temperature was relatively easy to change, an intermediate factor level was employed. This allowed for the inclusion of a quadratic term in the model, which accounts for the observed curvature. .

A table of the factors and setpoints is given in Table 7.4-1.

Table 7.4-1. List of Test Factors and Ideal Setpoints.

Factor	Factor Level Set
Wires per Bundle (WPB)	[1, 32]
Wire Gauge (AWG)	[20, 26]
Insulation	[XL-ETFE, TKT]
Pressure (atm)	[0 (Vacuum), 1]
Environmental Temperature (°C)	[-50, 20, 70]

The full test matrix follows as Table 7.4-2. Chamber load delineates the eight whole plots. The test matrix is shown in randomized order.

Table 7.4-2. Originally Planned Test Matrix[2]

Run No	Chamberload	Wires per Bundle	Wire Gauge Setpoint AWG	Insulation	Pressure Setpoint atm	Environmental Temperature Setpoint C
1	1	1	26	XL-ETFE	0	20
2	1	1	26	XL-ETFE	1	70
3	1	1	26	XL-ETFE	1	-50
4	2	32	26	XL-ETFE	0	70
5	2	32	26	XL-ETFE	0	-50
6	2	32	26	XL-ETFE	1	20
7	3	1	26	TKT	1	20
8	3	1	26	TKT	0	70
9	3	1	26	TKT	0	-50
10	4	1	20	TKT	1	-50
11	4	1	20	TKT	1	70
12	4	1	20	TKT	0	20
13	5	32	20	TKT	0	-50
14	5	32	20	TKT	1	20
15	5	32	20	TKT	0	70
16	6	32	26	TKT	0	20
17	6	32	26	TKT	1	70
18	6	32	26	TKT	1	-50
19	7	1	20	XL-ETFE	0	-50
20	7	1	20	XL-ETFE	1	20
21	7	1	20	XL-ETFE	0	70
22	8	32	20	XL-ETFE	1	70
23	8	32	20	XL-ETFE	0	20
24	8	32	20	XL-ETFE	1	-50

7.5 Thermal Analysis and Model Correlation

Thermal mathematical models were developed to analyze the single wire and wire bundle configurations, and to correlate to data obtained during the test campaign.

7.5.1 Wire Insulation Effective Thermal Conductivity

Heat transfer through wire insulation is part of the overall wire heat balance, and determination of the wire insulation effective thermal conductivity was required for single wire and wire bundle thermal analyses. The wire insulation is represented as an infinitely long cylinder with inner and outer radii of r_c and r_s, respectively. For a single layer of insulation, the thermal conductance per unit length is given by Eq. 1:

[2] A ninth test article (22 AWG XL-ETFE) was added during the test program resulting in a total of 27 runs with 9 chamber loadings.

$$G_L = \frac{G}{L} = \frac{2\pi k_w}{ln\left(r_s/r_c\right)} \quad \text{Eq. 1}$$

Insulations (e.g., TKT) are comprised of multiple layers. If the thickness and thermal conductivity of each constituent layer is known, then the equivalent thermal conductance, $(G_L)_{eq}$ may be determined by calculating the series conductance using Equation 2:

$$\left(\frac{1}{G_L}\right)_{eq} = \sum_{i=1}^{N}\left(\frac{1}{G_L}\right)_i \quad \text{Eq. 2}$$

Wire insulations used during this pathfinder phase used XL-ETFE or TKT. The thermal conductivities assumed for the constituent materials is presented in Table 7.5.1-1.

Table 7.5.1-1. Insulation Layer Thermal Conductivity

Material	Thermal Conductivity $(W/m \cdot K)$	Notes
XL-ETFE	0.238	Used 0.238 as seen in other resources, but the following link reports 0.24: https://www.chemours.com/Teflon_Industrial/en_US/assets/downloads/tefzel-etfe-film-properties.pdf
Kapton®	0.12	Measured at 296 K. Data from: http://www.dupont.com/content/dam/dupont/products-and-services/membranes-and-films/polyimde-films/documents/DEC-Kapton-summary-of-properties.pdf
PTFE	0.238	Assumed same as XL-ETFE

Effective thermal conductance as calculated using specification data[3] for wire insulation and is presented in Table 7.5.1-2.

Table 7.5.1-2. Effective Thermal Conductivities Used in Analysis

AWG	Insulation	Effective Thermal Conductivity $(W/m \cdot K)$
20	XL-ETFE	0.2380
26	XL-ETFE	0.2380
20	TKT	0.1921
26	TKT	0.1904
22	XL-ETFE	0.2380

7.5.2 Single Wire Thermal Model and Test Correlation

The original single wire thermal model was based on work presented in References 1 and 13. The wire insulation steady state surface temperature, T_s, is solved iteratively using Equation. 3:

$$I^2R_{L0}\left\{1+\alpha\left[\frac{I^2R_{L0}(\alpha T_0-1)-\frac{2\pi k_W T_S}{ln(r_S/r_C)}}{\alpha I^2R_{L0}-\frac{2\pi k_W}{ln(r_S/r_C)}}-T_0\right]\right\} = 2\pi r_s[\varepsilon\sigma(T_s^4-T_e^4)+f_h h(r_s,T_s)(T_s-T_e)] \quad \text{Eq. 3}$$

[3] These calculations were performed early in the assessment before measured data were available. Future analyses should include as-measured data, where practical.

Where:

I	wire current (A)
R_{L0}	wire electrical resistance per unit length at T_0 (Ω/m)
α	temperature coefficient of resistance $(1/K)$
T_0	reference temperature $(293.15\ K)$
k_w	wire insulation thermal conductivity $(W/m\ K)$
r_s	wire insulation jacket outer radius (m)
r_c	wire conductor radius (m)
ε	wire insulation or wire bundle external jacket infrared emissivity
σ	Stefan-Boltzmann constant $(5.67 \times 10^{-8}\ W/m^2\ K^4)$
T_s	wire insulation jacket surface temperature (K)
T_e	ambient environment temperature (K)
f_h	convective heat transfer scaling factor
h	convective heat transfer coefficient $(W/m^2\ K)$

Calculation of the convective heat transfer assumed a horizontal wire in air[4] at 1 atm under 1-g conditions. The convective heat transfer coefficient, h was determined by noting the relationship to Nusselt number, Nu (Eq. 4):

$$Nu = \frac{h(2r_s)}{k} \quad \text{Eq. 4}$$

and the Nusselt number was a function of the Grashof-Prandtl number, $GrPr$ (Eq. 5):

$$Nu = f(GrPr) \quad \text{Eq. 5}$$

where $GrPr$ is given by Eq. 6:

$$GrPr = \frac{\rho^2 \beta c_p g \Delta T (2r_s)^3}{\mu k} \quad \text{Eq. 6}$$

T_{film} is defined as (Eq. 7):

$$T_{film} \equiv \frac{T_s + T_e}{2} \quad \text{Eq. 7}$$

Note that ρ, c_p, μ, and k for air are $f(T_{film})$, $\beta = (1/T_{film})$ and $\Delta T = (T_s - T_e)$. Air properties used for this analysis are presented in Table 7.5.2-1.

[4] Air is used in the thermal models, but gaseous nitrogen was used in the 1 atm chamber tests. Select analysis runs were performed to compare the correlation between air and nitrogen cases and resulted in no change to the convection scaling factor, f_h.

Table 7.5.2-1. Air Properties Used in the Thermal Model

T_{film} (K)	ρ (kg/m^3)	c_p $(J/kg \cdot K)$	μ $(kg/m \cdot s)$	k $(W/m \cdot K)$
200	1.7684	1006.1	1.33E-05	0.01809
250	1.4128	1005.3	1.49E-05	0.02270
300	1.1774	1005.7	1.98E-05	0.02624
350	0.9988	1009.0	2.08E-05	0.03003
400	0.8826	1014.0	2.29E-05	0.03365
450	0.7833	1020.7	2.48E-05	0.03707

The relationship between Nu and $GrPr$ in Eq. 5 is dependent on the magnitude of $GrPr$ and the geometry to be analyzed. For this analysis, data extracted from plot [ref. 14] were used to formulate a curve fit. Hence, the Nu was determined for a calculated $GrPr$.

Since the fluid properties are a function of T_s and T_e which was assumed fixed, the convective heat transfer coefficient can be stated as $h = h(r_s, T_s)$.

A convective scaling factor, $f_{h,}$ is also used in the analysis to make final adjustments on h. For the vacuum case, $f_h = 0$.

Once T_s is known, Eq. 8 may be used to solve for the steady state conductor temperature, T_c:

$$T_c = \frac{I^2 R_{L0}(\alpha T_0 - 1) - \frac{2\pi k_w T_s}{ln\left(r_s / r_c\right)}}{\alpha I^2 R_{L0} - \frac{2\pi k_w}{ln\left(r_s / r_c\right)}} \qquad \text{Eq. 8}$$

The algorithm was implemented as a Microsoft® Excel® spreadsheet.

The original model exhibited a shortcoming when correlating to vacuum test data during the initial assessment [ref. 1] and the current study, and consistently over-predicted steady state conductor temperatures for the high temperature cases. While the over-prediction in Reference 1 may have been partially attributed to uncertainties or assumptions made for key modeling parameters, the current study went to great lengths to measure these parameters. When used in the overall heat balance, the over-prediction remained evident.

Three unmodeled effects were considered as potential contributors to the discrepancy between the predicted and measured temperatures:

1) End Effects – The heat balance model assumed an infinitely long wire. Heat loss from conduction to a cooler boundary condition at the wire terminations was not considered in the final analytical models. Such heat loss from a wire under test would reduce the measured temperature. The result would be a model over-prediction. This explanation is unlikely because the test set up was designed to minimize/negate the effect of end terminations by testing a sufficiently long wire (> 3 m). Pre-test analysis showed that temperature drop off occurs within approximately 1 foot (~0.30 m) of each end termination and, beyond that, did not affect the temperature of the middle length of the wire. Furthermore, an analysis comparing a heated wire with and without connections to end terminations showed about a 0.35℃ temperature difference.

2) Segments of Energized Wire Outside of the Temperature Controlled Shroud – While most of the wire under test was within the confines of the temperature-controlled shroud, some of the wire was outside of the shroud but subject to test chamber environmental conditions. For cases where the shroud was warmer than the volume outside the shroud, this would effectively lower the overall wire resistance and, for a specified current, would result in a lower power dissipation. For the case where the shroud was colder than the surrounding volume, the opposite would be true. Since the model assumed a higher power dissipation by assuming the entire wire is at the same temperature, the model would calculate a higher resistance and temperature. Attempts to calculate an aggregate resistance based on the measured central length temperature and ramped down temperatures approaching the terminations proved unnecessary as the measured power draw (VI) correlated with wire power dissipation using resistance ($I^2R(T_{meas})$) calculated using the measured wire central length temperature. Therefore, aggregate resistance was deemed unlikely as a contributor.

3) Insulation Jacket Infrared Transmissivity – Wire insulation materials such as XL-ETFE and Kapton® are not opaque and can allow energy to pass through them. While no data were found for the specific XL-ETFE and TKT insulations used in wire manufacturing, Reference 15 provides some data to support this hypothesis that XL-ETFE is transmissive in some infrared bands. Furthermore, Reference 16 hypothesizes the effect of infrared transmissivity on wire test results.

With end effects and the effect of wiring outside of the temperature-controlled shroud excluded, additional evidence of the possibility of wire jacket transmissivity was pursued. A 20 AWG wire with XL-ETFE insulation was heated by passing electrical current and infrared images collected at steady state conditions. The test set-up is shown in Figure 7.5.2-1. Four different levels of current were applied to the wire: 6.63, 10.48, 16.63, and 17.00A.

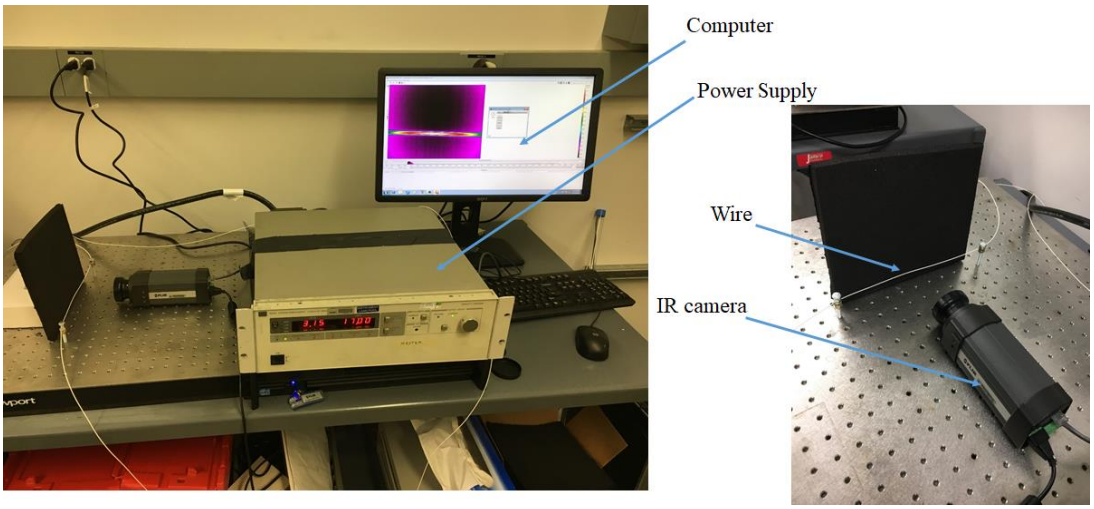

Figure 7.5.2-1. Wire Jacket Infrared Transmissivity Test Set-up

An image of a similarly sized wire in the visible spectrum was overlaid onto the infrared image is shown in Figure 7.5.2-2.

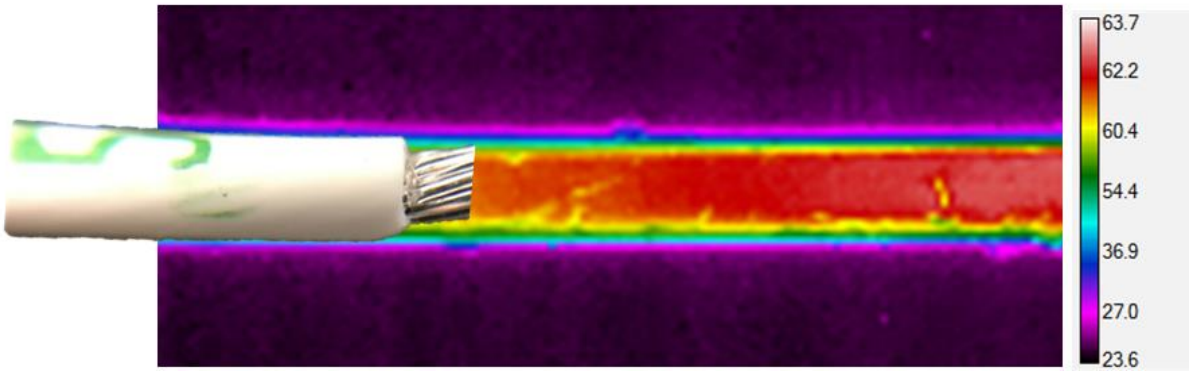

Figure 7.5.2-2. 20 AWG XL-ETFE-Jacketed Wire Visible image Overlaid onto Infrared Image

Visual inspection suggests the temperature gradient corresponds to the conductor location. While not conclusive, the results suggest the radial gradient seen in infrared image is due to the transmissivity of the insulation jacket.

To improve the single wire thermal model, steady state heat balance presented in Eq. 3 was reformulated to include a transmissivity term allowing heat transfer from the copper conductor directly to the environment via thermal radiation through an IR transmissive wire jacket. The heat balance for the wire is given in Eq. 9. Note that, for this derivation, it is assumed the jacket does not absorb any of the energy radiated from the conductor. Also, to account for the emissive properties and the jacket IR transmissivity, an effective IR transmissivity[5] (τ) was used that established through correlation to vacuum case test data.

$$I^2 R_{L0} L[1 + \alpha(T_c - T_0)] = 2\pi r_s f_h h L(T_s - T_e) + 2\pi r_s \sigma \varepsilon L(T_s^4 - T_e^4) + 2\pi r_c \sigma \tau L(T_c^4 - T_e^4) \quad \text{Eq. 9}$$

Eq. 9 contains references to T_s and T_c. To solve this equation, a relationship between T_s and T_c must be established. Eq. 10 is a heat balance focused on the conductor and states the heat generation within the conductor is equal to that which conducts through the wire jacket to the surface plus that which radiates from the conductor through the jacket due to IR transmissivity.

$$I^2 R_{L0} L[1 + \alpha(T_c - T_0)] = \frac{2\pi k_w L(T_c - T_s)}{\ln(r_s/r_c)} + 2\pi r_c \sigma \tau L(T_c^4 - T_e^4) \quad \text{Eq. 10}$$

Rearranging Eq. 10 yields an expression that relates T_s and T_c, which is given in Eq. 11:

$$T_s = \frac{[2\pi k_w/\ln(r_s/r_c)]T_c - I^2 R_{L0}[1+\alpha(T_c - T_0)] + 2\pi r_c \sigma \tau (T_c^4 - T_e^4)}{[2\pi k_w/\ln(r_s/r_c)]} \quad \text{Eq. 11}$$

Thermal modeling of the test configuration required knowledge of key wire parameters (R_{L0}, α, r_s) and environment temperature (T_e). The wire parameters (R_{L0} and α) were derived from oil bath testing and is described in Section 7.5.6. Infrared emissivity, ε for all wire jackets was

[5] The effective transmissivity is a means of accounting for some radiation through the wire insulation. As currently modeled, the use of this parameter does not strictly obey conservation of energy nor does it account for wire conductor plating emissivity. Additional study of this phenomenon is suggested as forward work.

assumed to be 0.9. Attempts to obtain this data by measurement produced data inconsistent with published values. The wire jacket radius, r_s (actually diameter, $2r_s$) and wire conductor radius, r_c (actually diameter, $2r_c$) were measured directly and represents an average of 8 to 20 measurements made along the length of the wire/bundle and converted to SI units. Model parameters are summarized in Table 7.5.2-2.

Model correlation was performed using data from the 22 AWG XL-ETFE jacketed wire test runs as there was a total of 16 data points covering a variety of temperature boundary conditions under vacuum and 1 atm conditions. Correlation of the vacuum case was attempted first as it afforded an opportunity to correlate the model without the effects of convection. Under vacuum conditions, with an assumed $\varepsilon = 0.9$ and all other model parameters measured, the effective transmissivity, τ term was adjusted until correlation with the test measured conductor temperature was achieved. Correlation was best achieved assuming a $\tau = 0.13$. With the transmissivity established, correlation proceeded to the 1 atm cases. The convection correlation of Reference 14 was selected, but a convection scaling parameter, f_h was used to make final adjustments to the convection correlation. Once these parameters were established, all subsequent test cases were correlated using these parameters in a "hands-off" mode. From the testing conditions, 48 steady state correlation cases were extracted. The model was run using the parameters from Table 7.5.2-2 in conjunction with average shroud temperature and current obtained data from each test condition.

Table 7.5.2-2. Single Wire Thermal Model Analysis and Correlation Parameters

Test Article	AWG	Insulation Material	k_w $(W/m \cdot ℃)$	R_{L0} (Ω/m)	α $(1/℃)$	ε	τ	f_h	$2r_s$ (mm)	$2r_c$ (mm)
1	26	XL-ETFE	0.2380	0.1298	0.00363	0.9	0.13	0.9	0.803	0.4572
3	26	TKT	0.1904	0.1651	0.00282	0.9	0.13	0.9	0.822	0.4674
4	20	TKT	0.1921	0.0327	0.00359	0.9	0.13	0.9	1.263	0.9373
7	20	XL-ETFE	0.2380	0.0326	0.00363	0.9	0.13	0.9	1.278	0.9398
8	22	XL-ETFE	0.2380	0.0522	0.00363	0.9	0.13	0.9	1.102	0.7366

Note: R_l, α, $2r_s$, and $2r_c$ were measured parameters. ε is assumed based on published data for XL-ETFE. τ and f_h are correlation parameters.

A comparison of measured steady state conductor temperatures (orange column) with the model-predicted steady state conductor temperature (blue column) is presented in Table 7.5.2-3.

Table 7.5.2-3. Single Wire Thermal Model Analysis Correlation Results

Run Identifier	AWG	Insulation	Pressure	Average Shroud Temp (°C)	Current (A)	Conductor $T_{measured}$ (°C)	Conductor $T_{predicted}$ (°C)
1	26	XL-ETFE	Vacuum	20.2	1.998	54.3	55.2
2	26	XL-ETFE	Vacuum	20.9	5.251	199.6	202.0
3	26	XL-ETFE	Vacuum	78.7	4.692	198.5	199.3
4	26	XL-ETFE	1 atm	70.0	2.006	77.2	76.5
5	26	XL-ETFE	1 atm	70.5	3.994	95.5	94.7
6	26	XL-ETFE	1 atm	71.4	8.005	167.6	168.0
7	26	XL-ETFE	1 atm	71.9	9.205	200.1	201.2
8	26	XL-ETFE	1 atm	-46.9	1.997	-41.7	-41.1
9	26	XL-ETFE	1 atm	-46.1	6.000	-0.4	1.3
10	26	XL-ETFE	1 atm	-43.0	11.992	172.5	188.0
11	26	XL-ETFE	1 atm	-42.2	12.553	199.0	215.5
12	26	TKT	1 atm	21.4	10.314	200.9	216.5
13	26	TKT	Vacuum	69.0	4.580	199.8	203.1
14	26	TKT	Vacuum	78.5	4.427	197.7	200.6
15	26	TKT	Vacuum	-48.1	5.226	198.0	200.6
16	20	TKT	1 atm	-48.9	28.958	196.7	214.7
17	20	TKT	1 atm	68.2	20.989	198.4	197.4
18	20	TKT	Vacuum	78.6	11.445	199.3	191.9
19	20	TKT	Vacuum	20.4	12.683	198.2	189.6
20	20	XL-ETFE	Vacuum	-49.5	14.034	199.7	199.9
21	20	XL-ETFE	Vacuum	-49.9	4.995	4.0	3.7
22	20	XL-ETFE	Vacuum	-50.2	7.968	66.8	65.7
23	20	XL-ETFE	Vacuum	-50.0	10.976	134.0	132.8
24	20	XL-ETFE	Vacuum	-49.4	14.050	200.7	200.3
25	20	XL-ETFE	1 atm	20.3	7.984	39.3	39.4
26	20	XL-ETFE	1 atm	20.5	13.990	75.2	76.7
27	20	XL-ETFE	1 atm	21.0	19.984	132.6	136.9
28	20	XL-ETFE	1 atm	21.7	25.203	203.3	210.7
29	20	XL-ETFE	Vacuum	68.7	4.987	95.2	94.3
30	20	XL-ETFE	Vacuum	68.8	7.984	132.5	130.9
31	20	XL-ETFE	Vacuum	78.7	11.978	201.2	199.6
32	22	XL-ETFE	Vacuum	22.4	9.700	200.6	200.6
33	22	XL-ETFE	Vacuum	40.2	9.438	200.1	199.8
34	22	XL-ETFE	1 atm	66.6	8.987	108.4	107.8
35	22	XL-ETFE	1 atm	72.5	11.986	145.7	145.1
36	22	XL-ETFE	1 atm	80.3	15.291	200.2	199.0

Run Identifier	AWG	Insulation	Pressure	Average Shroud Temp (°C)	Current (A)	Conductor $T_{measured}$ (°C)	Conductor $T_{predicted}$ (°C)
37	22	XL-ETFE	1 atm	40.4	17.595	200.1	201.1
38	22	XL-ETFE	Vacuum	59.2	5.471	118.1	117.2
39	22	XL-ETFE	Vacuum	59.8	9.260	203.9	203.2
40	22	XL-ETFE	1 atm	22.2	7.984	54.6	54.6
41	22	XL-ETFE	1 atm	22.5	11.978	93.9	94.6
42	22	XL-ETFE	1 atm	22.9	15.384	142.2	143.9
43	22	XL-ETFE	1 atm	22.5	18.539	199.8	202.7
44	22	XL-ETFE	Vacuum	78.6	4.987	123.7	122.9
45	22	XL-ETFE	Vacuum	78.6	6.991	161.9	160.9
46	22	XL-ETFE	Vacuum	78.8	8.784	201.6	200.7
47	22	XL-ETFE	1 atm	58.9	9.981	110.5	109.5
48	22	XL-ETFE	1 atm	59.8	16.556	200.9	200.5

A comparison of the predicted conductor temperature vs. the test measured conductor temperature is presented in Figure 7.5.2-3. Note the dashed line in this figure represents a 1:1 line showing the correlation between the measured and predicted conductor temperatures.

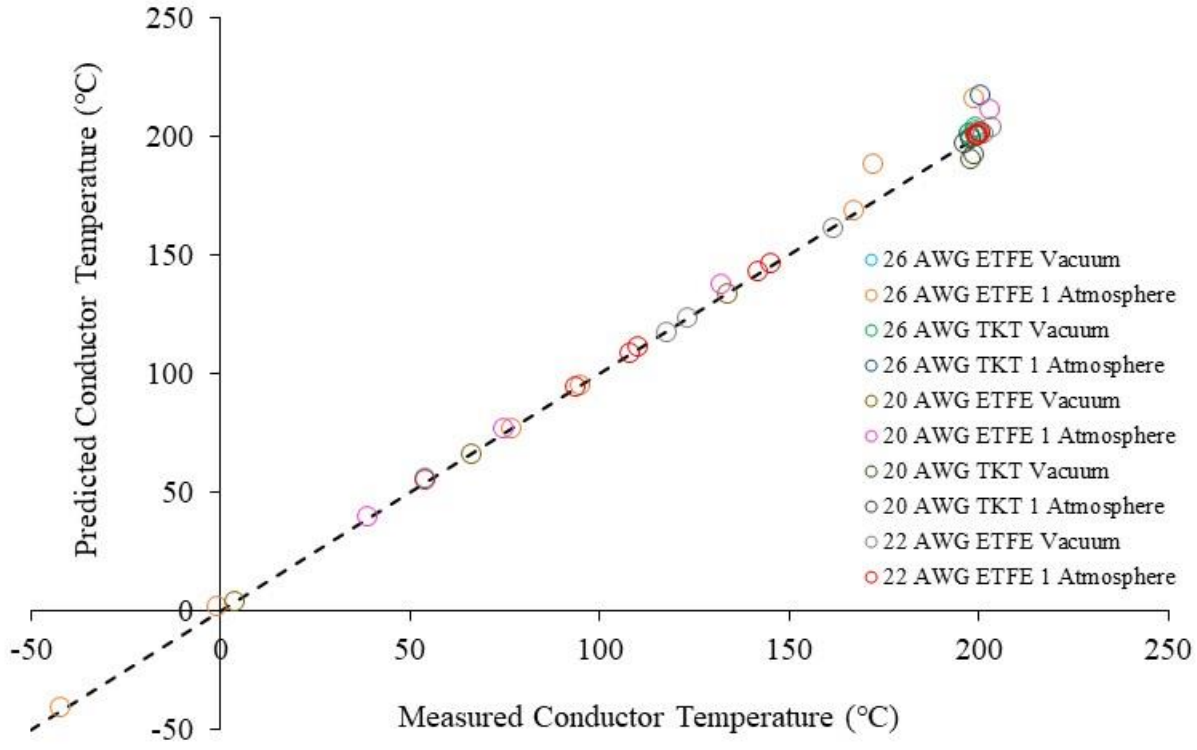

Figure 7.5.2-3. Single Wire Analysis Results Summary

Given that a single transmissivity value was used across all wire sizes and types tested, the correlation between the model and the test data was generally good. Temperature differences between predicted and measured conductor temperatures are summarized in Figure 7.5.2-4. In most cases, steady state temperature differences were <5℃. The figure shows increasing variance by $T_{measured}$. Because of the limited amount of TKT data (red points), it appears there is more variability in $T_{measured}$. However, this is likely because TKT data analyzed represents only the high-temperature (i.e., most-variable) cases. A regression analysis using the thermal model output to predict the temperature measured in test showed that the average difference was inconsequential: the regression line's slope was not significantly different from 1, meaning the 1:1 line shown in Figure 7.5.2-3 is a good description of the comparison.

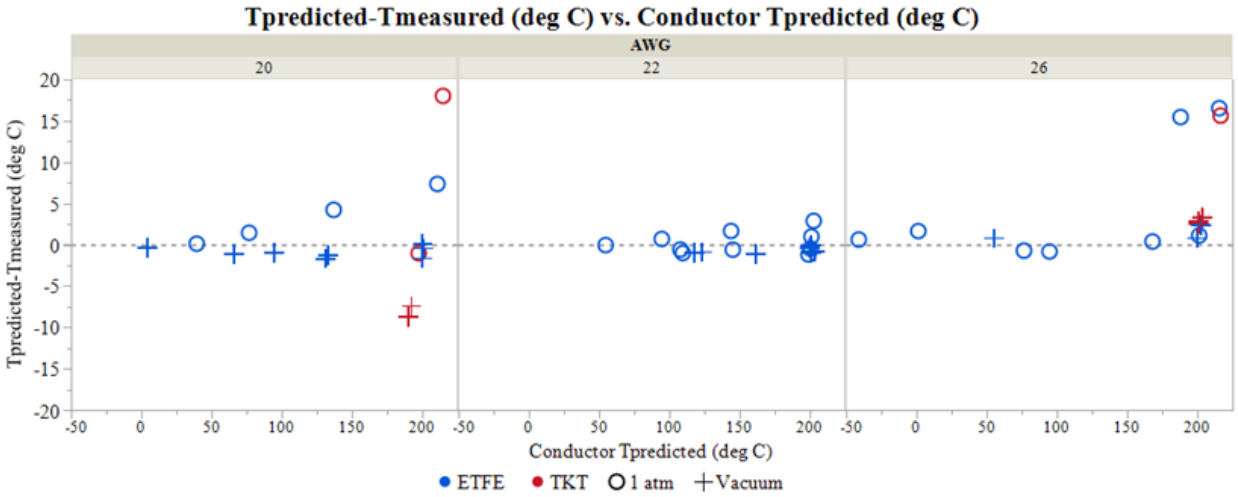

Figure 7.5.2-4. Steady State $T_{predicted} - T_{measured}$ for Single Wire Analysis

It is also useful to compare the test measured delta temperature (i.e., conductor temperature minus environment temperature), and the model predicted delta temperature as is shown in Figure 7.5.2-5. Again, in this figure the 1:1 line is a measure of correlation between the test and model prediction.

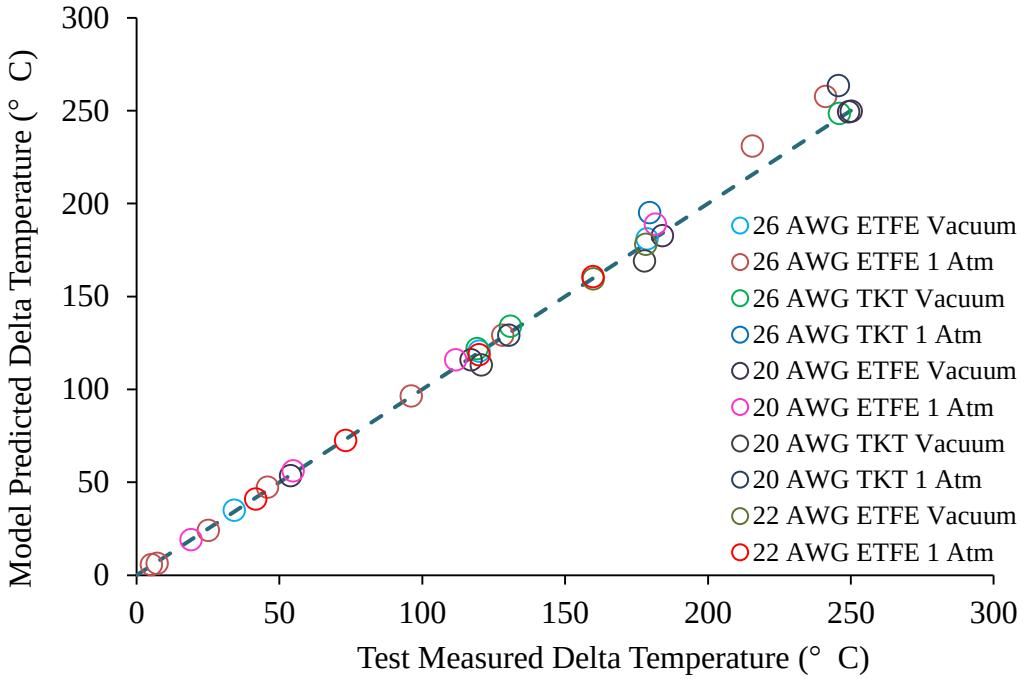

Figure 7.5.2-5. Comparison of Test Measured and Model Predicted Steady State Delta-Temperatures for the Single Conductor Wire Test Articles

7.5.2.1 Single Wire Monte Carlo Thermal Analysis

The previous analysis was performed with known or measured values for many of the analysis parameters. However, if a model is to be useful as a predictive tool, then it must be able to give insight into how conductor temperatures are affected if there is some variability to the key parameters.

The output distribution was meant to describe how a wire would respond, so the input distributions were designed to mimic production quality. Unfortunately, the team was not privy to quality data, so information regarding distributional form was lacking.

Nevertheless, some usable information was available. Wire specifications state an allowable maximum and minimum radius for the conductor and the insulation jacket. As a result, a wire procurement may result in wire delivered with conductor and insulation jacket radii anywhere within the specification range. Triangular distributions were chosen for r_c and r_s.

This demonstration assumed a single 22 AWG, XL-ETFE-jacketed conductor. The NESC team experiences were that wire diameters are generally manufactured to the low end of the specification to reduce materials cost and reduce the overall weight of the wire. However, the NESC team did not want to conclude that no wires would be produced at the high end of the specification, so while the distribution's peak (i.e., mode) should be lower than specification center, it should reach the upper and lower thickness limits.

A triangular distribution is a simple method for mimicking a distribution with an off-center mode (i.e., skew). This distribution is adequate if the data form (e.g., normal or Weibull) cannot be easily decided on, but a uniform (i.e., equal probability at any point within a range) is not desirable.

The left-hand distribution in Figure 7.5.2.1-1 illustrates the right skewed (i.e., heavy right tail, mode canted to the left) triangular r_c distribution assumed. The right-hand distribution shows the left skew for the r_s assumption employed in the Monte Carlo analysis. Its parameters are presented in Table 7.5.2.1-1.

The remaining analysis parameters are taken for Test Article 8 (Table 7.5.2-2) and Run Identifier 48 (Table 7.5.2-3) except for the conductor and insulation jacket radii.

Table 7.5.2.1-1. Triangular Distribution Parameters for the Conductor (r_c) and Insulation Jacket (r_s) Radii

Value	r_c (m)	r_s (m)
Min	3.6195e-4	5.2070e-4
Max	3.9878e-4	5.7150e-4
Mode*	3.6830e-4	5.5100e-4

*The as-tested value is assumed to be Mode for the purpose of this demonstration.

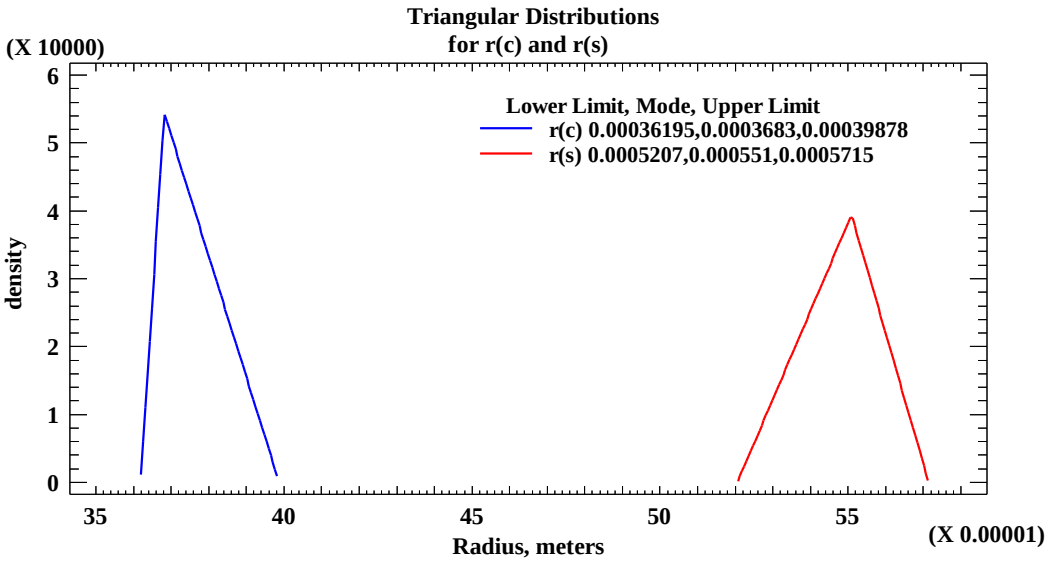

Figure 7.5.2.1-1. Triangular Distribution Shapes for the Conductor (r_c) and Insulation Jacket (r_s) Radii

Two thousand (2000) points, each using two input scenarios, were produced in this way. The output is shown in the histogram in the Figure 7.5.2.1-2. It is not described well by a normal distribution (red trace) because that red trace does not fit the data well, particularly in the tails – it appears to have a right skew. Two thousand runs is usually considered low for determining a distribution; typically, an order of magnitude or two total points are used. However, it was decided the fidelity that would result from this set of runs would be sufficient and useful given this relatively early stage in investigations.

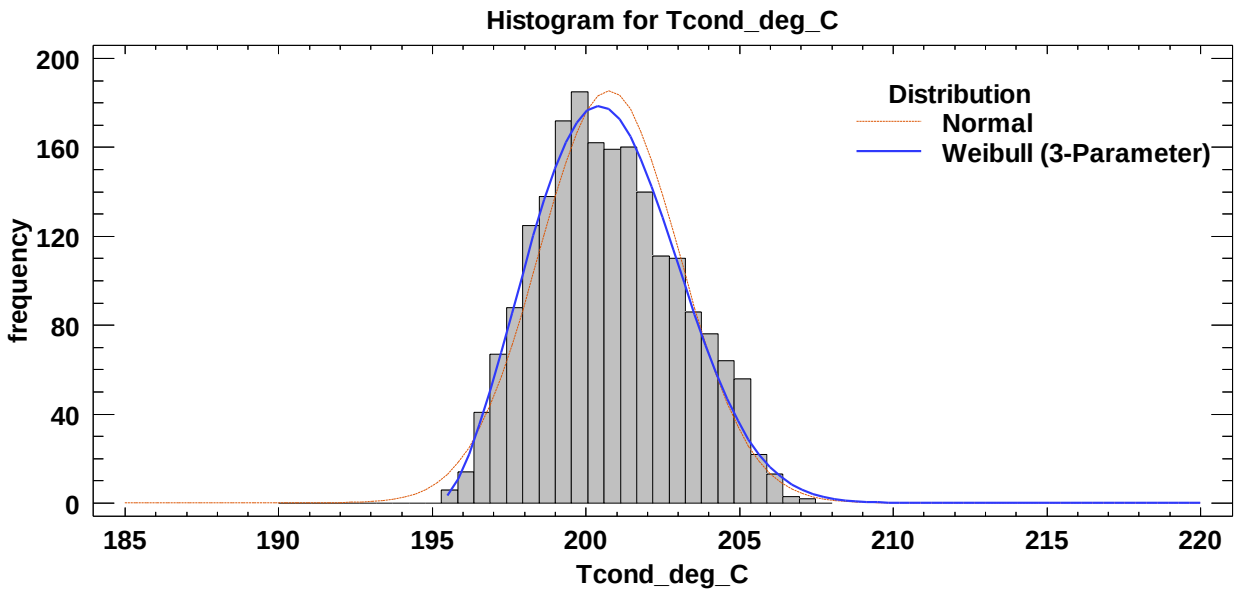

Figure 7.5.2.1-2. Insulation Radius (r_s) and Conductor Radius (r_c) Monte Carlo Model Results

A manual search for an adequate distributional fit was performed using standard Statgraphics® statistical analysis software. Fits to a number of distributions were attempted, and compared graphically and using the Anderson-Darling A^2 fit metric. Using this process on this dataset, a 3-parameter Weibull distribution was found to be an adequate fit. Its parameters were:

- Shape = 2.64984
- Scale = 6.27574
- Lower threshold = location = 195.188℃

The location parameter normally implies there is a lower physical bound below which the temperature cannot fall. Again, this assumption is not necessary. The distribution is meant only to represent the data, and be useful for visualization and further modeling.

Percentiles of this distribution are in Table 7.5.2.1-2.

Table 7.5.2.1-2. Percentiles of the Weibull (2.65, 6.28, and 195.2) Distribution

Lower Tail Area (<=)	*Percentile of the Distribution*	*Value Given the Distribution, °C*
0.01	1st	196.294
0.05	5th	197.234
0.5	50th (Median)	200.654
0.95	95th	204.683
0.99	99th	206.356

It is, perhaps, more informative to explore the variation in other parameters that were not (or could not) be explicitly measured (e.g., insulation jacket thermal conductivity and the convective heat transfer coefficient).

As a demonstration of capability, analysis of output from an additional Monte Carlo simulation run was performed assuming the same triangular distributions for r_s and r_c described above, but also assuming +/-10% variation (normally distributed) for, both, the wire insulation thermal conductivity, k_w and the convective heat transfer coefficient[6], h. The output was again compared to candidate distributions. A lognormal having the following parameters was found to be an adequate fit.

- Mean = 200.813℃
- Standard deviation = 3.95471℃
- Lower threshold = location = 132.914℃

Figure 7.5.2.1-3 depicts the fit of the 3-parameter lognormal against a histogram of the data, with a normal trace to show how it is different. While the disparity is not as apparent, the normal tries to imply there is a higher likelihood of lower temperatures than the Monte Carlo results show, and underestimates the high-temperature tail more than the 3-parameter lognormal does.

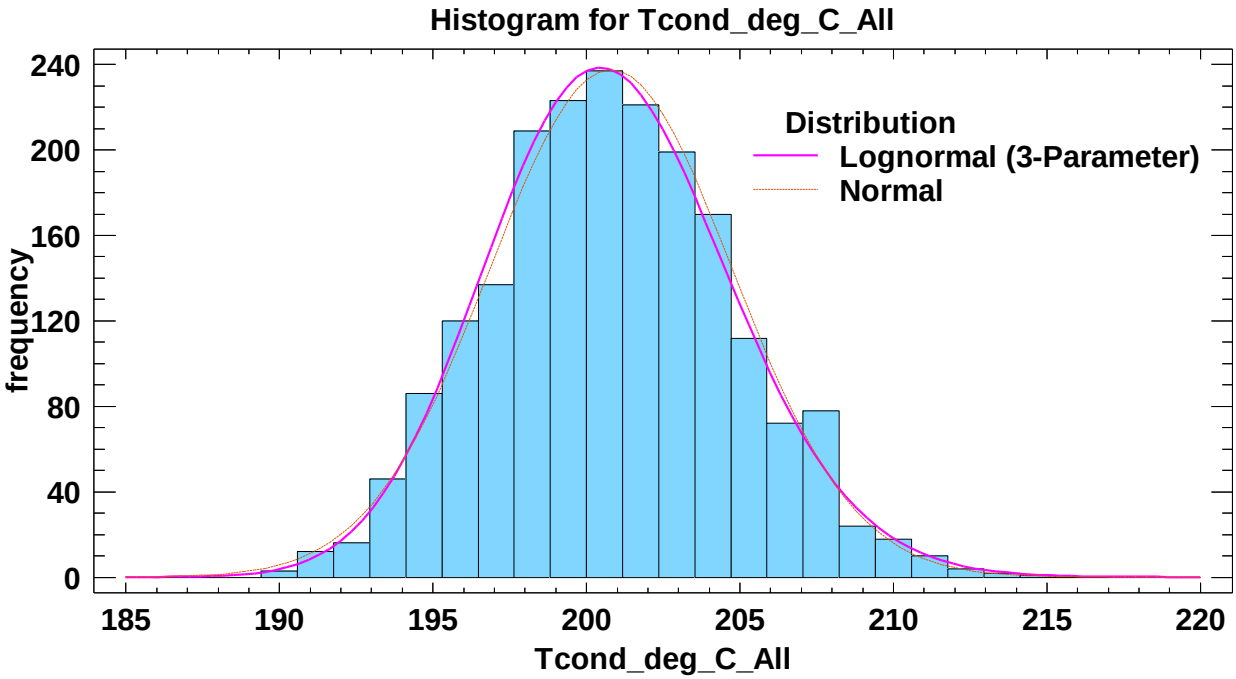

Figure 7.5.2.1-3. Monte Carlo Analysis Results for Varying r_s, r_c, k_w, and h

[6] The h value used was that calculated within the model using the correlation from Reference 11, and adjusted using for the best correlation by the factor, f_h. Adjustment during the Monte Carlo analysis was performed on $f_h h$.

A normal distribution is probably adequate, judging by the Figure 7.5.2.1-3. The lognormal was chosen instead because it is slightly better fitting because it reflects a physical process wherein spread increases with increasing temperature, where the normal may not. This relationship is seen in test data.

Percentile statistics for the lognormal distribution are shown in the Table 7.5.2.1-3.

Table 7.5.2.1-3. Percentiles of the Lognormal (200.8, 3.95, 132.9) Distribution

Lower Tail Area (<=)	*Percentile of the Distribution*	*Value Given the Distribution, °C*
0.01	1st	192.115
0.05	5th	194.510
0.5	50th (Median)	200.698
0.95	95th	207.507
0.99	99th	210.525

The data used to fit these distributions is archived on the assessment SharePoint site as a Microsoft® Excel® file (see Section 10.0).

This analysis suggests the range of possible solutions and the sensitivity to uncertainty in analysis parameters may be explored using Monte Carlo analysis. Once predictions for the nominal case are performed, Monte Carlo analysis may be used to determine how much additional margin should be applied to account for unknowns.

7.5.2.2 Wire Bundle Thermal Model

Modeling of the wire bundles was accomplished using the Complex Wire Bundle Thermal Model Builder (CWBTMB) developed during the previous assessment [ref. 1]. The model builder is a Microsoft® Excel® spreadsheet that provides users a means of inputting key model parameters. Once entered, Microsoft® Visual Basic for Applications (VBA) scripts are executed and the user inputs are transformed into a thermal network model in the Systems Improved Numerical Differencing Analyzer/Fluid Integrator (SINDA/FLUINT, a.k.a., SINDA) format. The CWBTMB was updated during this study to improve the convective heat transfer correlation, extend the air database properties and correct some other shortcomings. Some modification to the SINDA input deck was performed to allow rapid reconfiguration of the model for different currents, environmental temperatures and vacuum/atm cases.

A schematic representation of a segment of a typical bundle thermal network model is presented in Figure 7.5.2.2-1.

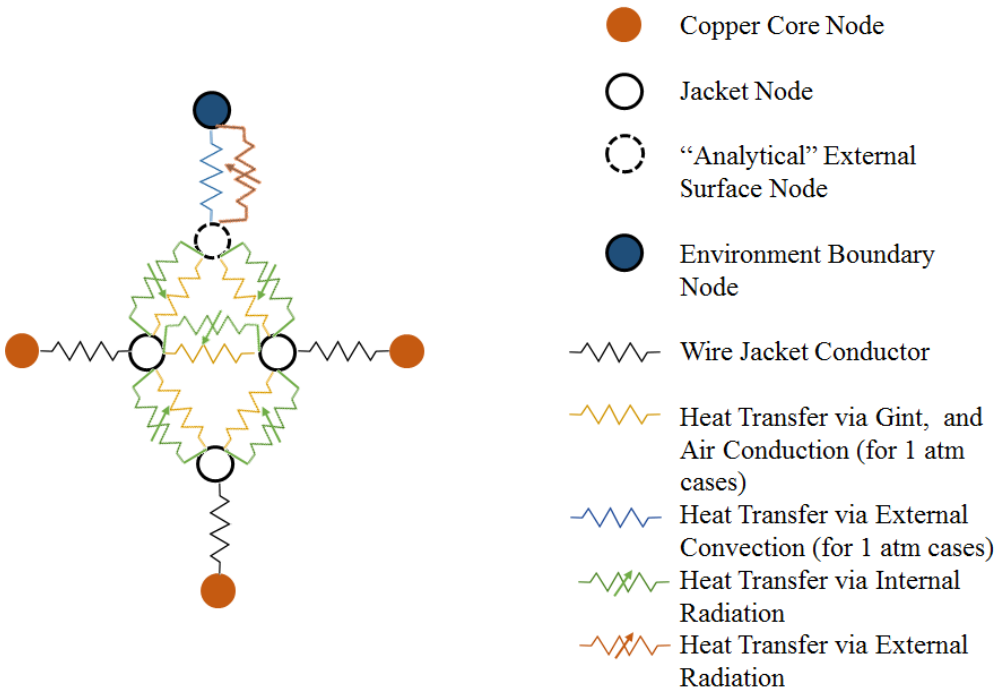

Figure 7.5.2.2-1. Representative Segment of Wire Bundle Thermal Network

This pathfinder study considered bundle sizes consisting of 32 conductors using two wire sizes and two wire insulation types. These are described in Table 7.5.2.2-1 along with parameters used in the model.

Table 7.5.2.2-1. 32 Conductor Wire Bundle Thermal Model Parameters

Test Article	AWG	Insulation Material	k_w $(W/m \cdot ℃)$	R_{L0} (Ω/m)	α $(1/℃)$	ε	f_h	$2r_s$ (mm)	$2r_c$ (mm)	Bundle Diameter (mm)
2	26	XL-ETFE	0.2380	0.1298	0.00363	0.9	0.96	0.803	0.4572	5.330
5	20	TKT	0.1921	0.0327	0.00359	0.9	0.96	1.263	0.9373	8.119
6	26	TKT	0.1904	0.1651	0.00282	0.9	0.96	0.822	0.4674	5.096
8	20	XL-ETFE	0.2380	0.0326	0.00363	0.9	0.96	1.278	0.9398	8.035

Note: Wire insulation transmissivity was not incorporated into the CWBTMB. However, the effective coupling to adjacent wire insulation is represented in G_{int} value. Determination of G_{int} is discussed in detail in the paragraphs below.

Analysis runs were performed for each wire bundle configuration for cases corresponding to steady state temperature data points obtained during testing. Steady state was assumed for testing using the second-to-last time point at each test condition to allow for temperature stabilization. The environment temperature used assumed a mathematical average of all test measured shroud temperatures.

Separate model correlations were performed for the vacuum and 1 atm cases as each was expected to have a different wire insulation-to-wire insulation thermal contact conductance due to the absence/presence of air.

For the vacuum cases, the correlation parameter assumed was the wire insulation-to-wire insulation interface conductance. For the 1 atm cases, the calculated external bundle convective heat transfer coefficient was scaled (using the f_h parameter) by 96% (i.e., 0.96) of the calculated value to produce the best correlation and held constant across all bundle correlation cases for 1 atm. This was true even for different wire insulation and wire sizes and was done to reduce the correlation effort to a single parameter, again, the wire insulation-to-wire insulation thermal contact conductance.

Correlation was first performed on the 20 AWG XL-ETFE bundle with 32 conductors as it provided numerous vacuum and 1 atm cases across a variety of steady state temperatures. For each run, the average of the test measured bundle inner conductor and outer surface temperatures was used to establish a best-fit thermal contact conductance by trial and error. When aggregated across all 1 atm cases for the 20 AWG XL-ETFE bundle test article, the contact conductance per unit length vs. bundle average temperature curve shown in Figure 7.5.2.2-2 was established. For vacuum cases, a constant value of $G_{int} = 0.285\ W/m \cdot ℃$ across all temperatures resulted in good correlation for all wire sizes, environment temperature conditions, and currents.

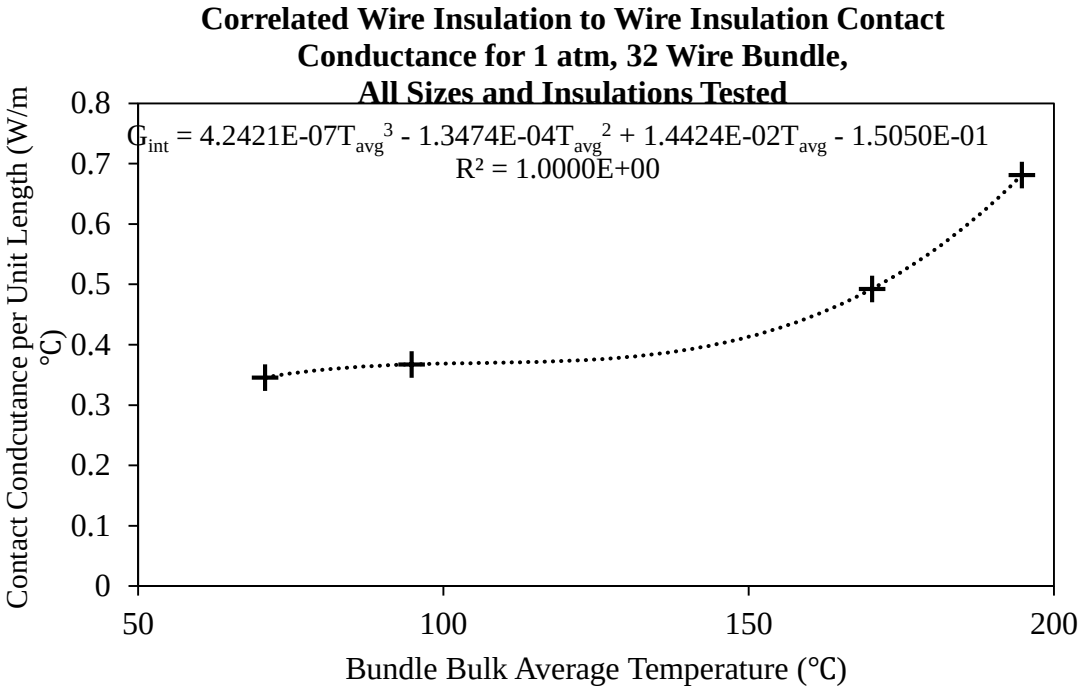

Figure 7.5.2.2-2. Correlated Wire Insulation-to-Wire Insulation Conductance

Subsequently, the convection-scaling factor and the contact conductance array were used across all subsequent bundle thermal analyses to determine the predictive power of the correlation in a "hands off" mode. A comparison between tests measured and predicted central conductor temperatures across all wire bundle test articles is presented in Table 7.5.2.2-2.

Table 7.5.2.2-2. 32 Conductor Element Wire Bundle Thermal Model Analysis Correlation Results[7]

Run Identifier	AWG	Insulation	Pressure	Average Shroud Temp (°C)	Current (A)	Central Conductor $T_{measured}$ (°C)	Central Conductor $T_{predicted}$ (°C)
1	26	XL-ETFE	Vacuum	69.9	1.972	197.3	198.3
2	26	XL-ETFE	Vacuum	73.0	1.488	156.3	149.2
3	26	XL-ETFE	Vacuum	71.7	1.701	164.0	169.6
4	26	XL-ETFE	Vacuum	77.9	1.794	182.8	183.1
5	26	XL-ETFE	Vacuum	79.5	1.896	194.2	195.0
6	26	XL-ETFE	Vacuum	-50.5	1.002	19.6	21.5
7	26	XL-ETFE	Vacuum	-47.0	2.294	199.4	202.4
8	26	XL-ETFE	1 atm	22.8	1.998	88.1	86.3
9	26	XL-ETFE	1 atm	19.3	3.307	196.5	187.1
10	20	TKT	Vacuum	-43.8	5.259	199.9	188.0
11	20	TKT	1 atm	24.3	7.638	200.6	191.9
12	20	TKT	Vacuum	70.2	4.453	198.1	185.5
13	26	TKT	Vacuum	21.2	2.014	200.6	207.4
14	26	TKT	1 atm	69.1	2.703	200.0	197.7
15	26	TKT	1 atm	-44.7	3.621	199.6	201.3
16	20	XL-ETFE	1 atm	66.9	0.995	70.9	70.5
17	20	XL-ETFE	1 atm	67.5	2.991	95.9	96.1
18	20	XL-ETFE	1 atm	69.5	5.990	175.9	175.2
19	20	XL-ETFE	1 atm	70.3	6.864	202.6	202.3
20	20	XL-ETFE	Vacuum	20.0	0.994	28.3	28.4
21	20	XL-ETFE	Vacuum	20.3	1.997	52.7	53.1
22	20	XL-ETFE	Vacuum	20.8	3.492	115.3	114.0
23	20	XL-ETFE	Vacuum	21.8	4.886	187.9	188.4
24	20	XL-ETFE	Vacuum	22.1	5.182	205.9	205.8
25	20	XL-ETFE	1 atm	-47.0	2.991	-20.2	-20.8
26	20	XL-ETFE	1 atm	-42.2	6.992	104.0	110.9
27	20	XL-ETFE	1 atm	-37.1	8.794	202.9	198.1

A comparison of the predicted central conductor temperature vs. the test measured central conductor temperature is presented in Figure 7.5.2.2-3. Again, the 1:1 line indicates an ideal correlation between the measured and predicted central conductor temperature.

[7] For the 26 AWG XL-ETFE bundle, the temperature measured on a wire on the external surface of the bundle was warmer than the centrally located conductor suggesting a shift in wire positions and could have been due to the placement of the bundle within the test apparatus. This was not observed during subsequent bundle tests. These data were retained as part of the overall test data and, in the end, compared well with the correlation parameters established for the other wire bundles.

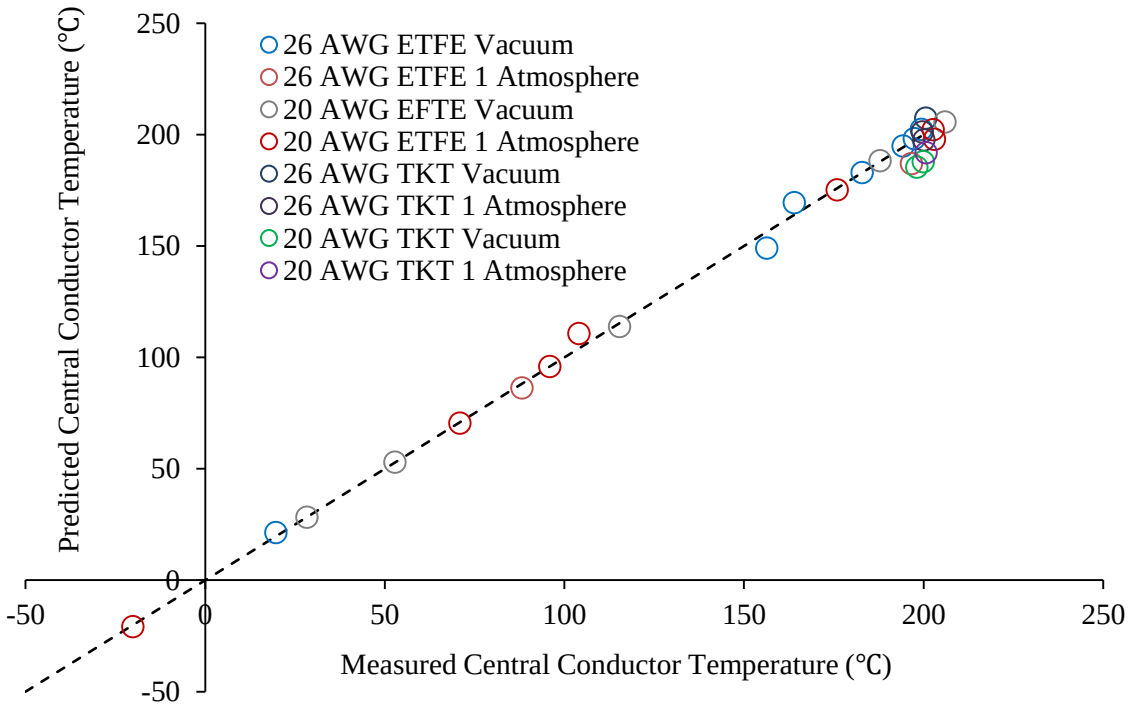

Figure 7.5.2.2-3. Comparison of Measured vs. Predicted Central Conductor Temperature for 32 Conductor Bundle, All Cases

Temperature differences between predicted and measured conductor temperatures are summarized in Figure 7.5.2.2-4. In most cases, steady state temperature differences were < 5°C. While only 6 of the 27 observations in this dataset were from bundles having TKT insulation, 4 of the 8 cases with prediction error > 5°C were TKT-insulation bundles. Again, this is likely due to only having TKT steady state data for high wire temperature observations. This is likely explained by the application of the G_{int} array (for the 1 atm case), or the single value (for the vacuum cases) derived for XL-ETFE bundle correlation to the TKT cases. This was a deliberate attempt to see whether these correlation parameters could successfully be used to correlate across all cases. If TKT-insulated wire is to be widely used, then it may be useful to establish a separate correlation for TKT. However, adding insulation-specific parameters may diminish the usefulness of a generic analysis approach.

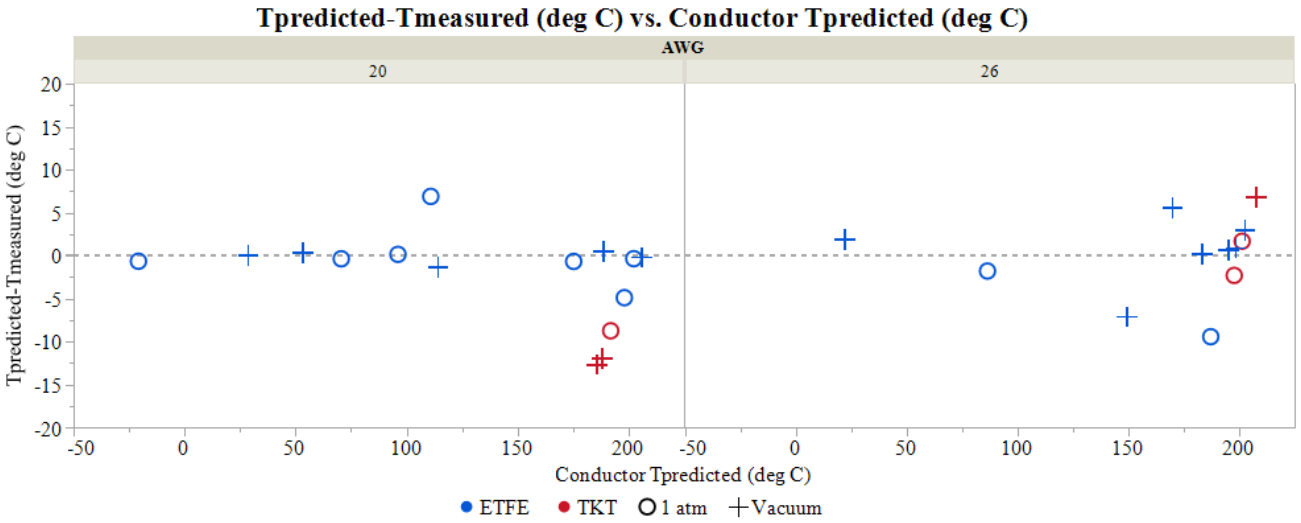

Figure 7.5.2.2-4. Central Conductor Steady State $T_{predicted} - T_{measured}$ for Wire Bundle Analysis

A comparison of the test measured delta temperature and the model predicted delta temperature for the 32 wire bundle configurations is presented in Figure 7.5.2.2-5. The 1:1 line represents ideal correlation between the model predicted and measured temperature delta. Regression modeling of the relationship determined that the 1:1 line does a good job of showing that, on average, the model output predicts the measured test data.

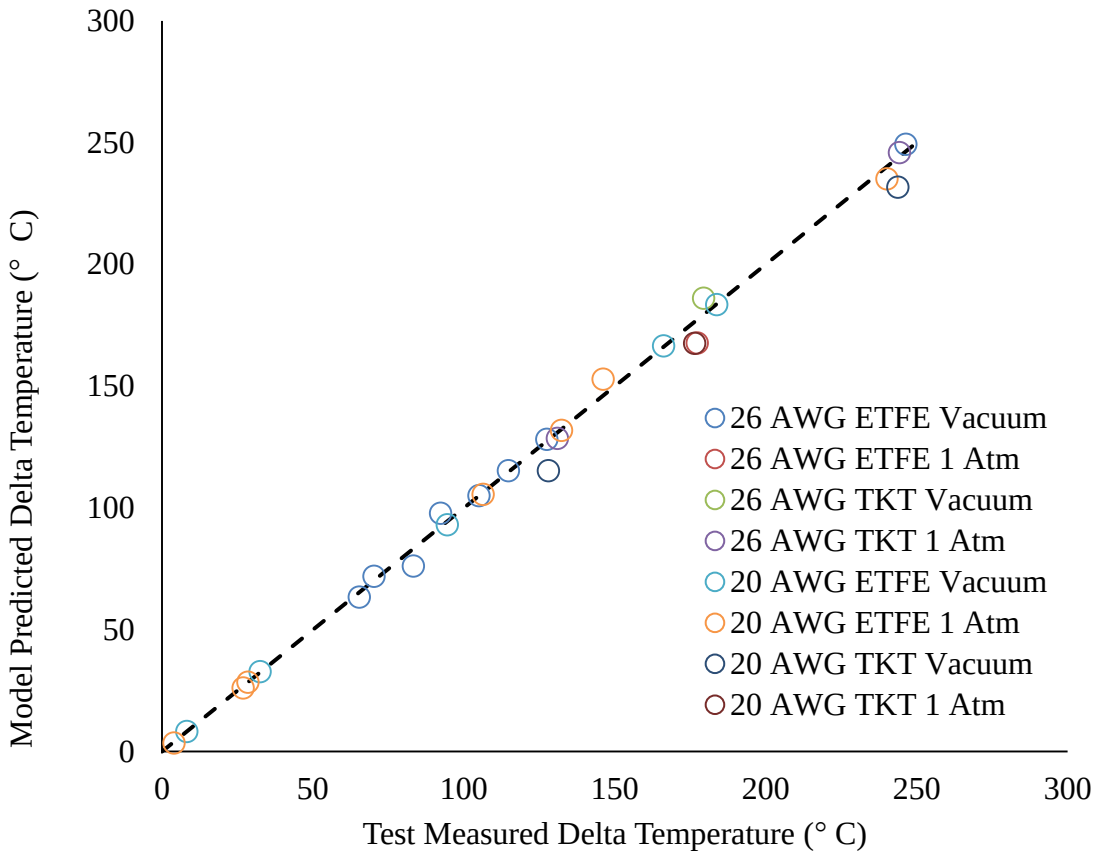

Figure 7.5.2.2-5. Comparison of Test Measured and Model Predicted Steady State Delta-Temperatures for the 32 Wire Bundle Test Articles

It is important to note some key differences when comparing the results obtained from the current investigation to those obtained from the previous assessment.

a. In the current assessment, a single value for the wire insulation-to-wire insulation contact conductance per unit length ($G_{int} = 0.285\ W/m \cdot ℃$) was sufficient to correlate all four wire bundles for the vacuum case. For the previous assessment, the contact conductance, per unit length started close to this value at lower temperatures ($G_{int} = 0.248\ W/m \cdot ℃$), but higher values were required at the higher temperatures ($G_{int} = 3.669\ W/m \cdot ℃$). It is not fully understood why there is this difference between the current and previous work. However, it should be noted the previous assessment used a wire bundle comprised mostly of 22 AWG XL-ETFE insulation wire with some 20 AWG XL-ETFE insulation wire. Additionally, the wire bundle used in the previous assessment was comprised of 105 multi-wired and insulation cables, which included triplets, quads, and twisted pairs. Furthermore, only a small number of correlation test points were obtained. The use of triplets, quads, and twisted pairs may have contributed to a temperature sensitivity in the interface conductance. Additionally, restraint on the bundle may have been different from that used for the current work. It has been hypothesized thermal expansion of the XL-ETFE may have increased the contact between adjacent wire insulations resulting in increased contact conductance [ref. 17].

b. The contact conductance per unit length varied with temperature for the 1 atm cases, but the magnitude of variation was considerably different from that observed during the previous assessment. Whereas the bundle bulk average temperature reached a maximum value of approximately $G_{int} = 0.7\ W/m \cdot ℃$ at 200℃ for bundles tested during this assessment, the maximum value required at a bundle bulk average temperature of 200℃ during the previous assessment was $G_{int} = 3.669\ W/m \cdot ℃$. Again, factors such as bundle size, restraint and use of twisted pairs, triplets and quads within the bundle may complicate bundle-to-bundle comparisons.

The difference in results obtained during this assessment compared to those obtained during the previous work raise serious questions about the characterization and repeatability of what is, arguably, the most critical correlation parameter, G_{int}. The results from the current work suggests that suitable correlations are found for the four bundles tested using consistent values or arrays for G_{int} and a consistent f_h across all pertinent cases where convection is present. Since these configurations did not contain twisted pairs, triplets, and quad wire components, it can only be concluded the results obtained are valid for the cases tested (without twisted pairs, triplets and quad constituents). Additional testing is warranted to see whether the G_{int} and f_h values apply to different bundle sizes. If the correlation is extensible to different bundle sizes, then, a model based approach to wire bundle derating is likely possible.

7.5.3 Response Surface (Linear Regression) Modeling

This section describes how the test data was brought from a dataset supplied by an SME team through engineering statistical analysis and a model due to an earlier similar investigation.

The values reported for the regression models here are expected (i.e., median) values, not a lower worst case bound. The AS50881 current rating curves of a wire in free air [ref. 4, Figure 3] are intended to be worst cases and conservative.

In Figure 3 in Reference 4, the figure plots applied current by multiple wire sizes against the resulting temperature rise of the wire minus the ambient temperature of the wire values represent expected values or lower bounds.

7.5.3.1 General Comments on Regression and Response Surfaces

Linear regression, which will subsequently be identified as regression, modeling is an engineering statistical tool commonly used in approximating the relationship between inputs, known in statistical literature as factors, predictors or regressors, and responses based on data. The methods are well-studied and well-known for a large number of applications [ref. 18]. The techniques required here were moderately advanced, but required no novel analysis methods.

The general form of a regression model relating two inputs x_1 and x_2 to a response variable y looks like the following Eq. 11.

$$E(y) = \beta_0 + \beta_1 x_1 + \beta_2 x_2 + \beta_{11} x_1^2 + \beta_{22} x_2^2 + \beta_{12} x_1 x_2 \qquad \text{Eq. 11}$$

This form shows the equation of a $y = mx + b$ equation of a line. In fact, $E(y)$, is simply the expected or predicted value of y, β_0 might be thought of as analogous to y-intercept b, x_1 is an input variable similar to x in the simple equation and the coefficient β_1 is thus similar to slope m. x_2 is an additional regressor variable. There can be any number of these, each with their own β

coefficients. Interactions, such as x_1x_2, allow for complexities in the relationship between the x's and y's.

When graphed, the regression model $(y) = \beta_1 x_1 + \beta_0$returns a line. Adding another input x_2 results in a plane, and so on. Adding quadratic terms such as x_1^2 result in curvature in the line or plane. Since a curved surface is not strictly a plane, it is then commonly called a *response surface*. A response surface relating two factors to a response is shown in Figure 7.5.3.1-1.

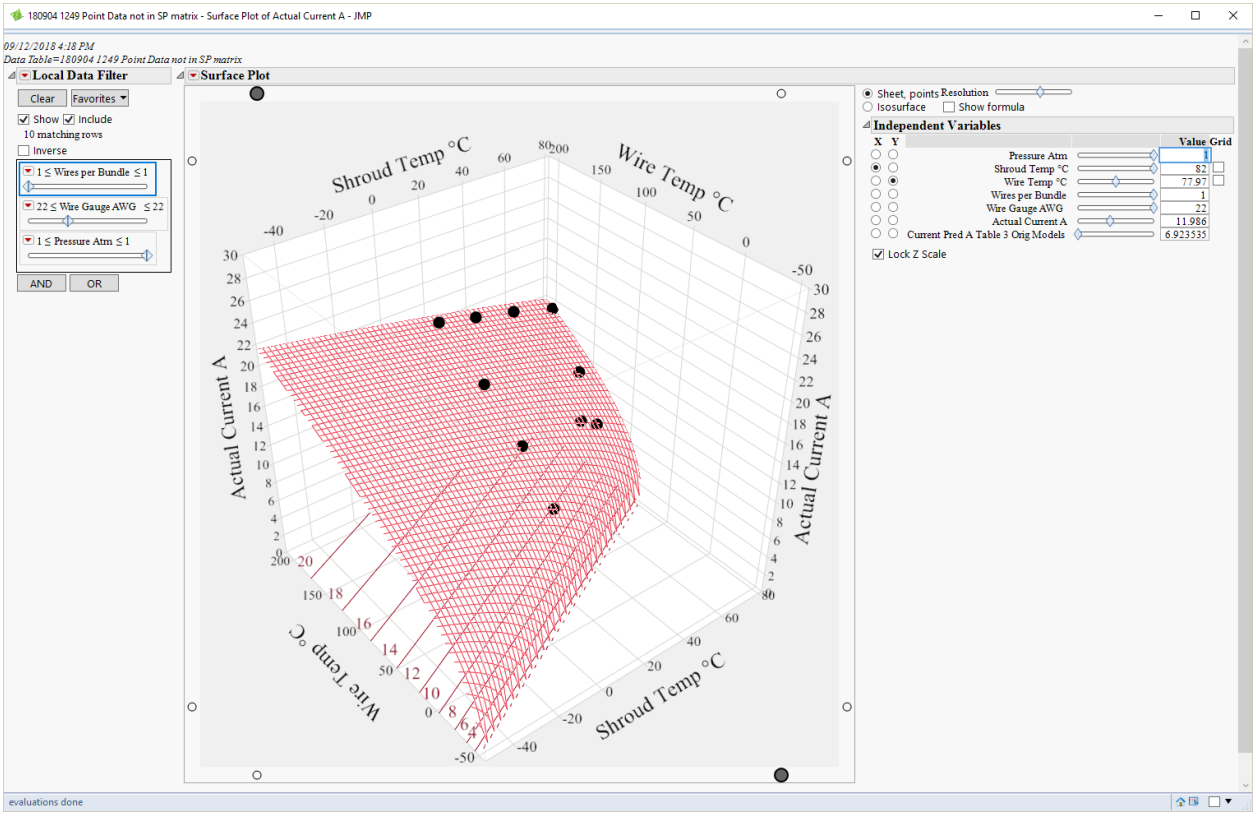

Figure 7.5.3.1-1. Example plot of the response surface generated by the AS50881 wire current rating curves [ref. 4, Figure 3] model for a single 26 AWG wire at 1 atm along with the steady-state data from test at this set of conditions.

It is important to note that Eq. 11 looks similar to a Taylor series decomposition of a complex function. It is not likely the mathematics of the true physical relationship take this form exactly, but that is not a regression model's function. A regression model works to trace the features of the physical relationship between regressors and responses. A good-fitting model is one that adequately traces the physics well enough that input parameter values $x$can be exercised in the model to return an expected $y$response of sufficient fidelity to the physical process for the purpose at hand. It should be noted that while the physics may not be strictly spelled out in the model, that model could nevertheless be studied to interpret how responses respond to inputs. Feeding values through the equation, running mathematical processes such as taking partial derivatives to find maxima, inflection regions etc., or simply examining the equation itself can be useful strategies to this end.

7.5.3.2 The Data

Data was reduced and collated by an SME team and this was put into analyzable form in a Microsoft® Excel® table. Only data from XL-ETFE-insulated wire was used in this analysis because insufficient steady state data was available for TKT trials to form a response surface model. Reference 4, Figure 3 predictions using the original equations in Table 7.5.3.2-1 are given for reference. The equations are valid only for single wires at 1 atm so predictions are made in the rightmost column for applicable cases.

Table 7.5.3.2-1. Reduced XL-ETFE Data used in Analysis with Predictions due to Existing Models

t	Group	Wires per Bundle	Wire Gauge AWG	Pressure atm	Shroud Temp °C	Wire Temp °C	Measured Current A	*50881 Figure 3 Predicted Current A*
1	1	1	20	0	-49.4752	199.703	**14.034**	
2	1	1	20	0	-49.9000	4.017	**4.995**	
3	1	1	20	0	-50.2315	66.760	**7.968**	
4	1	1	20	0	-50.0282	134.002	**10.976**	
5	1	1	20	0	-49.4397	200.679	**14.050**	
6	1	1	20	0	68.6884	95.236	**4.987**	
7	1	1	20	0	68.8094	132.497	**7.984**	
8	1	1	20	0	78.7096	201.172	**11.978**	
9	2	32	20	0	20.0372	28.257	**0.994**	
10	2	32	20	0	20.2544	52.737	**1.997**	
11	2	32	20	0	20.8096	115.276	**3.492**	
12	2	32	20	0	21.7812	187.871	**4.886**	
13	2	32	20	0	22.1441	205.902	**5.182**	
14	3	1	22	0	22.3724	200.567	**9.700**	
15	3	1	22	0	40.1773	200.056	**9.438**	
16	3	1	22	0	59.1714	118.102	**5.471**	
17	3	1	22	0	59.8249	203.937	**9.260**	
18	3	1	22	0	78.5551	123.706	**4.987**	
19	3	1	22	0	78.5991	161.926	**6.991**	
20	3	1	22	0	78.7747	201.588	**8.784**	
21	4	1	26	0	20.1687	54.338	**1.998**	
22	4	1	26	0	20.9397	199.558	**5.251**	
23	4	1	26	0	78.6513	198.453	**4.692**	
24	5	32	26	0	69.9477	197.327	**1.972**	
25	5	32	26	0	72.9897	156.267	**1.488**	
26	5	32	26	0	71.7448	163.964	**1.701**	
27	5	32	26	0	77.8756	182.826	**1.794**	
28	5	32	26	0	79.5135	194.226	**1.896**	
29	5	32	26	0	-50.5251	19.643	**1.002**	
30	5	32	26	0	-47.0225	199.354	**2.294**	
31	6	1	20	1	20.2599	39.253	**7.984**	*8.50*
32	6	1	20	1	20.4578	75.233	**13.990**	*13.87*
33	6	1	20	1	20.9820	132.646	**19.984**	*19.29*
34	6	1	20	1	21.7461	203.316	**25.203**	*24.15*
35	7	32	20	1	66.9325	70.885	**0.995**	
36	7	32	20	1	67.5033	95.910	**2.991**	
37	7	32	20	1	69.5344	175.886	**5.990**	
38	7	32	20	1	70.3340	202.639	**6.864**	
39	7	32	20	1	-46.9777	-20.183	**2.991**	

t	Group	Wires per Bundle	Wire Gauge AWG	Pressure atm	Shroud Temp °C	Wire Temp °C	Measured Current A	*50881 Figure 3 Predicted Current A*
40	7	32	20	1	-42.1670	103.960	**6.992**	
41	7	32	20	1	-37.1332	202.938	**8.794**	
42	8	1	22	1	66.6459	108.360	**8.987**	*9.29*
43	8	1	22	1	72.5057	145.670	**11.986**	*12.00*
44	8	1	22	1	80.2792	200.157	**15.291**	*15.03*
45	8	1	22	1	40.3911	200.088	**17.595**	*17.12*
46	8	1	22	1	22.2329	54.618	**7.984**	*8.28*
47	8	1	22	1	22.5054	93.884	**11.978**	*11.87*
48	8	1	22	1	22.8602	142.212	**15.384**	*15.00*
49	8	1	22	1	22.4766	199.789	**18.539**	*17.96*
50	8	1	22	1	58.9452	110.476	**9.981**	*10.23*
51	8	1	22	1	59.8448	200.936	**16.556**	*16.18*
52	9	1	26	1	69.9913	77.188	**2.006**	*2.41*
53	9	1	26	1	70.4589	95.500	**3.994**	*4.24*
54	9	1	26	1	71.4433	167.585	**8.005**	*7.79*
55	9	1	26	1	71.9153	200.064	**9.205**	*8.87*
56	9	1	26	1	-46.8624	-41.748	**1.997**	*2.07*
57	9	1	26	1	-46.1391	-0.373	**6.000**	*5.57*
58	9	1	26	1	-42.9589	172.530	**11.992**	*11.22*
59	9	1	26	1	-42.2444	198.957	**12.553**	*11.81*
60	10	32	26	1	22.8153	88.113	**1.998**	
61	10	32	26	1	19.3081	196.531	**3.307**	

Column *t* is a row reference. *Group* refers to a set of changes of the factors WPB, AWG, and Pressure. These were examined as "hard-to-change factors", which are those where a large amount of effort (e.g., time, money, etc.) is needed to change. The number of changes to these factors is reduced to meet cost or schedule constraints. Keeping an accounting of this reduced change schedule is necessary because these factors were held constant while the easy-to-change temperature factors were varied, so there are fewer "samples" for the hard-to-change variables than for the easy-to-change ones, thus less information available to determine whether those variables are significant or not. This information on when factors are changed was used as an input for a split-plot analysis mentioned in Section 7.4. Note the split-plot assumptions are not strictly correct, but were deemed sufficient for this first phase.

WPB and AWG were clearly in the hard-to-change category. In fact, for each combination of WPB and AWG, only one test article was used. Other sources of variation with unknown impact such as differences due to wire lot, manufacturer, diameter of conductor, insulation thickness, wire test article construction and other factors were thus not represented in this data and model and no uncertainty information regarding them was estimated. The next wire bundle will include different values of these unstudied factors. Conclusions regarding any other wire bundle must be made with this in mind.

Atmospheric pressure also was not changed as often as temperature, so was considered a hard-to-change factor.

Temperatures and currents were recorded at nonzero currents at what were judged steady state conditions by an SME team. Steady state conditions at low and intermediate wire temperatures

were not achieved as often as those at high temperatures were, so the data is skewed in that direction. Regression models thus may not represent low currents and wire temperatures. Potential methods for using data at somewhat off-steady-state temperature/current conditions were not explored due to time constraints.

The experimental protocol varied current as an input and recorded wire temperature as a response. Most queries on this data are expected to be of the form, "Temperature *T* is a design threshold (enforced, e.g., by wire insulation integrity or proximity to electronics). What is the maximum current that can be passed through the wire and remain under *T*?" Hence, in analyses *wire temperature* was treated as an input factor and current as the response.

Steady-state temperatures and currents were reduced by taking an average over time during test. For this reason, the contribution of measurement error in current and temperature measurement systems was not calculated. These considerations were deemed unimportant to findings from this phase.

7.5.3.3 Analysis

The data were analyzed primarily in Design Expert® statistical analysis software, with some work performed in Statgraphics®, JMP®, and R [ref. 19] software.

Insight into the physical relationships between variables and responses was available and invaluable to the statistical analyses. In planning the test matrix based on historical data (Section 7.4), it was observed the difference between wire and environmental temperature was a key predictive factor for analysis. A NESC team member working on a related task provided current rating equations from AS50881which are given in the first two columns of Table 7.5.3.3-1. These equations provide the rated current given wire gauge, wire temperature, and environmental temperature for a single wire in free air at 1 atm. The form of the AS50881 wire current curves equations is $log(Current) = \beta_0 + \beta_1 log(\Delta T)$ (all logs used in this section are $\log_{10}$). This served as a model for a more accurate and defensible regression model.

A side analysis was performed to find out whether the constants (i.e., coefficients) in the equations in Table 7.5.3.3-1 were predictable using linear models. If they were, then it could simplify how this relationship is used. Those models might simplify the understanding of the relationship between area of a conductor, directly related to AWG, and its current-carrying capacity. Assuming that each wire gauge deserves its own equation requires the assumption there is another factor involved in predicting ampacity particular to each gauge. Results of that analysis are in the rightmost two columns of Table 7.5.3.3-1. Traces of the two models are shown in Figure 7.5.3.3-1. Both models predicting the coefficients were significant.

Table 7.5.3.3-1. Models describing ampacity of single copper wires in free air due to a related task along with coefficients from a regression analysis relating wire gauge to the trend in each coefficient.

Wire Size AWG	AS50881 Figure 3 Curves	Coef 1	Coef 2	Coef 1 Pred.	Coef 2 Pred.
26	x=10^((LOG$_{10}$(ΔT)-0.0116)/2.2113)	-0.0116	2.2113	-0.0460	2.2031
24	x=10^((LOG$_{10}$(ΔT)+0.295)/2.2365)	0.295	2.2365	0.1977	2.1884
22	x=10^((LOG$_{10}$(ΔT)+0.5069)/2.197)	0.5069	2.197	0.4413	2.1737
20	x=10^((LOG$_{10}$(ΔT)+0.7304)/2.1617)	0.7304	2.1617	0.6850	2.1590
18	x=10^((LOG$_{10}$(ΔT)+0.9326)/2.1083)	0.9326	2.1083	0.9287	2.1443
16	x=10^((LOG$_{10}$(ΔT)+1.0895)/2.122)	1.0895	2.122	1.1724	2.1296
14	x=10^((LOG$_{10}$(ΔT)+1.2923)/2.0753)	1.2923	2.0753	1.4161	2.1148
12	x=10^((LOG$_{10}$(ΔT)+1.5785)/2.0895)	1.5785	2.0895	1.6597	2.1001
10	x=10^((LOG$_{10}$(ΔT)+1.834)/2.0959)	1.834	2.0959	1.9034	2.0854
8	x=10^((LOG$_{10}$(ΔT)+2.1299)/2.0543)	2.1299	2.0543	2.1471	2.0707
6	x=10^((LOG$_{10}$(ΔT)+2.2747)/1.9948)	2.2747	1.9948	2.3908	2.0560
4	x=10^((LOG$_{10}$(ΔT)+2.515)/1.9833)	2.515	1.9833	2.6345	2.0413
2	x=10^((LOG$_{10}$(ΔT)+2.9844)/2.0642)	2.9844	2.0642	2.8781	2.0265
1	x=10^((LOG$_{10}$(ΔT)+3.1733)/2.085)	3.1733	2.085	3.0000	2.0192
0	x=10^((LOG$_{10}$(ΔT)+3.2055)/2.0448)	3.2055	2.0448	3.1218	2.0118
00	x=10^((LOG$_{10}$(ΔT)+3.2937)/2.0282)	3.2937	2.0282	3.2437	2.0045
000	x=10^((LOG$_{10}$(ΔT)+3.2965)/1.9767)	3.2965	1.9767	3.3655	1.9971
0000	x=10^((LOG$_{10}$(ΔT)+3.479)/1.9893)	3.479	1.9893	3.4873	1.9898

Note 1 Temperature Difference (Wire Rating Minus the Ambient = ΔT in C)

Note 2 Single Copper Wire Current in Amperes in Free Air = X

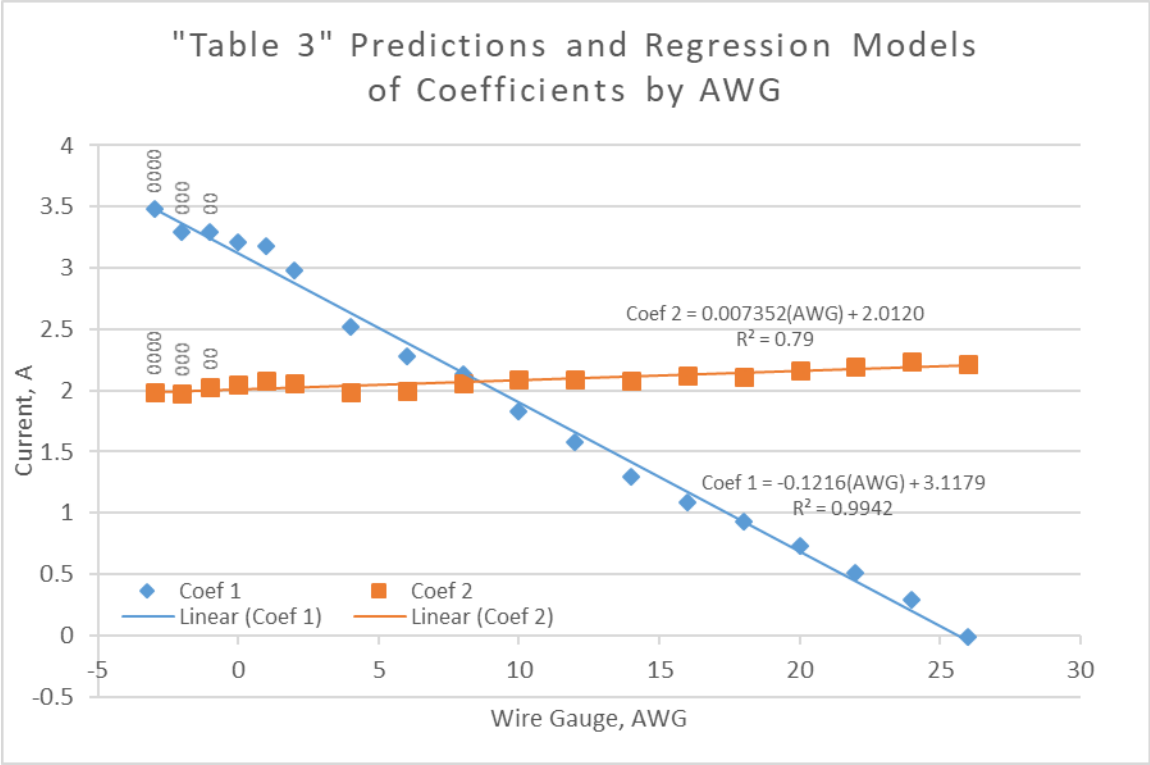

Figure 7.5.3.3-1. Predicted Models of Coefficients in Table 7.5.3.3-1

Response surfaces due to the original-coefficient model (Figure 7.5.3.3-2) and the linearized-coefficient model (Figure 7.5.3.3-3) are illustrated for the 22 AWG 1 atm 1 WPB case. It can be seen the fit to the test data generated during this assessment is better for the original wire current rating curves [ref. 4, Figure 3] model than the linearized-data model, but it is not conservative to the data for high shroud temperatures and low wire temperatures. The linearized coefficient model is the more conservative across the range of the data. This is true for all three wire gauges tested.

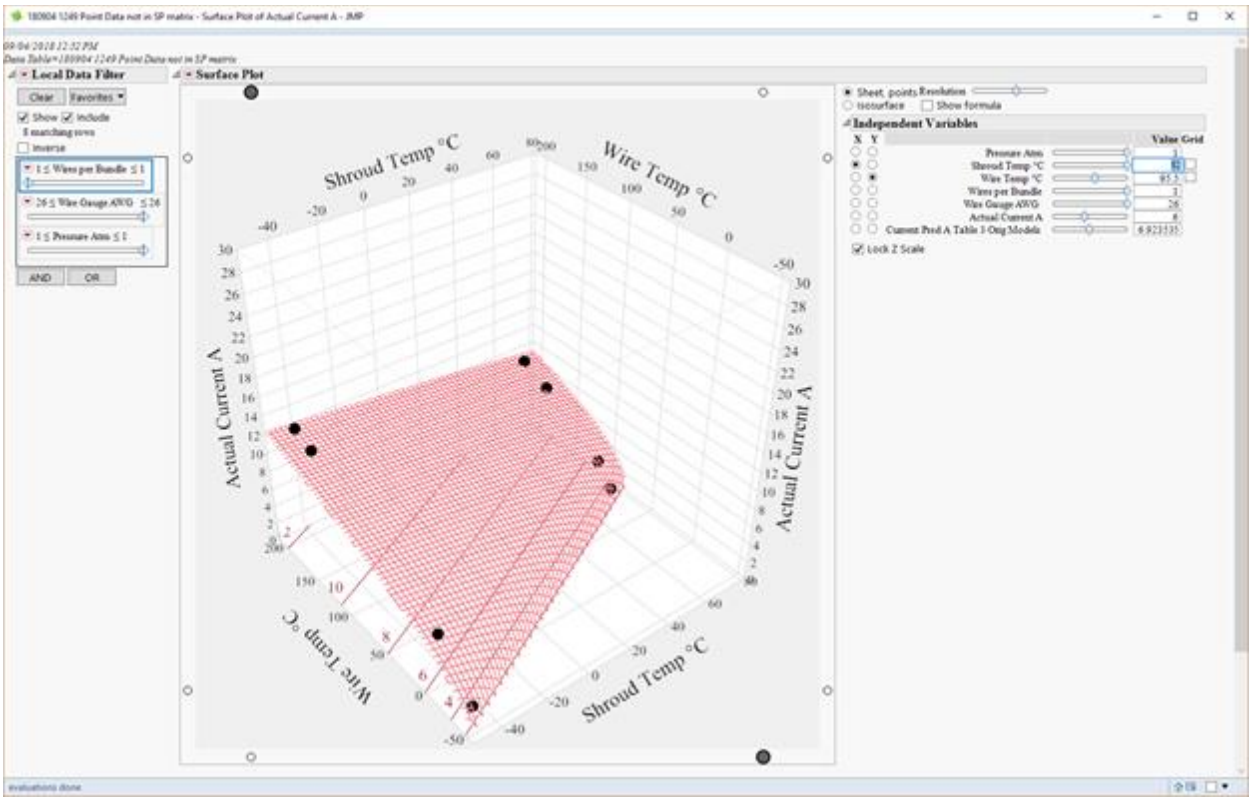

Figure 7.5.3.3-2. Response surface using coefficients from prediction surface generated by an AS50881 wire current rating curves [ref. 4, Figure 3] model using original coefficients describing a single 26 AWG wire at 1 atm. See also Figure 7.5.3.1-1.

Regression analysis of the data was performed in phases. Initial phases looked at WPB, AWG, Pressure, Wire Temperature in °C (Wire Temp), and Shroud Temperature in °C (Shroud Temp), but not the difference between Wire and Shroud Temperatures (ΔT). Analysis produced response surfaces that did not match credible physics.

Analysis was then performed considering WPB, AWG, Pressure, and ΔT, with quadratic terms for AWG and ΔT, and a number of interactions between terms. Some interactions were not able to be included in the model because they were too highly correlated or were not analyzable given the steady state dataset. An example of an unanalyzable term would be WPB^2. This factor was tested at two levels (i.e., 1 and 32 wires per bundle). Three or more points, including 16-wire bundles in testing, would be required to detect curvature characterized by a WPB^2 term in the response.

The analysis produced model Eq. 12 that followed the data adequately. The model is expected to be useful for the ranges of the input factors listed in Table 7.5.3.2-1.

Eq. 12:

If Pressure = 0 (vacuum),

$$Current = 10^{1.07691+0.512364*\log_{10}(Wire\ Temp\ °C - Shroud\ Temp\ °C)-0.0146692*WPB-0.0556236*AWG}$$

If Pressure = 1 atm,

$$Current = 10^{1.34513+0.512364*\log_{10}(Wire\ Temp\ °C-Shroud\ Temp\ °C)-0.0146692*WPB-0.0556236*AWG}$$

Eq. 12 should be considered a single model. They were calculated using the entire dataset rather than treating the vacuum and 1 atm data separately. This allowed for quantitative evaluation of the differences between the two pressure conditions, and maximizing the number of observations available in creation of the model (i.e., the more data, generally, the more information available for building a model. It is recommended the coefficients be left at the above number of significant figures for calculating that result to reduce unnecessary rounding errors, then rounding the result of the calculation for presentation.

Note there are no quadratic or interaction terms in this model, even though they were considered during analysis. Terms found to be unnecessary or detrimental to describing the phenomenon adequately were removed. When a dataset is orthogonal and balanced, as comes from a well-designed experiment, statistical significance can often be used as a screen to identify the important predictors from variables that have little or no influence on the response. In this case, the dataset analyzed was neither orthogonal nor balanced, meaning there were significant correlations between factors and the ability to detect some effects was weakened somewhat. Significance alone, in this case, was not a sufficient screen for choosing appropriate regression model terms.

Instead, the Bayesian information criterion (BIC) [ref. 20] metric was used to winnow down the set of factors to a level that was most efficient in using the data to describe a response surface. Development and strict statistical interpretation of the BIC metric can be found in that reference [ref. 20] and will not repeated here. Its calculation is moderately difficult, but fortunately is built into the Design Expert® DOE experiment design and analysis software used here. The metric is calculated by the software for each candidate model. The metric can then be compared between models formed using the same dataset. The analyst looks for the model with the minimum value of the metric.

There is a set of structured analysis methods for performing this task known as best subsets analysis, but that method was not available to the analysts during this phase. Standard software and currently available macros and packages have not been developed to apply best subsets analysis to split-plot analyses. The analysts used a brute-force manual approach for this task, removing or adding factors into models one at a time to find those with low BIC values that defined credible response surfaces.

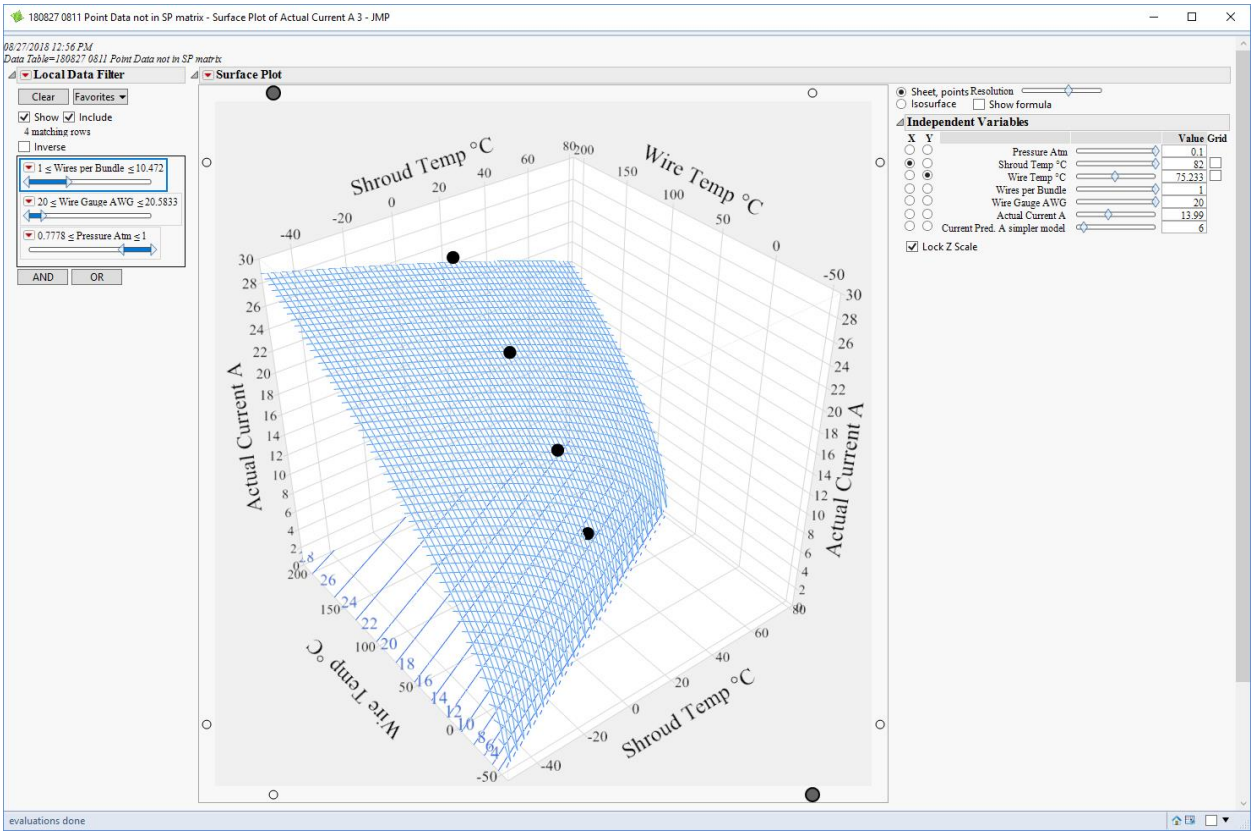

Figure 7.5.3.3-3. Original regression model response surface showing how current was affected by the wire surrounding environmental temperatures in the case of a single 26-gauge wire at 1 atm.

The resulting model given in Eq. 12 resulted in the minimum BIC given this set of starting factors of -150.26. R^2 was more than 0.991. A representative response surface plot for the case of a single 26 AWG wire at 1 atm is in Figure 7.5.3.3-3.

Further analysis resulted in an improved final model. Plots of the model-predicted values compared to the data are shown in Figure 7.5.3.3-4 for the simpler model (left) and the more-complex model chosen to describe the data. These graphs are analogous to the 1:1 plots described earlier (e.g., Figure 7.5.2.2-3).

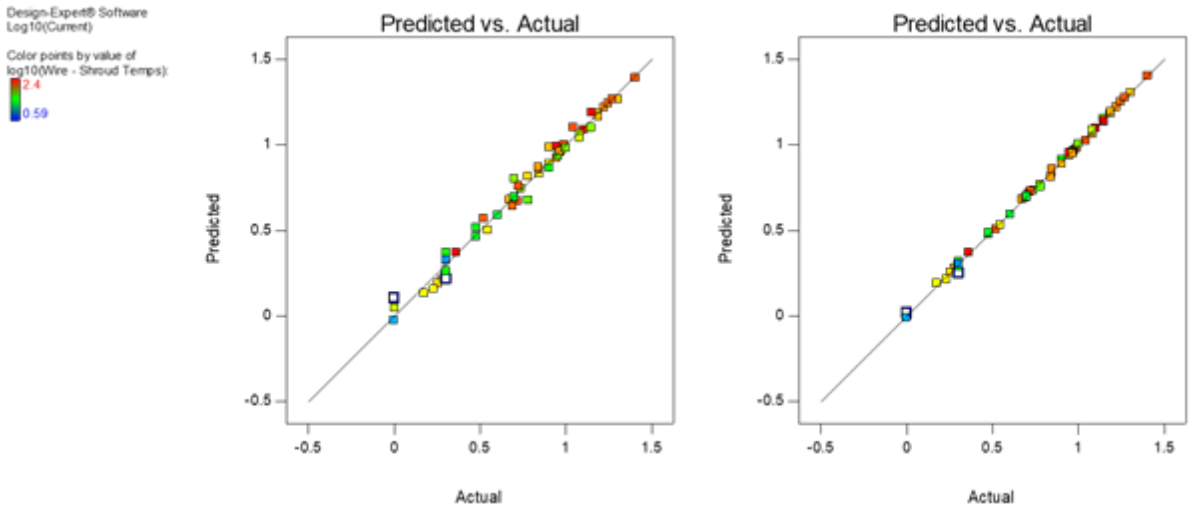

Figure 7.5.3.3-4. Plots of model-predicted vs. actual test data for the original simpler model (left) and the model finally chosen to predict current (right).

The improved model's BIC statistic was lower/better at -219.06. The R^2 value was also improved at more than 0.999. Both models are probably useful but, including another main effect term (wire temperature), interactions between terms and the quadratic appeared to have produced a better match to the data. As will be seen, they may also illuminate the underlying physics a little better.

A plot showing regression model traces of the various cases, assuming a 200°C wire temperature along with the original AS50881 wire current rating curves [ref. 4, Figure 3] models' prediction traces, the predictions made using the estimated coefficients from the above regression analysis along with points showing steady state test data at wire temperatures between 195 to 205°C is shown in Figure 7.5.3.3-5.

Below and following similar figures (7.5.3.3-11 through 7.5.3.3-14):

- Round points and single-line traces indicate single-wire cases. Square points and double-line traces indicate 32 WPB cases.
- Green points and traces indicate 20 AWG. Blue indicates 22 AWG. Red indicates 26 AWG.
- Solid points and lines indicate 1 atm traces. Hollow points and dashed lines indicate vacuum traces.
- Dash-dot traces indicate the AS50881 wire current rating curves [ref. 4, Figure 3] models, all of which are single wire at 1 atm.

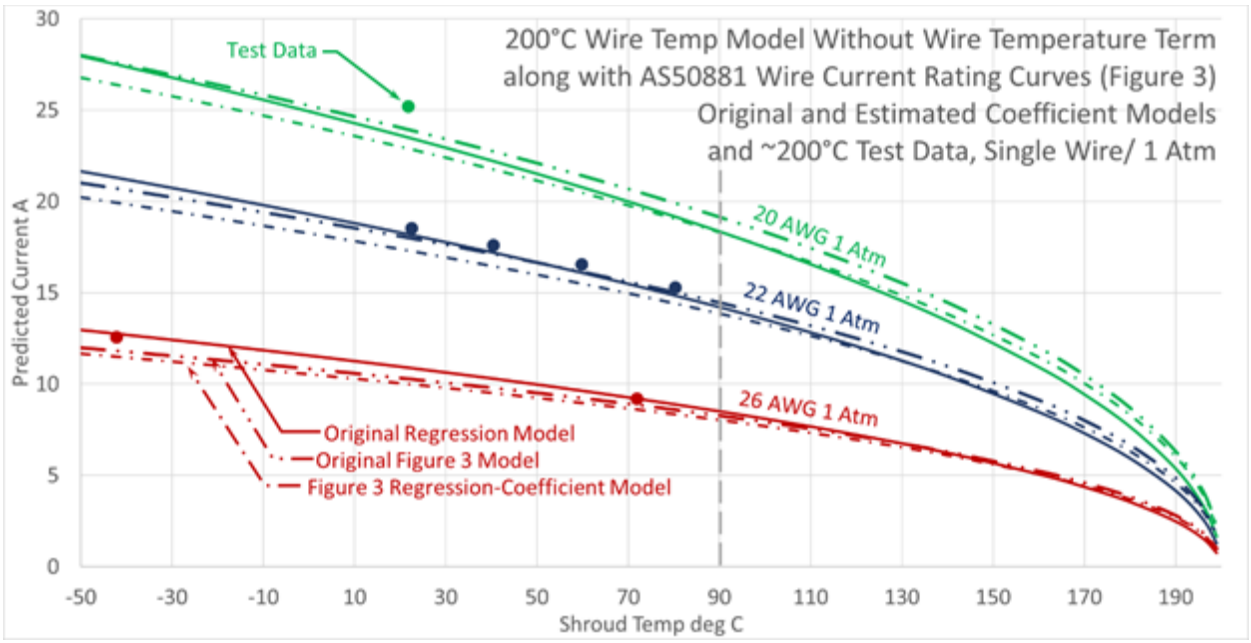

Figure 7.5.3.3-5. Traces for wire temperature = 200°C for the single-wire, 1 atm cases generated by the regression model with no adjustment for wire temperature, along with the AS50881 wire current rating curves [ref. 4, Figure 3] models and relevant test data.

The regression and AS50881 wire current rating curves ref. 4, Figure 3 original and estimated-coefficient models follow each other reasonably well. No data was collected at shroud temperatures over 90°C (vertical grey dashed line), and no data above 80°C is in the steady state dataset used in analysis, so this might be expected. This domain of the graph is shown to illustrate model behavior in that region, but extrapolations using this regression model may or may not be correct in that range.

During examination, the problem with the model was seen to be related to wire temperature. Analysis was rerun with the same factors, quadratic terms and interactions as before, but now including Wire Temp as a factor. (Another analysis was performed replacing Wire Temp with $log(Wire\ Temp)$, but the model returned was less satisfactory.)

Addition of this factor led to the improved model Eq. 13. The model was highly significant ($p < 0.0001$), R^2 was nearly 1, and BIC was -219.06. This equation is expected to be useful within the input parameter ranges seen in Table 7.5.3.2-1.

Eq. 13:

For Pressure = 0 (i.e., vacuum):

$$Current = 10\text{^}(1.06978 + 0.66227 * \log_{10}(Wire\ Temp\ °C - Shroud\ Temp\ °C\ ) - 0.0127531 * WPB - 0.0617644 * AWG + 0.00121145 * Wire\ Temp - 0.088395 * \log_{10}(Wire\ Temp\ °C - Shroud\ Temp\ °C)^2)$$

For Pressure = 1 (i.e., atmospheric):

$$Current = 10\text{^}(1.50056 + 0.520098 * \log_{10}(Wire\ Temp\ °C - Shroud\ Temp\ °C) - 0.0167922 * WPB - 0.0617644 * AWG - 0.000262997 * Wire\ Temp + 0.006662 * \log_{10}(Wire\ Temp\ °C - Shroud\ Temp\ °C)^2)$$

Response surface plots for four cases are below.

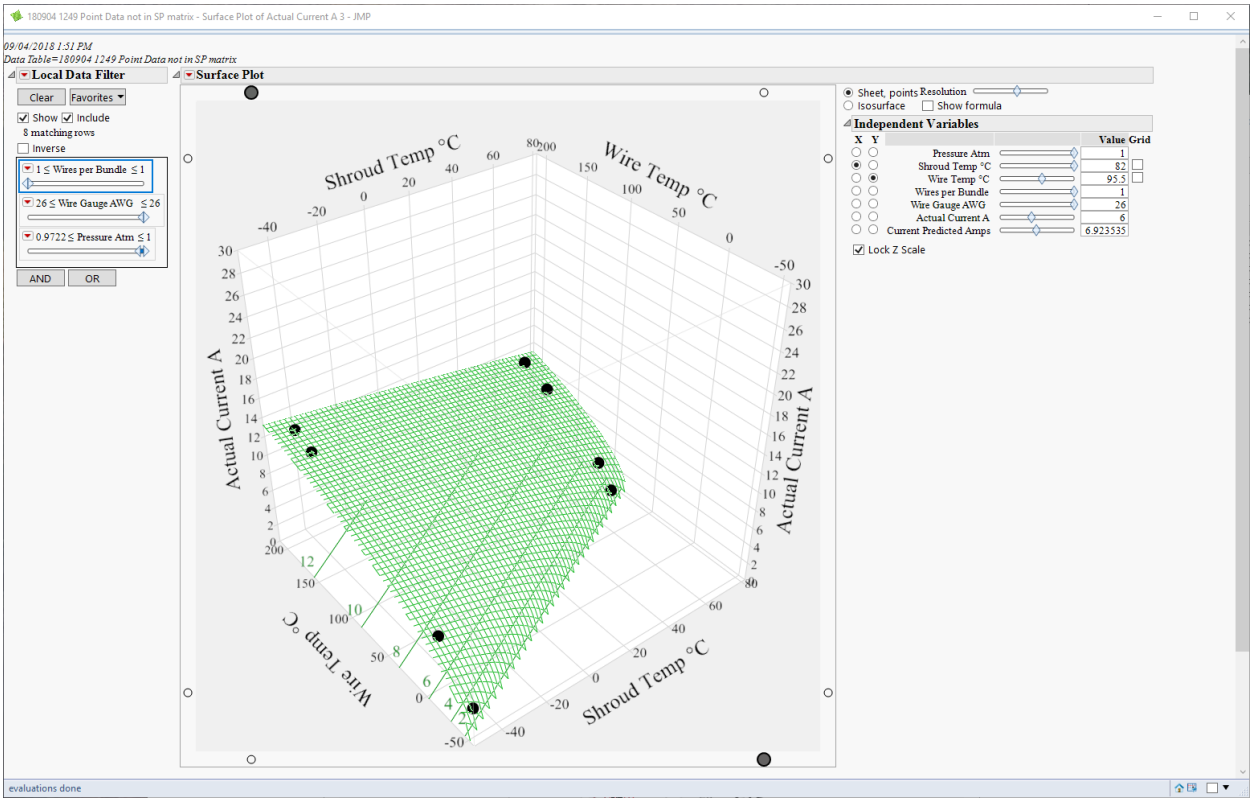

Figure 7.5.3.3-6. Response surface for the regression model that includes wire temperature showing how current was affected by the wire temperature and the surrounding environmental temperatures in the case of a single 26-gauge wire at 1 atm.

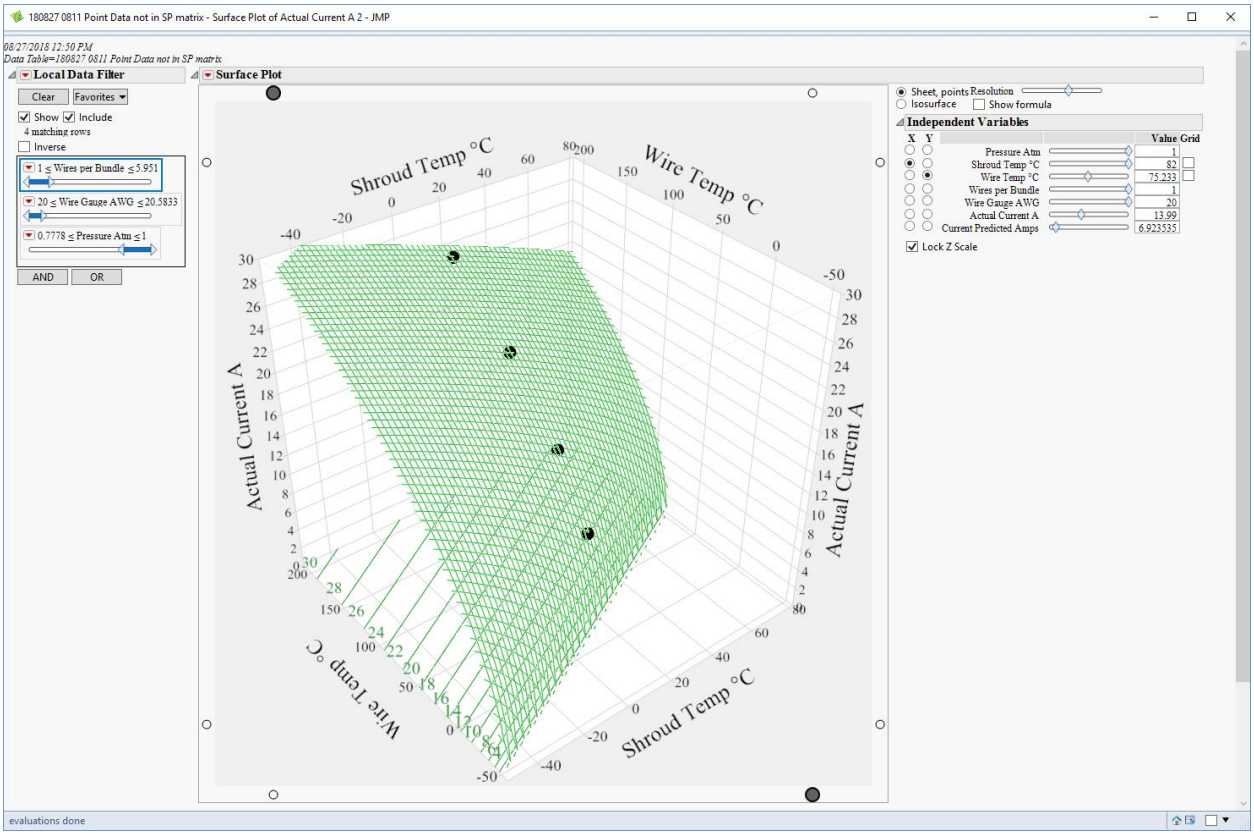

Figure 7.5.3.3-7. Response surface for the regression model that includes wire temperature showing how current was affected by the wire temperature and the surrounding environmental temperatures in the case of a single 20-gauge wire at 1 atm.

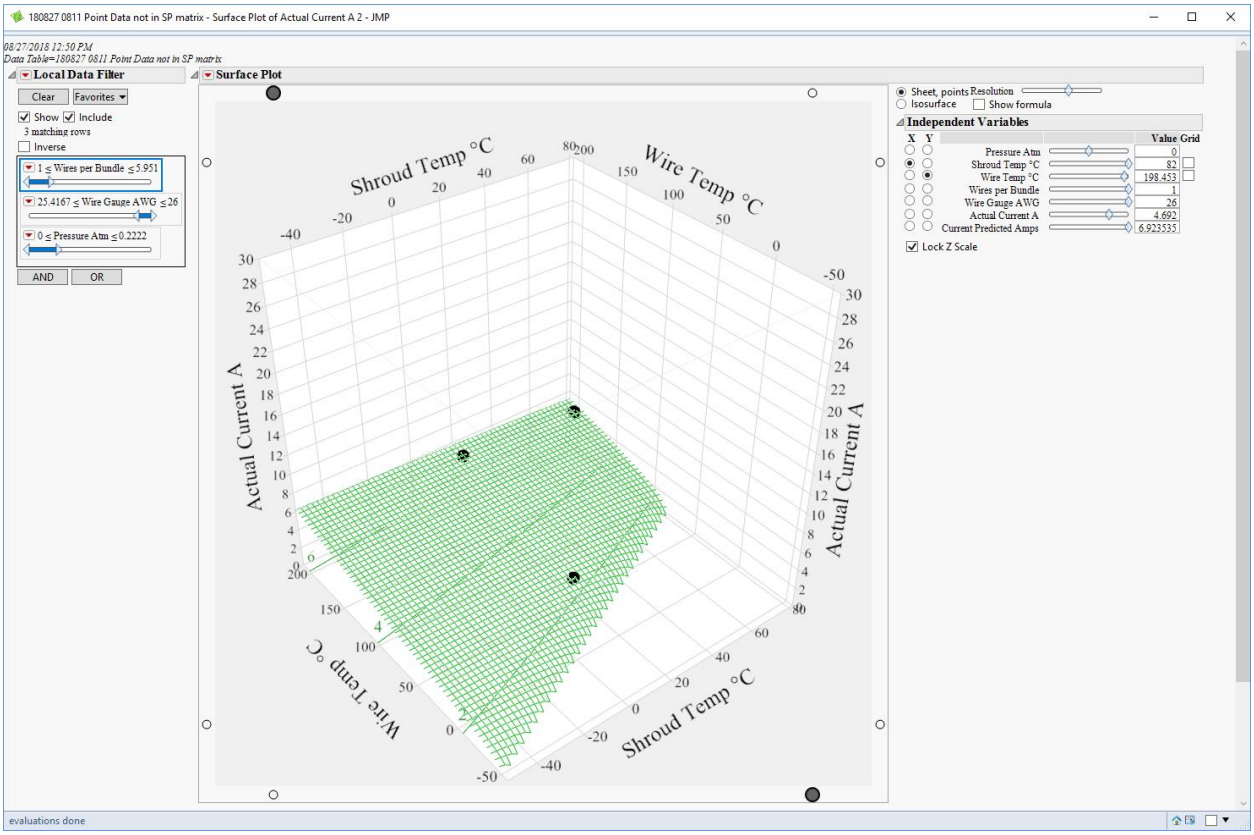

Figure 7.5.3.3-8. Response surface for the regression model that includes wire temperature showing how current was affected by the wire temperature and the surrounding environmental temperatures in the case of a single 26-gauge wire in vacuum.

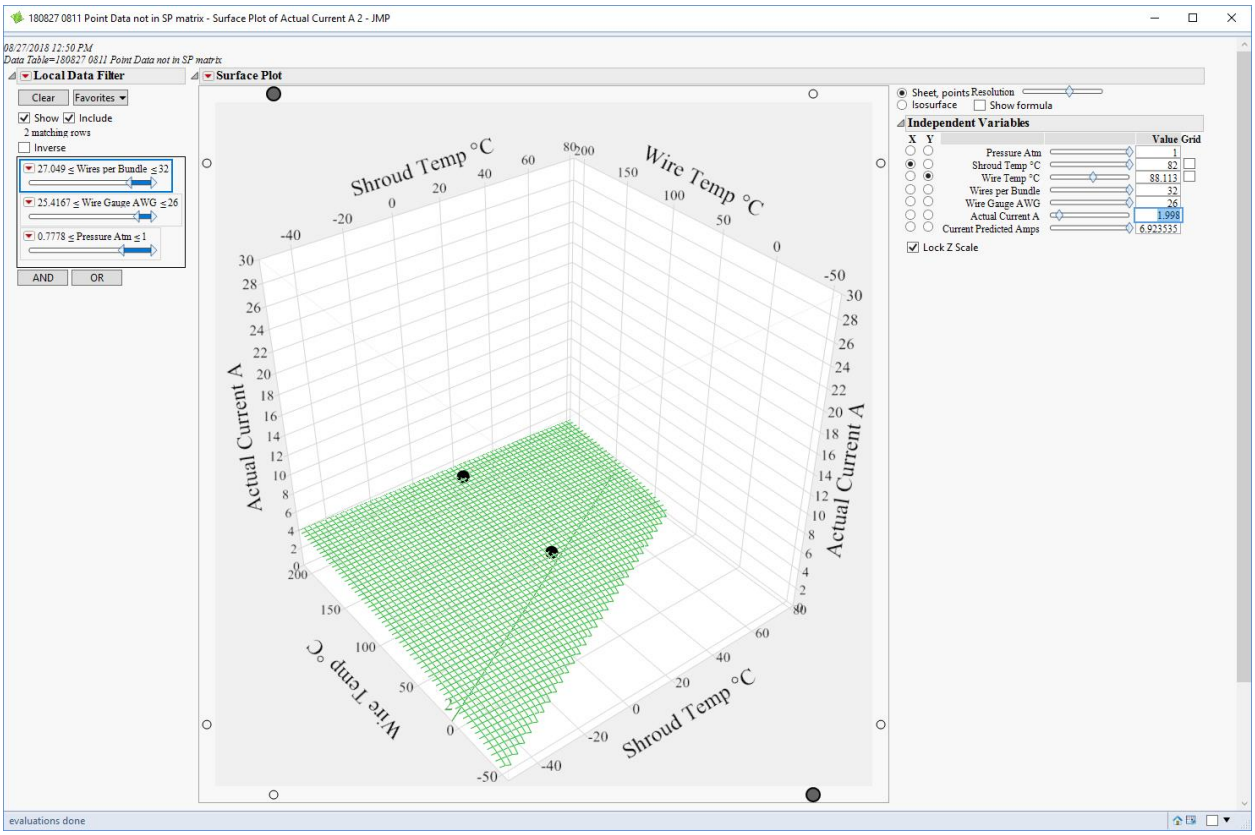

Figure 7.5.3.3-9. Response surface for the regression model that includes wire temperature showing how current was affected by the wire temperature and the surrounding environmental temperatures in the case of a bundle of 32 26-gauge wires at 1 atm.

Eq. 13 is a reduced form of the equation evaluated in analysis. Analysis was performed using coded factors, meaning that each factor was converted to a scale between -1 and +1. This avoided a mathematical problem with bias in calculating coefficients and significances in interaction terms, but it also results in a model equation where all the variables are on the same scale (i.e., -1 to +1). The coded model's coefficients partially indicate the relative contributions of the individual factors to the predicted result. This equation is shown in Table 7.5.3.3-2.

Table 7.5.3.3-2. Model Equation including Wire Temperature in Terms of Coded Factors

Coefficient	Coded Term	What Term Represents
Log_{10}(Current)	=	
+0.46		Location (intercept)
+0.43	* A	Log(Δ*T*)
-0.23	* B	WPB
-0.19	* V	AWG
+0.062	* D	Wire Temp
+0.12	* E	Pressure
+0.064	* AE	Log(Δ*T*) x Pressure interaction
-0.033	* BE	WPB x Pressure interaction
-0.092	* DE	Wire Temp x Pressure interaction
-0.040	* A^2	Curvature in log(Δ*T*)
+0.039	* A^2E	Curvature in log(Δ*T*) x Pressure interaction

The coefficients for the main effects (i.e., single-letter, nonquadratic coded terms) appear to show that $log(\Delta T)$ has the largest effect, which are shown in Figures 7.5.3.3-6 through 7.5.3.3-9. It is positive where current increases with increasing $log(\Delta T)$. However, it is involved in two quadratic terms and interactions with pressure.

For the following example, assume factors WPB, AWG, and Wire Temp are held constant at their midpoint (even though that may not make physical sense), so their contribution to current through this model is constant at 0 in coded terms. (If this is difficult, one can assume any more-representative coded value, but the math may not be done as easily in one's head.)

Then (Eq. 16):

$$\log(Current) = 0.46 + 0.43 * A + 0.12 * E + 0.064 * A * E - 0.040 * A^2 + 0.039 * A^2 * E$$

The Pressure variable in the test was binary, either vacuum or 1 atm. In the coded formulation, *E* is either -1 (vacuum) or +1 (1 atm).

Now assume a high temperature difference of about 251°C, meaning $A = +1$. When run in 1 atm, the total contribution of the curvature terms involving A^2 is nearly 0(i.e., $(-0.040 + 0.039) * A = 0.001$) – hardly enough to see in a trace. However, when run in vacuum, the contribution of the curvature term to current is $(-0.040 - 0.039) * A^2$, nearly -0.08 log current units at 251°C.

The engineering effect is that using a wire in vacuum does not reduce the ampacity compared to sea level conditions. Ampacity in a vacuum is *additionally* reduced as a function of the square of the difference between wire temperature and the temperature of the surroundings. In practice, it works to noticeably flatten the current response in vacuum as compared to at 1 atm.

There is an additional adjustment, the derivative (i.e., the slope at any point) of current as a function of ΔT depending on pressure, contributed by the AE (log(ΔT) x Pressure interaction).

The other terms can be interpreted in this fashion. The effect of wire gauge was large, and its effect did not change much with pressure – it was not involved in an interaction. The difference in effect of wire temperature in vacuum vs. 1 atm; however, was relatively pronounced at about 0.184 log current units difference between the two conditions considering the DE (Wire Temp x Pressure interaction).

The graph of the traces generated by the model including the Wire Temp term at 200°C single-wire temperatures at 1 atm are shown in Figures 7.5.3.3-10 through 7.5.3.3-14. The error between the steady-state test data and the associated regression model traces are considerably smaller than those for the model without Wire Temp in Figure 7.5.3.3-10, but are farther from – and less conservative than the AS50881 wire current rating curves [ref. 4, Figure 3] models at environmental temperatures below 90°C for this condition. This may serve to dampen enthusiasm for employing this engineering statistical model's use until it can be confirmed, or improved, with data from further testing. However, the general form of the models should be correct, so offer utility for comparisons and findings.

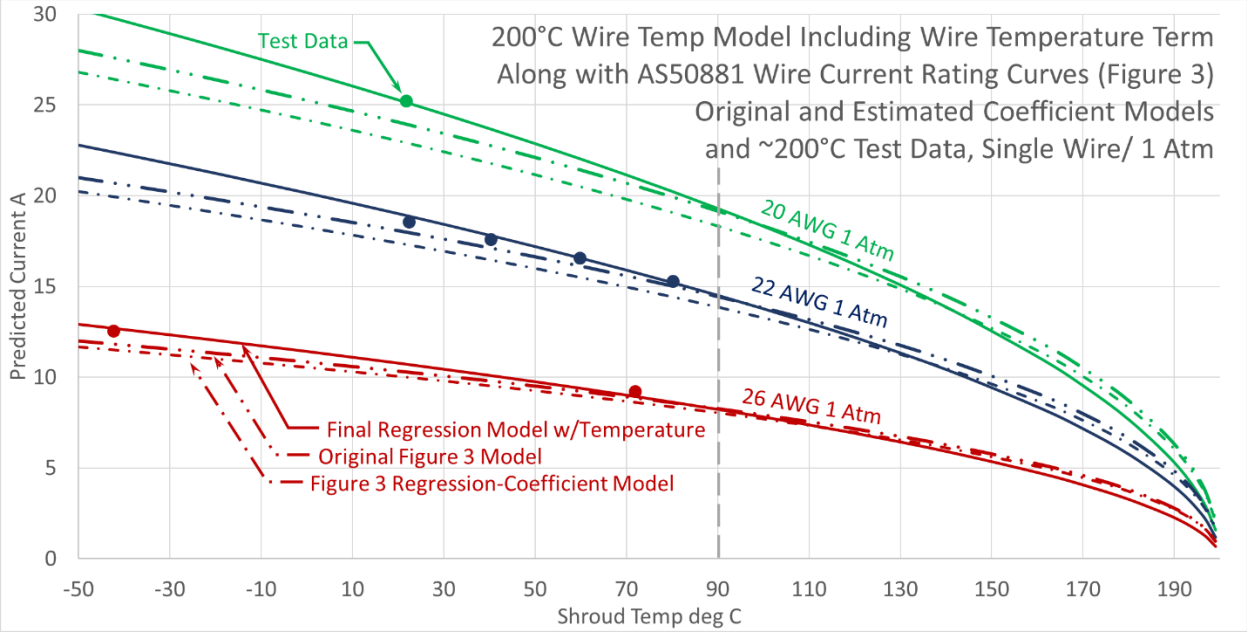

Figure 7.5.3.3-10. Traces for single wires at wire temperature = 200°C generated by the regression model including adjustment for wire temperature, along with the AS50881 wire current rating curve [ref. 4, Figure 3] original and estimated-coefficient models and relevant test data.

Figure 7.5.3.3-11 compares ampacity at 200°C in a vacuum with that at 1 atm. As expected in the model description above, losing the convective heat loss component results in ampacity that is much reduced and little affected by the temperature of the environment.

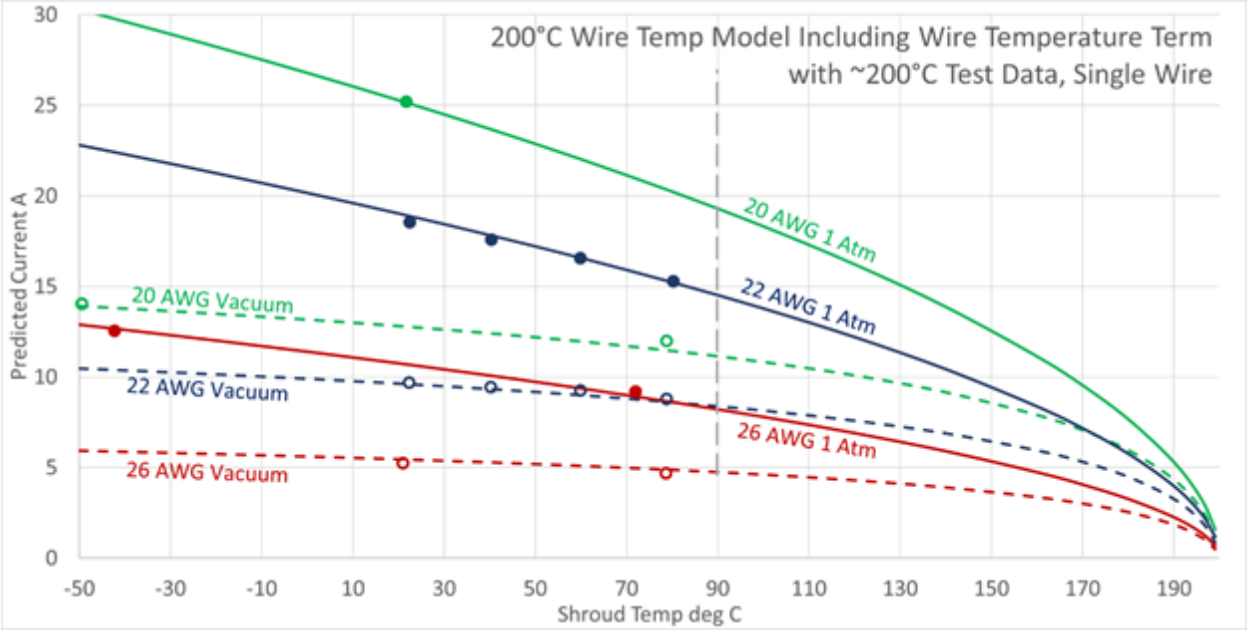

Figure 7.5.3.3-11. Traces for single wires at wire temperature = 200°C generated by the regression model including adjustment for wire temperature with relevant test data.

Figures 7.5.3.3-12 through 7.5.3.3-14 shows the impact to ampacity when a wire is bundled with other conductors carrying similar current. Predicted 32-wire bundle ampacity in vacuum is nearly constant at shroud temperatures below about 125°C.

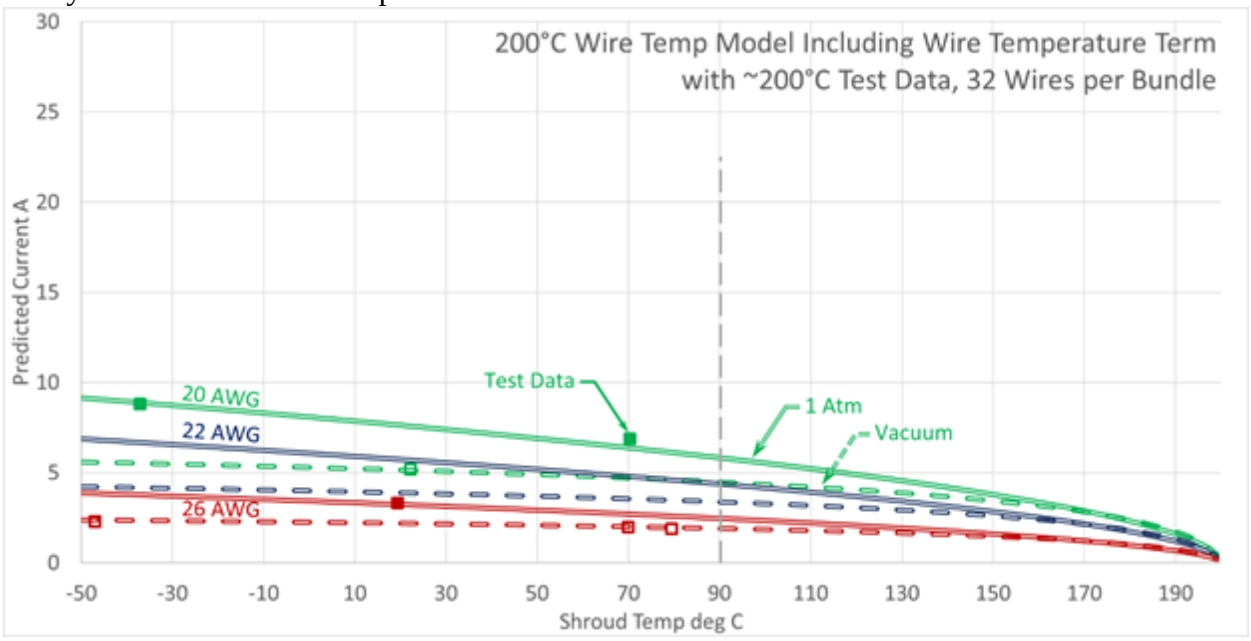

Figure 7.5.3.3-12. Traces for 32-wire bundles at wire temperature = 200°C generated by the regression model including adjustment for wire temperature with relevant test data comparing effects of pressure.

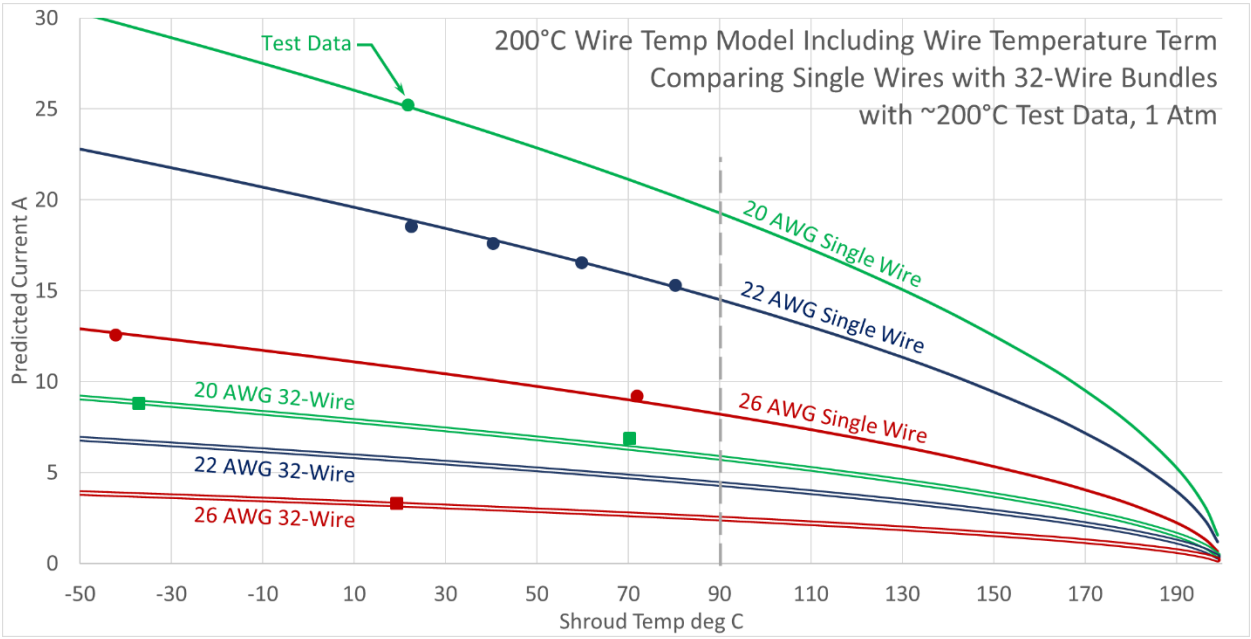

Figure 7.5.3.3-13. Traces at wire temperature = 200°C generated by the regression model including adjustment for wire temperature with relevant test data comparing single wires and 32-wire bundles at 1 atm pressure.

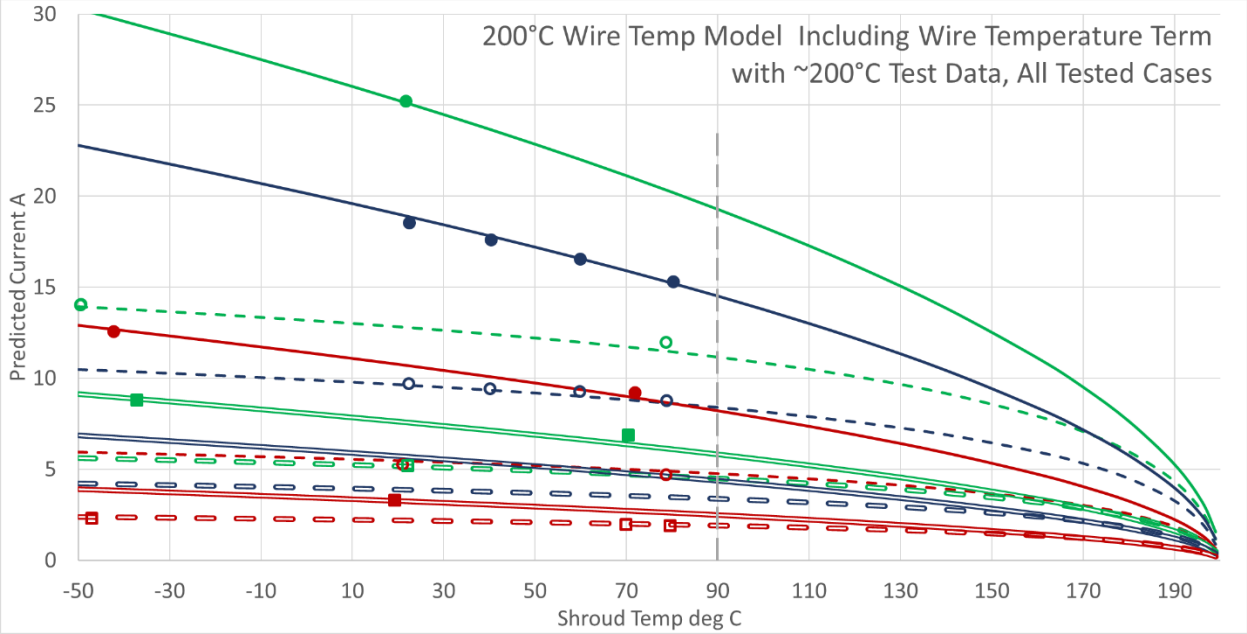

Figure 7.5.3.3-14. Traces at wire temperature = 200°C generated by the regression model for all tested AWG, WBP and Pressure cases including adjustment for wire temperature with relevant test data.

7.5.4 Comparison of Correlated Model Predictions with the AS50881 Standard and JPL Standard

7.5.4.1 Single Wire Comparison

The correlated single wire thermal model was compared to the pertinent single wire curves in the AS50881 standard [ref. 4] for XL-ETFE and TKT insulations for the 1 atm case. The environment temperature was subtracted from the predicted maximum conductor temperature to obtain the steady state Delta Temperature (y-axis) for the corresponding current (x-axis). A summary of the comparison is presented in Figure 7.5.4.1-1. It should be noted the analysis points shown represent a variety of environment temperatures. It is also apparent from the figure that use of XL-ETFE or TKT insulations produce results in accordance with the standard for the cases examined and are equivalent to the results predicted by the standard or slightly less conservative for the higher current cases. Lower currents, corresponding to lower temperature delta above the environment temperature are more conservative than that dictated by the standard.

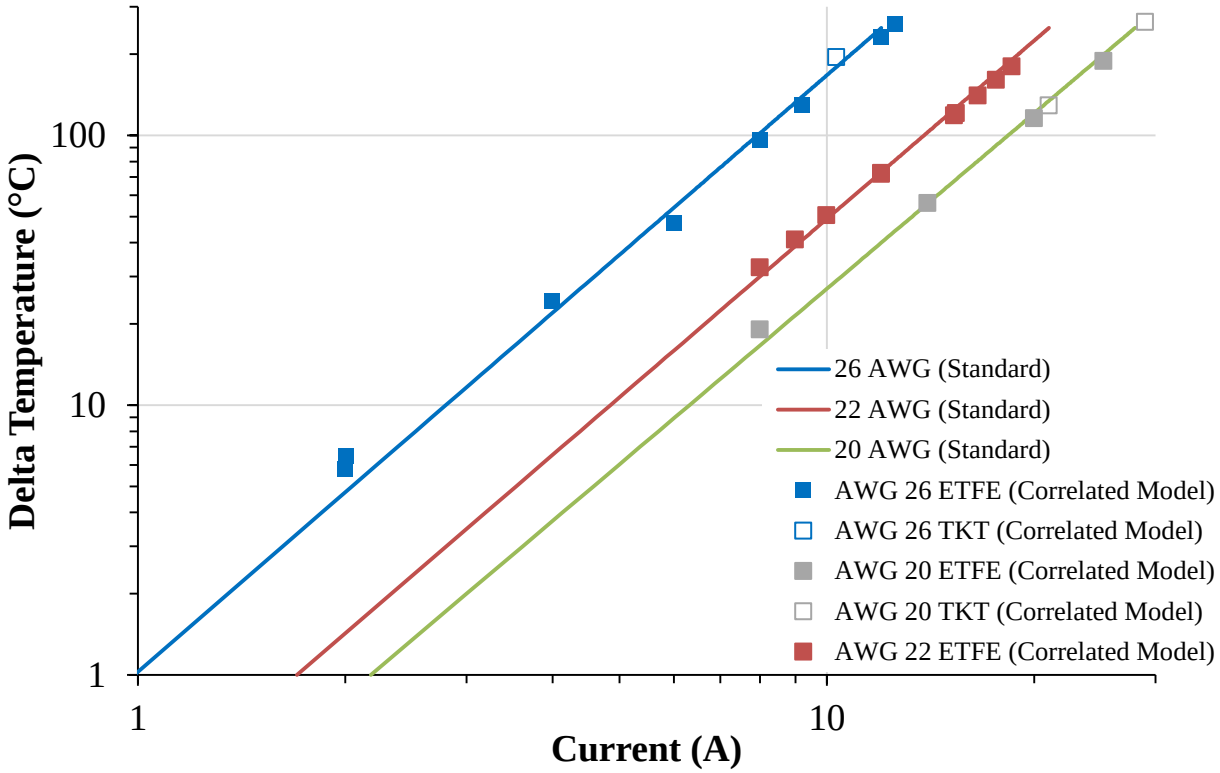

Figure 7.5.4.1-1. Comparison of the Correlated Single Wire Thermal Model to AS50881 for the 1 atm Case

7.5.4.2 Wire Bundle Comparison

To compare the AS50881 standard with the correlated 32-wire bundle thermal model, it was necessary to obtain single wire data [ref. 4, Figure 3] and derate it according to the standard. For a 32-wire fully loaded bundle in 1 atm, the derating factor [ref. 4, Figure 4] is ~0.28. When multiplied with the ampacity curves, the solid curves on Figure 7.5.4.2-1 are obtained. As was the case for the single wire comparison, the environment temperature was subtracted from the predicted maximum conductor temperature to obtain the steady state Delta Temperature (y-axis) for the corresponding current (x-axis). The analysis points shown represent a variety of environment temperatures. It is apparent from the figure that use of XL-ETFE or TKT insulations produce results in accordance with the standard. For the cases examined, the results

predicted by the standard are more conservative than those predicted by the model for virtually all cases.

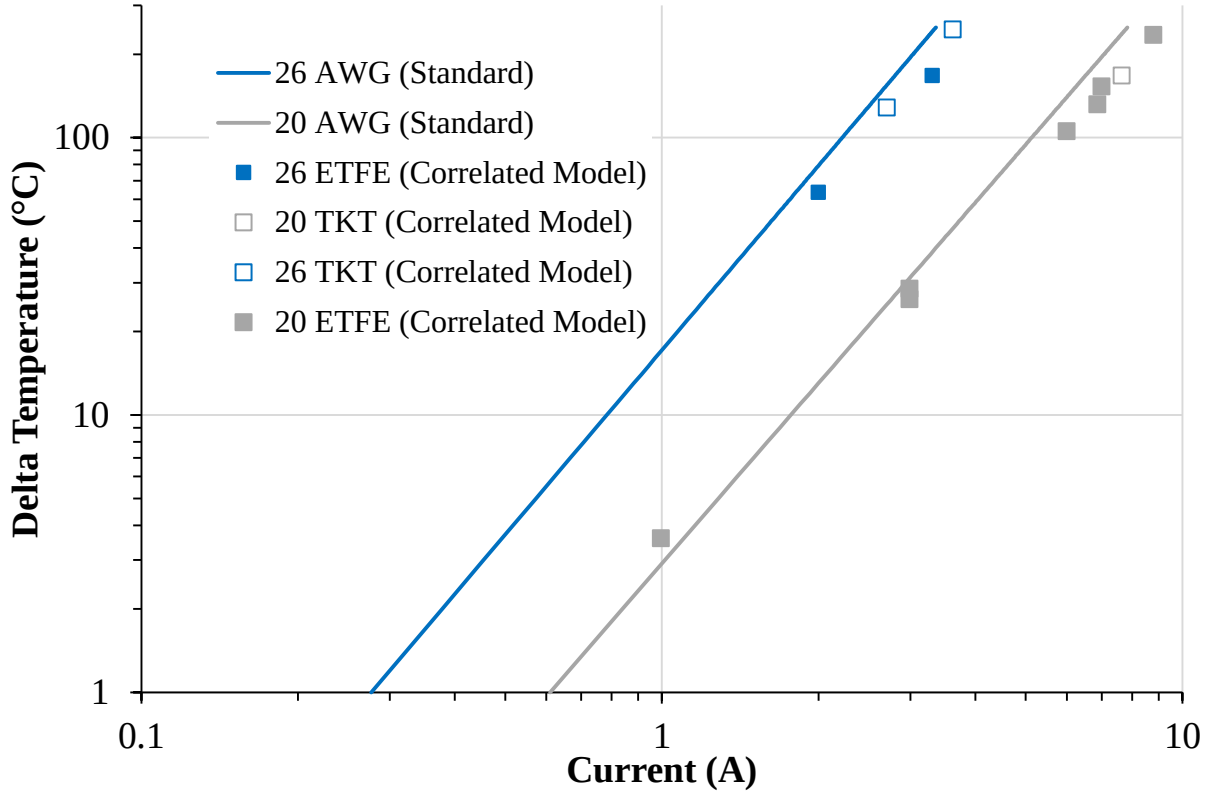

Figure 7.5.4.2-1. Comparison of the Correlated 32-Wire Bundle Thermal Model to AS50881 for the 1 atm Case

7.5.4.3 Comparison to JPL Flight Standards

The wire ampacity derating table used for JPL flight projects [ref. 6] is spot checked using relevant test data acquired during the test campaign. The JPL wire derating table purportedly gives the maximum allowed current a wire or wire bundle can carry before exceeding 200°C in vacuum or 1 atm conditions. It assumes the ambient environment is +80°C.

For the limited testing and analyses performed during this pathfinder study, the environmental conditions described in the JPL wire derating table were matched for six cases and the amount of current was measured that caused the conductor to reach 200°C. This data is compared with the JPL wire derating values in Table 7.5.4.3-1. In all vacuum cases, the JPL derating tables are conservative. However, the level of conservatism varies with margins between 0.5 and 3.5A. For the one data point taken in atmospheric conditions, the JPL standard showed a negative margin of 0.7A. Note the derating values used in the JPL standard for 1 atm, pressure conditions were taken from the AS50881 standard. As shown, this standard shows little margin for single wires, and limited margin for wire bundles.

Table 7.5.4.3-1. Comparison of Test Data to JPL Derating Standards

Shroud Temp. (°C)	Wire Temp. (°C)	Pressure (-)	Wire Gauge /Insulation AWG/(-)	Wire Configuration (-)	JPL –Max allowable current (A)	Measured Current (A)	Margin (A)	Percent Difference (%)
78.5	198.5	vacuum	26/XL-ETFE	Single wire	2.7	4.7	2	74
79.5	201	vacuum	26/XL-ETFE	32-Wire bundle	1.4	1.9	0.5	36
78.7	197.7	vacuum	26/TKT	Single wire	2.7	4.4	1.7	63
78.6	199.3	vacuum	20/TKT	Single wire	8.0	11.45	3.5	43
78.8	201.6	vacuum	22/XL-ETFE	Single wire	5.6	8.78	3.2	57
80.3	200.2	1 atm	22/XL-ETFE	Single wire	16	15.29	-0.7	-4

7.5.5 Model Sensitivity Analysis

To determine the ampacity of a conductor or conductor bundle, experiments were conducted to examine a given conductor or conductor bundle's temperatures as a function of the current through the conductor. Uncertainty and error propagation analysis was used to inform the instrumentation selection and the experimental setup for measuring current and temperature. Equation 17 describes the relationship between a conductor's resistivity and temperature.

$$R(T) = R_{L0}L[1 + \alpha(T - T_0)] \quad \text{Eq. 17}$$

where T is the conductor temperature (°C), T_0 is the reference temperature (20°C), R_{L0} is the resistance per unit length at T_0, L is the wire length (m), α is the temperature coefficient of resistance ($°C^{-1}$).

The resistive power dissipation through the conductor can be expressed as:

$$VI = I^2R(T) = I^2R_{L0}L[1 + \alpha(T - T_0)] \quad \text{Eq. 18}$$

where V is the applied voltage (V), I is the current (A).

Rearranging the resistive power dissipation equation gives the temperature as a function of current (Eq. 19):

$$T = \frac{\left(\frac{V}{IR_{L0}L} - 1\right)}{\alpha} + T_0 \quad \text{Eq. 19}$$

$where$: V (voltage) and I (current) are measured test variables, R_{L0} and α vary based on the selected conductor of interest, and L is the length of the test article. The partial derivatives with

respect to the parameters $V,\ I, R_{L0}, \alpha$, and L were taken to examine how uncertainties in these parameters' measurements affect the uncertainty in the calculated temperature (Eqs. 20 through 24):

$$\frac{\partial T}{\partial \alpha} = \frac{1-\left(\frac{V}{IR_{L0}L}\right)}{\alpha^2} \quad \text{Eq. 20}$$

$$\frac{\partial T}{\partial V} = \frac{1}{\alpha I R_{L0} L} \quad \text{Eq. 21}$$

$$\frac{\partial T}{\partial I} = \frac{-V}{\alpha I^2 R_{L0} L} \quad \text{Eq. 22}$$

$$\frac{\partial T}{\partial L} = \frac{-V}{\alpha I R_{L0} L^2} \quad \text{Eq. 23}$$

$$\frac{\partial T}{\partial R_{L0}} = \frac{-V}{\alpha I R_{L0}^2 L} \quad \text{Eq. 24}$$

Using the root-mean-square-error (RMS) method, the uncertainty in temperatures (U_T) due to a given uncertainties in measurements is defined as (Eqs. 25 and 26):

$$U_T = \sqrt{\left(\frac{dT}{d\alpha}U_\alpha\right)^2 + \left(\frac{dT}{dV}U_V\right)^2 + \left(\frac{dT}{dI}U_I\right)^2 + \left(\frac{dT}{dL}U_L\right)^2 + \left(\frac{dT}{dR_{L0}}U_{R_{L0}}\right)^2} \quad \text{Eq. 25}$$

$$U_T = \sqrt{\left(\frac{1-\left(\frac{V}{IR_{L0}L}\right)}{\alpha^2}U_\alpha\right)^2 + \left(\frac{1}{\alpha I R_{L0} L}U_V\right)^2 + \left(\frac{-V}{\alpha I^2 R_{L0} L}U_I\right)^2 + \left(\frac{-V}{\alpha I R_{L0} L^2}U_L\right)^2 + \left(\frac{-V}{\alpha I R_{L0}^2 L}U_{R_{L0}}\right)^2} \quad \text{Eq. 26}$$

The equation for U_T illustrates the uncertainty in temperature measurements is inversely proportional to the parameters α, I, R_{LO}, and L, and directly proportional to V. Upper and lower bounds of the experimental parameters were defined to determine the expected U_T. The error analysis assumes the testing of single and 32 wire bundle copper conductors between 20 to 28AWG. Given these assumptions, α is expected to be approximately 0.004 (1/℃), R_{L0} is expected to range from 0.0354 to 0.147 Ω/m, and L is expected to be approximately 3 m. The input currents will range from 0.5 to 25A. Expected voltages were calculated using Eq. 27:

$$V = IR_{L0}L[1 + \alpha(T - T_0)] \quad \text{Eq. 27}$$

To determine the upper bound U_T, the upper bound voltages were calculated assuming $T = 200^o C$.

Given the expected voltage and current ranges, the Agilent 34970 data acquisition system was initially selected due to its ability in the expected ranges. Table 7.5.5-1 shows the voltage measurement accuracy of the Agilent 34970 [ref. 21]. The Riedon 1 $m\Omega$ $\pm 0.1\%$ 10W resistance shunt was selected to measure current due to its low error reading and current measurement

ranges [ref. 22]. Uncertainty analysis was conducted to examine errors in temperature measurement given the initially selected instruments.

Table 7.5.5-1. Agilent 34970 Voltage Measurement Accuracies

VOLTAGE RANGE (V)	% READING ERROR	RANGE ERROR (V)
0.1	0.003	3.5E-06
1	0.002	0.000006
10	0.0015	0.00004
100	0.002	0.0006
300	0.002	0.006

The error analysis shows the error in temperature measurements is highly sensitive to the error in α and R_{L0} measurements due to these parameters being significantly less than one, and inversely proportion to U_T. For a less than 2°C uncertainty in temperature, α needs to be measured within a 0.5% accuracy, and R_{L0} needs to be measured within a 0.2% accuracy.

7.5.6 Oil Bath Testing to Determine R_{L0} and α

Resistance changes over specified temperature ranges were measured to determine α and R_{L0}. A 4-wire system was used to apply a sufficient current to measure a voltage drop and calculate the resistance. The length between probes was accurately measured and the wire temperature was controlled using an oil bath. The working fluid is capable of heating the conductor to its maximum useful temperature. The experimental work was performed with XL-ETFE and TKT insulation wires, sized 26, 22, and 20 AWG (see Table 7.5.6-1).

Table 7.5.6-1. Wires Characteristics

AWG	Insulation	Conductor
26	Lt. Wt. XL-ETFE AS22759/33	Ag plated High Strength Copper Alloy
22	Lt. Wt. XL-ETFE AS22759/33	Ag plated High Strength Copper Alloy
20	Lt. Wt. XL-ETFE AS22759/33	Ag plated High Strength Copper Alloy
26	Lt. Wt. TKT AS22759/181	Ag plated Ultra-High Strength Copper Alloy
20	Lt. Wt. TKT AS22759/181	Ag plated High Strength Copper Alloy

7.5.6.1 Instruments

The length between probes was measured using a ruler with an accuracy of 1/2 mm (Figure 7.5.6.1-1).

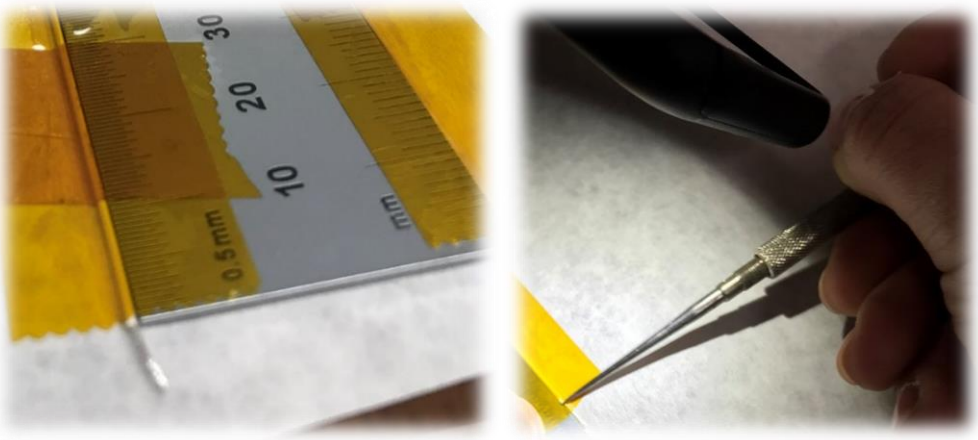

Figure 7.5.6.1-1. Wire Length Measurement

The AD15R-40-A11B Polyscience® Temperature Bath was used for these tests (Figure 7.5.6.1-2). System parameters are presented in Table 7.5.6.1-1.

Figure 7.5.6.1-2. Polyscience® Temperature Bath

Table 7.5.6.1-1. Polyscience® Temperature Bath

Polyscience® Temperature Bath	
Model	AD15R-40-A11B
Temperature Stability (°C)	0.01
Bath volume (L x W X H) (cm)	21.2 x 27.6 x 14
Maximum allowed temperature (°C)	202
Minimum allowed temperature (°C)	-52
Fluid Specific Heat (cal/g·°C)	0.23

The wire sample to be tested was coiled through four holes made into two plastic supports. This structure helps to keep the wire immersed into the working fluid, and in a stable position inside the bath (see Figure 7.5.6.1-3). The virgin Teflon™ Polytetraflouroethylene (PTFE) surpasses most plastics when it comes to chemical resistance and performance in extreme temperatures (see Table 7.5.6.1-2).

Table 7.5.6.1-2. Wire Support

Wire Support	
Material	Teflon™ PTFE
Temperature Range (°C**)**	-177 to 260

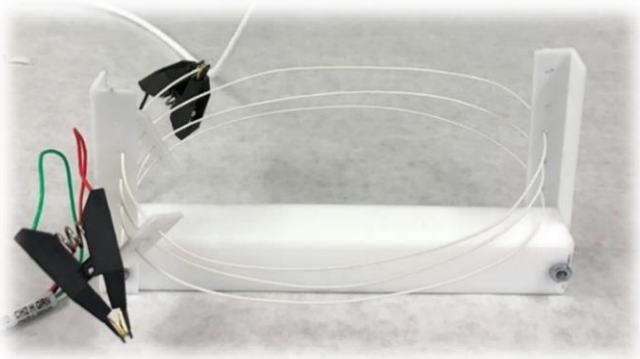

Figure 7.5.6.1-3. Wire Support

The Keysight 34420 Ohmmeter (see Figure 7.5.6.1-4) was selected to measure the wire resistance. A 4-wire system was used to apply a sufficient current to measure a voltage drop and calculate the resistance. The 4-wire measurement technique was used to remove lead and contact resistance. This is an advantage for precise measurement of low resistance values. Resistance fluctuations of the order of 10^{-5} ohms were observed over time when the fluid reached the stabilized temperature. The accuracy of the measurement was on the order of 10^{-4} ohms.

Figure 7.5.6.1-4. Keysight 34420 Ohmmeter

7.5.6.2 Working Fluid

Perfluoropolyether fluorinated heat transfer fluids (PFPE HT) shows excellent compatibility with most of the materials commonly present in heat exchangers. PFPE dielectric properties do not change with use with no risk of short circuiting. Environmentally safe, PFPE is non-toxic, non-explosive, and will not damage electronics should any leakage occur. No Flash or Fire Point and no auto-ignition point are additional advantages of PFPE HT. The boiling point is 240°C at 1 atm.

7.5.6.3 Test Set Up

The following steps were repeated to measure the resistance of the different wires:

1. pour the dielectric working fluid into the bath,
2. place the wire on the support,
3. connect the wire to the ohmmeter,
4. insert the system into the bath,
5. turn on the Polyscience® Temperature Bath and set the desired temperature,
6. turn on the ohmmeter and select the resistance measurement option.

The heating bath container was prepared using a sufficient quantity of liquid to keep the wire specimen temperature uniform. Resistance measurements were made when the fluid reached the stabilized temperature. The first measurement was made at 20°C. Four measurements were made between the maximum and minimum temperatures. The maximum temperature was set to 170°C since over temperature is registered when the bath reaches ~180°C (see Section 7.5.6.1). The minimum temperature (-20°C) is a requirement for the PFPE. The number of data collected during testing was increased to select the minimum value for which α does not depend on the amount of data collected (see Figure 7.5.6.3-1 and Figure 7.5.6.3-2). This shows the random error in estimating α is small given the test performed.

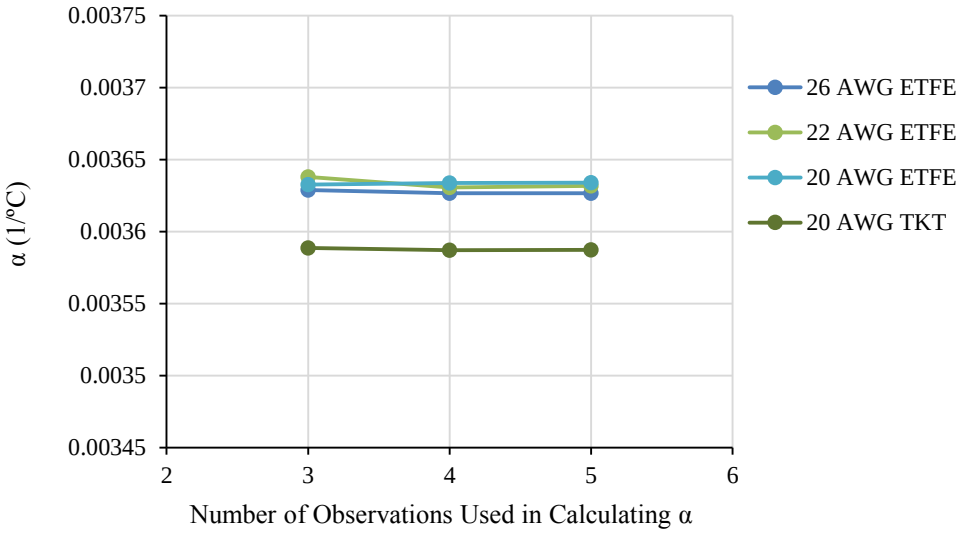

Figure 7.5.6.3-1. α Variation with Number of Observations Collected (26 to 20 AWG XL-ETFE, 20 AWG TKT)

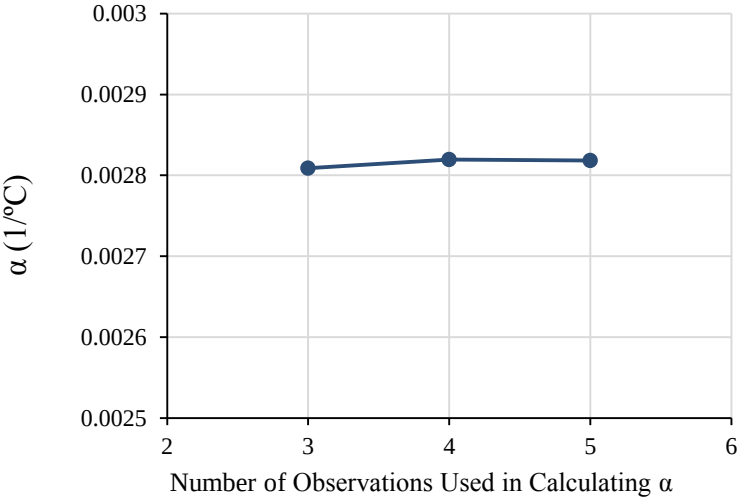

Figure 7.5.6.3-2. α Variation with Number of Observations Collected (26 AWG TKT)

7.5.6.4 Oil Bath Testing Results

Resistance measurements for each wire are reported in Table 7.5.6.4-1. A least-squares fit analysis on the data was performed. The intercept of the regression line and the R -squared statistic indicating of how closely the data fits the fitted regression line are reported in Figure 7.5.6.4-1. The resistance can be calculated using the Eq. 28:

$$R_m = R_0[1 + \alpha(T_m - T_0)] \qquad \text{Eq. 28}$$

where R_0 is the Wire Conductor Resistance in ohms at 20°C, T_0 is the temperature (°C) at which R_0 was measured (20°C), T_m is the measured temperature (°C), R_m measured resistance of the conductor at T_m and α. Laboratory generated resistance equations, L, and R^2 values are reported in Table 7.5.6.4-2.

Table 7.5.6.4-1. Measured Resistance

T (˚C)	Measured Resistance R_m [Ω]				
	XL-ETFE (AWG26)	**XL-ETFE (AWG22)**	**XL-ETFE (AWG20)**	**TKT (AWG26)**	**TKT (AWG20)**
-20	0.1137	0.0465	0.0287	0.1488	0.0308
20	0.1330	0.0543	0.0335	0.1678	0.0359
60	0.1522	0.0620	0.0384	0.1876	0.0411
100	0.1724	0.0699	0.0433	0.2066	0.0462
170	0.2054	0.0840	0.0518	0.2384	0.0553

Table 7.5.6.4-2. Resistance Equations obtained through Regression Analysis of Test Data

Wire Type	Wire Length(m)	Lab generated resistance equation	R^2
AS22759/33-26XL-ETFE	1.0245	0.000482*T + 0.123309	0.999994
AS22759/33-22XL-ETFE	1.0395	0.000197*T +0.050325	0.999900
AS22759/33-20XL-ETFE	1.028	0.000122*T+0.031105	0.999991
AS22759/181-26 (Ultra High Strength copper)	1.0165	0.000473*T + 0.158629	0.999704
AS22759/181-20	1.0975	0.000129*T + 0.033359	0.999994

The resistance per unit length is reported in Table 7.5.6.4-3. From a previous assessment, the resistance per unit length for the 22 AWG XL-ETFE at 20ºC was 0.052083 ohm/m, and α was 0.003925 [ref. 1]. It is possible that the difference between values obtained during this study and the previous study could be due to the measurement technique (oil bath vs. water bath) or lot to lot variability. Table 7.5.6.4-4 summarizes wires characteristics and test results. It includes α, the specification resistances and resistances from a conductor vendor, and the laboratory measured lower values. In the case of the 26 AWG TKT, it is an ultra-high strength alloy while all other wires are a high strength alloy so a different α and much higher resistance is expected.

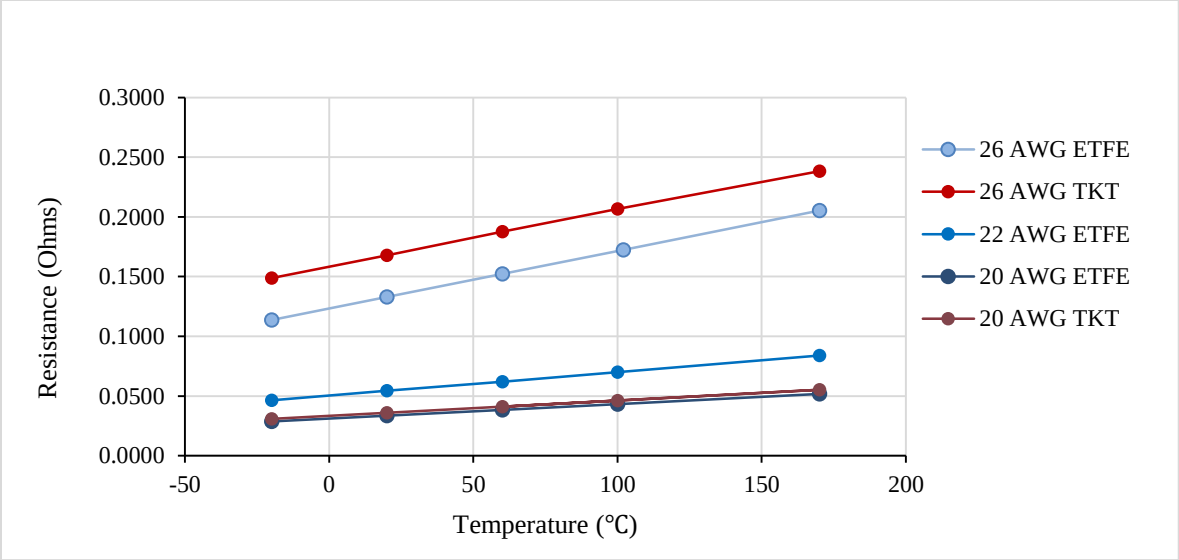

Figure 7.5.6.4-1. XL-ETFE Resistance for Wire used in this Assessment

Table 7.5.6.4-3. Resistance Per Unit Length for Wire used in this Assessment

T (˚C)	Resistance per unit length [Ω/m]				
	AS22759/33-26 XL-ETFE	AS22759/33-22 XL-ETFE	AS22759/33-20 XL-ETFE	AS22759/181-26 TKT	AS22759/181-20 TKT
-20	0.1110	0.0447	0.0279	0.1464	0.0281
20	0.1298	0.0522	0.0326	0.1651	0.0327
60	0.1486	0.0596	0.0374	0.1846	0.0374
100	0.1683	0.0672	0.0421	0.2032	0.0421
170	0.2005	0.0808	0.0504	0.2345	0.0504

Table 7.5.6.4-4. Wire Characteristics and Test Results

AWG	26	22	20	26	20
Construction	Lt. Wt. XL-ETFE AS22759/33	Lt. Wt. XL-ETFE AS22759/33	Lt. Wt. XL-ETFE AS22759/33	Lt. Wt. TKT AS22759/181	Lt. Wt. TKT AS22759/181
Finished Wire Dia. (in) Min/Max.	0.030/0.034	0.041/0.045	0.048/0.052	0.030/0.034	0.048/0.051
Insulation Thickness (in.)	0.006	0.006	0.006	0.006	0.006
Spec (min.) Conductor/Finished Wire Dia. (in) Min./Max.	0.0175/0.0204	0.0285/0.0314	0.0365/0.0395	0.0175/0.0204	0.0365/0.0395
Measured Conductor Dia. (in)	0.018	0.029	0.037	0.018	0.037
Lab Rep. Res./Length 20˚C (Ohms/m)	0.1298	0.0522	0.0326	0.1651	0.0327
Lab Rep. Res./Length 20˚C (milliohms/ft)	39.56	15.91	9.94	50.32	9.97
Spec (Max.) Res./Length 20˚C (milliohms/ft)	44.8	17.5	10.7	56.4	10.7
Vendor (Max.) Res./Length 20˚C (milliohms/ft)	41.1	16.5	10.1	56.4	10.1
Lab Rep. α (1/˚C)	0.00363	0.00363	0.00363	0.00282	0.00359
Res. (Ohms/m) using Lab Rep. Equation	0.1298	0.0522	0.0327	0.1654	0.0327
Temp. ˚C for Equation	20	20	20	20	20

The conductor resistance at 20°C after high temperature excursions was remeasured to determine if the resistance increased as a result of the high temperature exposure. It is known that high temperature aging will permanently increase the conductor resistance as shown is Table 7.5.6.4-5 where the increase was 14.3% after 1,000 hours exposure at 200°C. The durations at high temperature were much shorter in the present tests, but some impact on resistance was observed. The resistance of a 26 AWG, TKT silver plated conductor was compared before (i.e., 0.1651 ohms/m) and after an 8-hour exposure at 200°C (i.e., 0.16705 ohms/m), which equates to an increased resistance of 1.18% was calculated.

Table 7.5.6.4-5. DC Resistance Before and After Thermal Aging [ref. 28]

Conductor Type	Resistance (Ohms/1,000 Ft.) at 20˚C		Percent increase (%)
	Initial	Thermal Aged for 1,000 hrs. @200˚C	
24 gauge silver plated high strength copper	22.65	25.90	14.3

7.6 Potential Future Work

With the successful development and demonstration of a wire/wire bundle test apparatus, a capability exists to test additional configurations and collect data to further refine analytical and regression models. Opportunities for future work might include test verifying bundles of various constructions against established standards, investigation of "smart short" capabilities of wire bundle configurations, and exploration of specialized configurations (e.g., twisted pairs, triplets, quad, and other aggregate configurations). Once sufficient confidence in the test and analysis techniques have been established, refining the models and using them as the basis for an Agency-wide methodology for wire ampacity derating to replace the current wire derating standards may be possible.

Future work may include refinement of the testing techniques to include testing at pressures between atmospheric and high vacuum, further exploration of wire insulation infrared transmissivity and modeling techniques, and inclusion of nitrogen as a test gas in the thermal modeling tools. Accommodation to include more of the test samples within the temperature controlled test volume may also be explored.

7.7 Concluding Remarks

An apparatus for testing wire and wire bundles under vacuum and atmospheric conditions for a variety of environmental temperatures and currents has been developed and demonstrated. A wire and wire bundle test matrix was formulated using DOE techniques and successfully executed. Key wire parameter data were measured and provided critical information required to refine analytical models. The parameter data were analyzed, resulting in response surface models that were able to successfully model the data. Physics-based wire and wire bundle thermal models were refined and successfully correlated with test data.

Currently there is no general NASA standard for wire current rating/derating, or how to define the temperature of a wire or wire bundle. Most NASA Centers have a standard or technical memo that address certain aspects of wire current rating and derating. However, there is not a comprehensive Agency or Center standard similar to AS50881. As an example, the JSC Technical Memorandum NASA/TM-102179 for Space Shuttle Program payloads states wire current rating curves are based on insulation temperature: *"The actual level of allowable current*

in a selected environment is the amount of current required to raise the insulation temperature from that of the wire in a nonconducting state (insulation temperature is equal to ambient) to the maximum rated temperature of the insulation." This assessment assumed current rating curves (e.g., AS50881 and JPL D-8208) are directly associated with the conductor temperature and the actual temperature of the conductor (not insulation). The assumption is supported by the fact the temperature of a single wire or wire bundle is a function of heating from passing current through one or more wires and the surrounding ambient temperature. This assumption was successfully used to validate the correlation between published current rating curves, laboratory measurements, and the developed physics-based thermal and response surface models. The wire conductor and insulation materials both limit the actual current rating of the wire system. An aerospace grade copper conductor is plated with tin (rated at 150°C), silver (rated at 200°C), or nickel (rated at 260°C) to provide a stable conductive service over the range of expected temperatures. Each conductor system has a different temperature rating, and the plating systems will degrade electrically and physically because of high temperature exposure.

Insulation material surrounding the conductor limits the wire current rating since insulation can be electrically and physically degraded by high temperature exposure. Insulations such as XL-ETFE are thermally rated at 200°C, and TKT is rated at 260°C. Thermal ratings are determined by long-term exposure (typically 1,000 to 10,000 hours) of the conductor and insulation system as part of the wire qualification.

In human-rated space flight, the surface temperature of the wire is important since the wire or wire bundle may be accessible by a crew member. Typically, wiring in crewed areas is limited to 50°C and during maintenance, a crew member (per ISS Program SSP30312 [ref. 28]) would need to be aware uncovered wires could be at temperatures that may be hazardous without protection.

The ability to accurately model and predict temperatures of wiring will be a useful tool for designers optimizing and increasing the safety of human-rated and robotic spacecraft electrical systems, and for technical reviewers assessing the safety of these systems.

8.0 Findings, Observations, and NESC Recommendations

8.1 Findings

The following findings were identified:

F-1. Both the response surface model and physics-based thermal model developed during this assessment correlate with the pathfinder test data and AS50881.

F-2. For the limited scope of the pathfinder study, modern AS22759 wire constructions (e.g., XL-ETFE and TKT), showed good agreement with the models developed and wire current rating curves per AS50881.

F-3. Wire insulation to wire insulation contact conductance required to correlate bundle wire models during this assessment differ from the values obtained during the NESC-RP-14-00949 assessment and is believed to be due to the different bundle construction in the previous study.

F-4. Uncertainty in temperature measurements for a resistance-based temperature measurement is inversely proportional to the parameters temperature coefficient of

resistivity α, current I, resistance per unit length-at a reference temperature R_{L0}, and wire length L, and directly proportional to voltage.

F-5. The measured values of the qualified (i.e., certified to a wire specification) wire constructions used in this assessment were within specification requirements yet were different from the nominal specification values given for resistance at room temperature, conductor diameter, and overall finished wire diameter. An accurate measurement of the conductor resistance and temperature coefficient, conductor diameter, and overall finished wire diameter is required to develop thermal models that correlate well to lab measured single wire and wire bundle temperatures.

8.2 Observations

The following observations were identified:

O-1. An increase of wire conductor resistance of 1.18% was measured after limited thermal exposure during lab testing. Wire conductor resistance increases with aging at high temperatures. However, for the wire gauges studied during this pathfinder phase, literature suggests increases on the order of 14.3% after long exposure to high temperatures.

O-2. Type E, 36 AWG thermocouples can be successfully used to measure wire conductor temperature on wire gauges 26 AWG or larger. For the wire gauges tested, the estimated effect of the thermocouple was on the order of, at most, 3°C.

O-3. A wire combing technique developed during this assessment, in conjunction with spot ties along a bundle length, was successful in maintaining a wire of interest at or near the central location within a wire bundle. However, if the bundle is bent, it is not clear whether the relative wire positions are maintained.

O-4. The model coefficients used to construct the wire current curves in AS50881 are linearly related to wire gauge. This could be used to simplify both testing and modeling due to the smoothness of the design space.

O-5. It appears the JPL derating values for single wires in 1 atm shows no margin (or negative margin), while the derating values for single wires and bundles in vacuum show a wide variety of margin. Compared to limited test data for five vacuum cases called out in the JPL standard that were replicated in testing, the JPL standard had additional margins that fluctuated from 0.5A to 3.5A. However, it is unclear whether JPL takes into consideration wire aging and product variability.

O-6. NASA does not have an Agency-wide standard for defining wire and cable current ratings and derating guidance.

O-7. Operating wire bundles in vacuum, resulting in loss of the convective heat loss mode, makes ampacity relatively insensitive to environmental temperature. This effect is particularly pronounced when wire bundles as opposed to single wires are used

8.3 NESC Recommendations

The following NESC recommendations are intended for those performing wire and wire bundle testing, unless otherwise noted.

R-1. Resistance change, as a result of thermal aging, should be considered in any future work using 1000 hours at the rated temperature as the basic test. ***(O-1)***

R-2. Testing and analysis for other wires types, gauges and configurations should be conducted, with and without convection to further improve the physics-based and response surface models. ***(F-1)***

R-3. Oil bath testing to determine temperature coefficient of resistivity α and resistance per unit length at a reference temperature R_{L0} for all future wire tests is recommended. ***(F-5)***

R-4. NASA should consider adoption of a wire rating standard that applies to all programs and includes bounding variabilities. ***(O-6)***

R-5. Future testing and analysis should include unstudied factors such as wire lot, manufacturer, diameter of conductor, insulation thickness, and wire test article construction. ***(F-5)***

9.0 Alternative Viewpoint(s)

There were no alternative viewpoints identified during the course of this assessment by the NESC team or the NRB quorum.

10.0 Other Deliverables

Updates to the following tools will be archived on the NESC team's SharePoint site:

a. Single Wire spreadsheet thermal model (Filename: SINGLE WIRE MODEL WITH TRANSMITTANCE AND CORRECTED MCADAMS H ARCHIVE 17-01264.xlsm)

b. Complex Wire Bundle Thermal Model Builder (Filename: Complex Bundle SINDA Model Builder FOR 17-01264 ARCHIVE UPDATED.xlsm)

c. Monte Carlo Analysis Results (stored on the assessment SharePoint site in the folder "Final Report Deliverables" in "Single Wire Model Trans Mcadams Corr Monte Carlo with Tridist 10 August 2018 ETFE 22 AWG.xlsm)

d. Single Wire and 32-Wire Bundle spreadsheet thermal model including data on which the model was based, along with linear regression data and coefficient predictions for the AS50881 current rating curves of a wire in free air [ref. 4] (Response Surface Models.xlsx, rev. 181022 1601)

11.0 Lessons Learned

No lessons learned were identified as a result of this assessment.

12.0 Recommendations for NASA Standards and Specifications

No recommendations for NASA standards and specifications were identified as a result of this assessment.

13.0 Definition of Terms

Ampacity	The maximum amount of electrical current a conductor or device can safely carry before sustaining immediate or progressive deterioration. [May also be referred to as Current Carrying Capacity which is the maximum amount of current a given wire may be allowed to carry which is a function of the wire conductor and insulation material (maximum allowable temperature), ambient conditions (temperature and vacuum), and installed configuration (bundle size and heat rejection capability). (modified from JPL D-8208).]
Corrective Actions	Changes to design processes, work instructions, workmanship practices, training, inspections, tests, procedures, specifications, drawings, tools, equipment, facilities, resources, or material that result in preventing, minimizing, or limiting the potential for recurrence of a problem.
Finding	A relevant factual conclusion and/or issue that is within the assessment scope and that the team has rigorously based on data from their independent analyses, tests, inspections, and/or reviews of technical documentation.
Lessons Learned	Knowledge, understanding, or conclusive insight gained by experience that may benefit other current or future NASA programs and projects. The experience may be positive, as in a successful test or mission, or negative, as in a mishap or failure.
Observation	A noteworthy fact, issue, and/or risk, which may not be directly within the assessment scope, but could generate a separate issue or concern if not addressed. Alternatively, an observation can be a positive acknowledgement of a Center/Program/Project/Organization's operational structure, tools, and/or support provided.
Problem	The subject of the independent technical assessment.
Proximate Cause	The event(s) that occurred, including any condition(s) that existed immediately before the undesired outcome, directly resulted in its occurrence and, if eliminated or modified, would have prevented the undesired outcome.
Recommendation	A proposed measurable stakeholder action directly supported by specific Finding(s) and/or Observation(s) that will correct or mitigate an identified issue or risk.
Root Cause	One of multiple factors (events, conditions, or organizational factors) that contributed to or created the proximate cause and subsequent undesired outcome and, if eliminated or modified, would have prevented the undesired outcome. Typically, multiple root causes contribute to an undesired outcome.
Supporting Narrative	A paragraph, or section, in an NESC final report that provides the detailed explanation of a succinctly worded finding or observation. For example,

	the logical deduction that led to a finding or observation; descriptions of assumptions, exceptions, clarifications, and boundary conditions.
Temperature Rating of Wire Insulation	Maximum continuous temperature the wire construction (conductor and insulation) can reach according to the wire construction specification. The current-carrying capacity of a wire is the amount of current the wire construction can carry in its operating environment without causing the insulation temperature to exceed its rating. Consequently, a properly sized wire must be capable of carrying, for an indefinite period of time, the maximum continuous current of which the associated protective device is capable (modified from NASA TM 102179).
Wire	The term "wire" when used in this report refers to an insulated electrical wire manufactured with silver-coated conductor of copper alloy, insulated with ETFE or TKT.

14.0 Acronyms and Nomenclature List

atm	Atmosphere (unit of measure of pressure)
AWG	American Wire Gauge
BC	Boundary Condition
BIC	Bayesian Information Criterion
CAD	Computer-Aided Design
CCP	Commercial Crew Program
CWBTMB	Complex Wire Bundle Thermal Model Builder
DAQ	Data Acquisition System
DOD	Department of Defense
DOE	Design of Experiment
FEP	Fluorinated Ethylene Propylene
GPM	Gallons Per Minute
HT	Heat Transfer
IR	Infrared
OEM	Original Equipment Manufacturer
MPCV	Multi-purpose Crew Vehicle
PFA	Perfluoroalkoxy
PFPE	Perfluoropolyether Fluorinated Fluids
PTFE	Polytetrafluoroethylene
S/N	Signal-to-Noise Ratio
SAE	Society of Automotive Engineers
SI	Systeme International (i.e., International System of Units)
SLS	Space Launch System
TFE	Tetrafluorethylene
TKT	Teflon™-Kapton®- Teflon™
ULT	Ultra-Low Temperature
WPB	Wires per Bundle
XL-ETFE	Ethylene Tetrafluoroethylene

Nomenclature

A	Circumferential Surface Area of the Outer Layer Insulation
g	Acceleration due to Gravity ($9.8\ m/s^2$)
I	Wire Current
k	Air Thermal Conductivity
L	Wire/Wire Bundle Length
G_{int}	Wire Insulation-to-Wire Insulation Interface Conductance per Unit Length
G_{kapton}	Kapton® Layer Conductance (W/K)
G_{rad}	Wire Insulation-to-Wire Insulation Radiation Conductance per Unit Length
$GrPr$	Grashof-Prandtl Number
G_{teflon}	Teflon™ Layer Conductance (W/K)
k_w	Wire Insulation Thermal Conductivity
Nu	Nusselt Number
Q_c	Total Heat Dissipated by the Conductor in Watts
Q_{rad}	Radiation Heat between the Wire Outer Insulation Surface and the Shroud
r_b	Wire Bundle Radius
r_c	Wire Conductor Radius
r_s	Wire Insulation Outer Radius
R_0	Wire Resistance at the Reference Temperature of 20°C
R_L	Wire Electrical Resistance per Unit Length
R_m	Measured Resistance
R_{L0}	Wire Electrical Resistance per Unit Length at T_0
T_0	Reference Temperature ($20℃ = 293.15\ K$)
T_c	Wire Conductor Temperature
T_e	Ambient (shroud) Environment Temperature
T_{film}	Average of Insulation Surface Temperature and Gas Temperature
T_{kapton}	Kapton® External Surface Temperature (°C)
T_s	Wire Insulation Surface Temperature
T_{teflon}	Teflon™ External Surface Temperature (°C)
α	Temperature Coefficient of Resistance
σ	Stefan-Boltzmann constant ($5.67 \times 10^{-8}\ W/m^2\ K^4$)
β	$1/T_{film}$
c_p	Air Specific Heat
ε	Wire Insulation or Wire Bundle External Insulation Infrared Emissivity
f_h	Convective Heat Transfer Scaling Factor
μ	Air Viscosity
τ	Effective Wire Insulation Infrared Transmissivity
h	Convective Heat Transfer Coefficient

15.0 References

1. Iannello, C. J., et al., NESC-RP-14-00949, SpaceX Electrical Power System (EPS) Review Phase II, Volume I, March 30, 2017.
2. Raj S. Cornelius, "A History of the Development of New Current Ratings for Aerospace Wire," Raychem Corporation.
3. Military Specification, Wiring, Aerospace Vehicle, MIL-W-5088L, May 1991.
4. Aerospace Standard, Wiring Aerospace Vehicle, AS50881, Rev. F, SAE International, May 2015.
5. S. Taylor, "Thermal analysis of wiring for weight reduction and improved safety" AIAA/ICES Conference, Portland, Oregon, USA, 18-21 July 2011.
6. JPL D-8208, Rev I, dated 2002, Section 3.12, Spacecraft Design and Fabrication Requirements for Electronic Packaging and Cabling.
7. UTL Series Recirculating Chiller, FTS_UTLchiller---Brochure.pdf, https://www.spscientific.com/ProductCategory/102/FTS_Systems/
8. VHT PRODUCTS CO., Safety data sheet SP102, VHT® FlameProof Coating 1300-2000°F (704-1093°C) – Aerosol Flat Black.
9. Plastics Industry Trade Association (2015, September). Fact Finding Report on Power over Local Area Network Type Cables (white paper).
10. Anderson-Cook, C. M. (2006, March). What and When to Randomize. *Quality Progress*, 59 - 62.
11. Myers, R. H.; Montgomery, D. C. and Anderson-Cook, C. M. (2009). Response Surface Methodology: Process and Product Optimization Using Designed Experiments. 3rd Ed. Wiley, Hoboken, NJ.
12. Goos, P. and Vandebroek, M. (2004, January). Outperforming Completely Randomized Designs, *Journal of Quality Technology*, 36(1), 12-26.
13. Rickman, S. L., Iannello, C. J., Heat Transfer Analysis in Wire Bundles for Aerospace Vehicles, WIT Transactions on Engineering Sciences, Heat Transfer 2016, Wessex Institute, UK, 2016, vol. 106, pp. 53-63.
14. McAdams, W. H., Heat Transmission (Third Edition), New York, McGraw-Hill Book Company, Inc., 1954.15. Ramirez, A., & Cox, C. (2012, Fall). Improving on the Range Rule of Thumb. Rose-Hulman Undergraduate Mathematics Journal, 13(2). Retrieved September 25, 2016, from https://www.rose-hulman.edu/mathjournal/archives/2012/vol13-n2/paper1/V13n2-1pd.pdf.
15. Wentink, T, Planet, W. G., Infrared Transmission and Emission of Teflon, Contract No., AF 04(647)-278, Avco-Everett Research Laboratory, March 1960.
16. Malagoli, M., Benthem, R., Lacombe, D, Farhat, L, Allewaert, Y, Grave, W, and Vliet, A., Improvement of the Wire Rating Standards Based on TV Testing and Thermal Modeling, ICES-2018-162, International Conference on Environmental Systems, 2018, https://ttu-ir.tdl.org/ttu-ir/handle/2346/74138.
17. Rickman, S. L., Iannello, C. J., Shariff, K., Improvements to Wire Bundle Thermal Modeling for Ampacity Determination, Proceedings of the 3rd World Congress on Mechanical, Chemical and Material Engineering (MCM '17), 4th International

Conference on Heat Transfer and Fluid Flow (HTFF '17), HTFF 102, Rome, Italy, June, 2017.

18. Montgomery, D.C., Peck, E.A., and Vining, G.G. (2001). Introduction to Linear Regression Analysis. 3rd Ed. Wiley, New York, NY.
19. R Core Team (2013). R: A language and environment for statistical computing. R Foundation for Statistical Computing, Vienna, Austria. URL http://www.R-project.org/.
20. Buckland, S.T., Burnham, K.P., and Augustin, N.H. (1997, June). Model Selection: An Integral Part of Inference, *Biometrics*, 53(2), 603 – 618.
21. Agilent 34970 Service Guide p. 16.
22. Riedon RSN Series Specification Sheet.
23. AS22759/181 REV. A Specification Updated to include AS29606 Conductor Requirements, Rohs Restrictions, Harmonization with AS22759/191 and AS22759 Modifications, Federal Supply Class 6145.
24. E Type Thermocouple by OMEGA™, https://www.omega.com/kwbld/etypethermocouple.html
25. Wire Size Determination for Aerospace Applications, Report No. 88-220, Eagle Engineering/LMESCO under Contract to NASA (NAS-17900), December 1, 1988.
26. Gaston, D. M., Selection of Wires and Circuit Protective Devices for STS Orbiter Vehicle Payload Electrical Circuits, NASA TM 102179, June 1991.
27. Tom Eng, Joseph Saleh, Percon® 24 A New High Strength Conductor Alloy for Military Wire and Cable Applications, Proceedings of the 2011 Aerospace Interconnection System Symposium.
28. Electrical, Electronic, and Electromechanical (EEE) Parts Management and Implementation Plan for the Space Station Program, SSP 30312 Vol I, Revision K, September 1, 2011.

Appendices

Appendix A. Single Wire Design and Analysis in Thermal Desktop®
Appendix B. Test Article Preparation

Appendix A. Single Wire Design and Analysis in Thermal Desktop®

A.1 Single Wire Design and Analysis in Thermal Desktop®

To better understand the correlation between wire amperage and wire maximum temperature and the impact of the attached thermocouple on the wire maximum temperature, a single wire thermal model was built in Thermal Desktop®.

Temperature dependent wire resistance was implemented in the model. To validate the Thermal Desktop® model results, a theoretical formulation was implemented in Matlab®.

As shown in Figure A-1, copper properties were used for the wire conductor. Two layers of insulations made of Kapton® and Teflon™ covering the conductor were modeled [ref. 23].

Table A-1 shows the thermal properties and insulation thicknesses used in the model.

The current JPL cabling table shown in Figure A-2 indicates that 8 amp is the maximum current to be used for a 20 AWG wire in vacuum. The analysis was initiated for a 20 AWG wire at 8A.

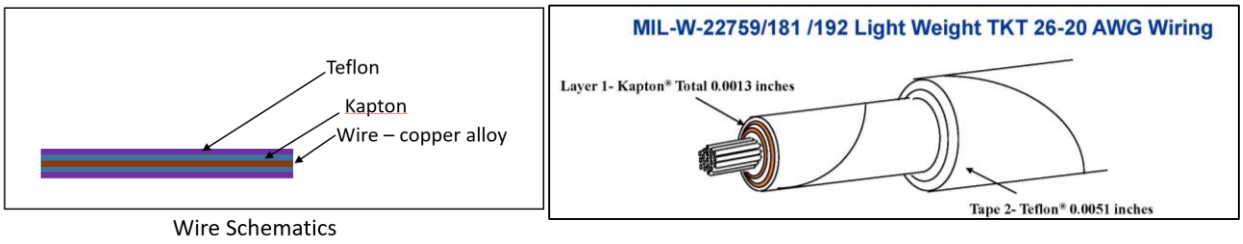

Figure A-1. Wire Configuration

Table A-1. Thermal Properties and Thickness

Material	Thermal Conductivity (W/m K)	Thickness (in) [mm]
Copper (wire conductor)	401	0.0395 [1.00] OD (20 AWG)
Kapton®	0.12	0.0013 [0.033]
Teflon™	0.26	0.0051 [0.13]

This tables gives the maximum allowable current in four different situations for silver-plated conductors with TKT, KT, and TFE Teflon insulation. The table assumes an ambient temperature of 176°F (80°C) with an allowable rise of 248°F (120°C) to the 392°F (200°C) rating of silver-plated conductors.

Wire Type	Wire Size	Maximum Allowable Current Rating Amperes			
		Single Wire		Wire Bundle	
		Air	Vacuum	<5 Wire	<33 Wire
Silver Coated Copper	12	66	23.0	17.7	12.0
	14	50	17.5	13.5	9.1
	16	36	13.0	10.0	6.8
	18	32	11.2	8.6	5.8
	20	23	8.0	6.2	4.2
	22	16	5.6	4.3	2.9
Silver Coated Alloy*	*24	10	3.5	2.4	1.6
	*26	7.7	2.7	2.1	1.4
	*28	5.9	2.0	1.6	1.0
* Copper alloy conductivity = 0.84 x copper conductivity					

Figure A-2. Current Carrying Ratings presented in current JPL Cabling Table [ref. 6]

Hand Calculation and Validation

To validate the single wire Thermal Desktop® model, an analytical model was coded in Matlab®. Figure A-3 shows the resistance model and the code flow chart. As shown in the flow chart, the code starts with a guess for the conductor temperature, T_c. Using the conductor temperature, temperature dependent resistance is calculated using Eq. A-1.

$$R(T) = R_0[1 + \alpha(T_c - T_0)] \qquad \text{Eq. A-1}$$

where, T_c is the wire temperature, T_0 is the reference temperature of 20°C. R_0 is the wire resistance at the reference temperature of 20°C, α is the temperature coefficient of resistivity, which was assumed constant at 0.003925/°C for copper in all the calculations and for the Thermal Desktop® model.

Using temperature dependent wire thermal conductance, wire conductive heat from the conductor to the outer surface of the insulation is calculated using Eq. A-2.

$$Q_c = R(T_c)I^2 \qquad \text{Eq. A-2}$$

where Q_c is the conductive heat from the conductor to the outer surface of the wire insulation, and I is the wire current.

All thermal conductances shown in the model including copper, Kapton®, and Teflon™ thermal conductances are calculated using the thermal conductivity and insulation layers thickness (Table A-1). Using the conductive heat, Q_c, and calculated thermal conductances, the outer insulation surface temperature is calculated and radiative heat between the outer insulation surface and the shroud is calculated using Eq. A-3:

$$Q_{rad} = \varepsilon\sigma A\left({T_{teflon}}^4 - {T_e}^4\right) \qquad \text{Eq. A-3}$$

where, ε is the insulation surface emissivity, σ is Stefan-Boltzmann constant (5.67e-8 W/m^2-K), A is the circumferential surface of the outer layer insulation, Q_{rad} is the radiation heat between the wire outer insulation surface and the shroud, T_{teflon} is Teflon™ outer surface temperature, and T_e is the shroud temperature which was assumed to be fixed at 80°C.

Wire temperature, T_c is modified in a calculation loop until energy balance is satisfied. The wire temperature at which energy balance reached is reported as the final wire conductor temperature.

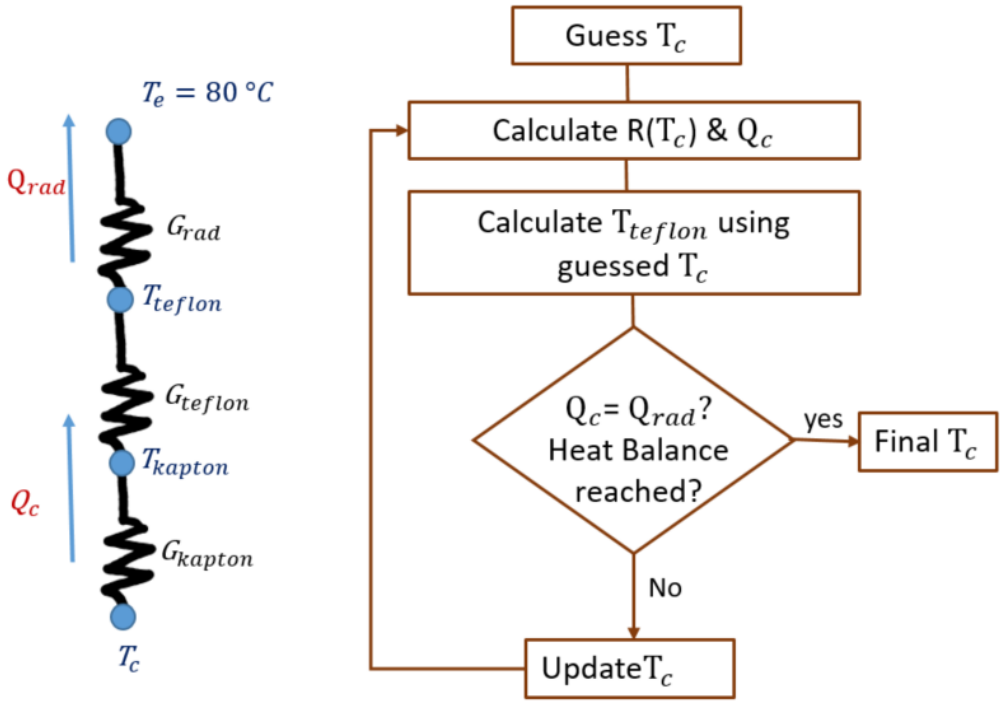

Figure A-3. Left – Resistance model, Right - Analytical algorithm coded in Matlab®

Figure A-4 shows the results for a 2 ft (0.6 m) vs. a 10 ft (3.3 m) 20 AWG wire using Thermal Desktop® model and the analytical code. As shown in the plots, the maximum wire temperature is influenced by the end conditions for a 2 ft (0.6 m) wire while increasing the length to 10 ft (3.3 m), makes the end conditions insignificant. The analytical model is in agreement with Thermal Desktop® model within 2%.

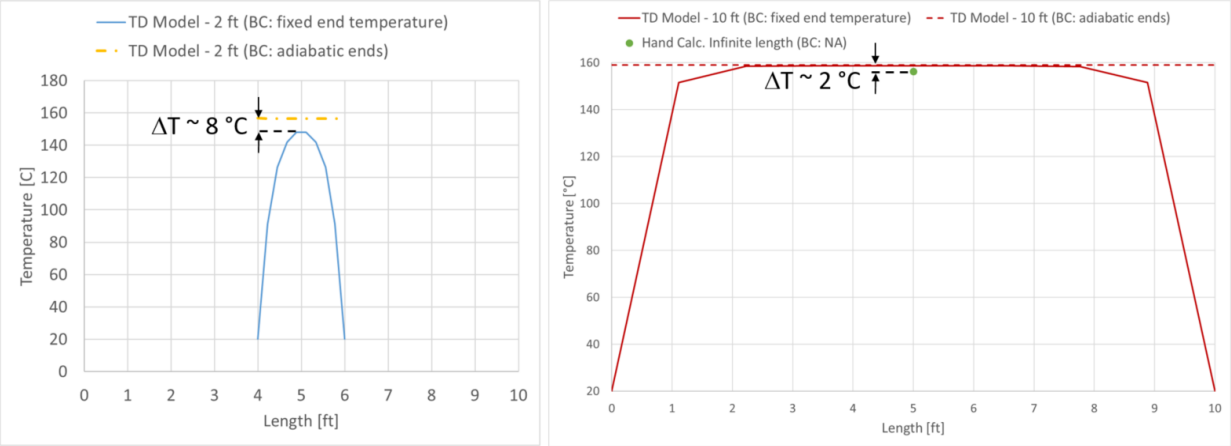

Figure A-4. Left – 2 ft (0.6 m) wire (adiabatic vs. fixed ends) – Right – 10 ft (3.3 m) wire (adiabatic vs fixed ends vs analytical model)

Max Temperature vs Current Correlation for 20 AWG Wire

A thermal model for single wire including the shroud was built in Thermal Desktop®. Temperature dependent wire resistance (Eq. A-1) was implemented in the model to ensure wire resistance and the heat dissipation increase as the nodal temperatures increase. A range of analyses was completed for 20 AWG wire for 8, 9, 10, 11, 11.5, and 12A. Shroud temperature and wire ends were fixed at -50°C for the cases including current. As shown in Figure A-5, maximum temperature reached was 204°C at 12A current.

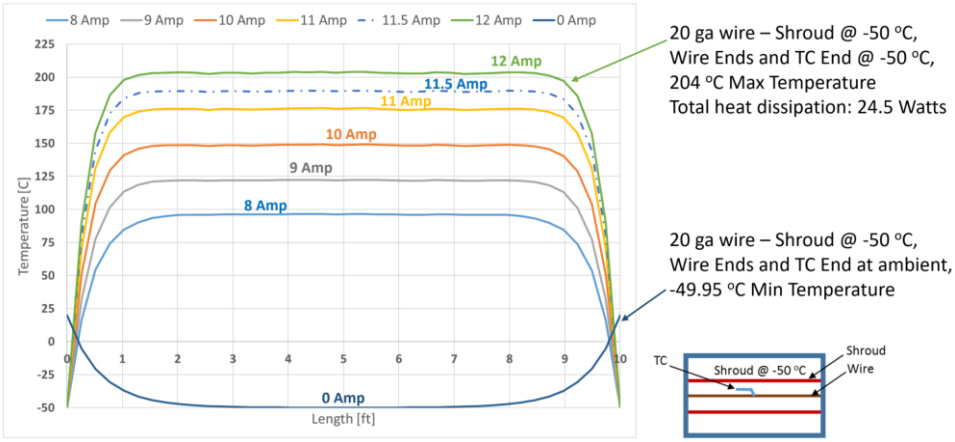

Figure A-5. Wire (20 AWG) Temperature Variation as a Function of Amp

Thermocouple Mounting Impact on Maximum Temperature

In the current test setup, a Type E thermocouple was soldered in the center of the wire conductor [ref. 24]. Thermocouple attached to the center of the wire conductor acts as a conductive heat sink. Moreover, soldering thermocouple to the conductor left about 0.05 inches (1.27 mm) of the wire and thermocouple partially without insulation as shown in Figure A-6. This will cause a heat sink at vacuum when this part is exposed to the cold shroud. In pressure cases there will be

additional convective losses. Exposed copper was covered with additional layer of FEP insulation to minimize the losses.

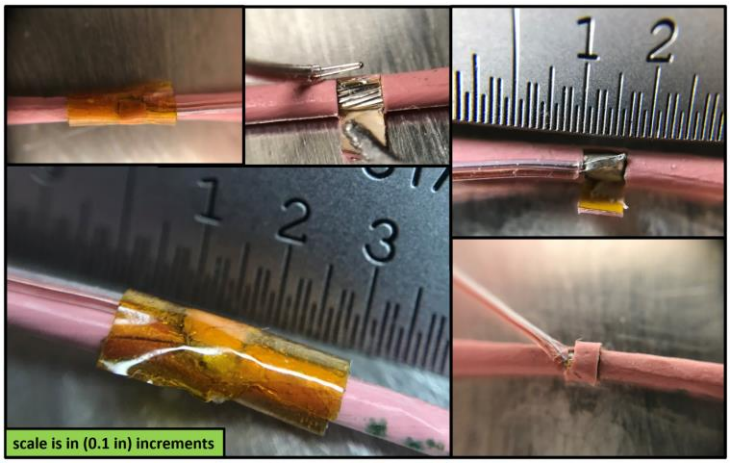

Figure A-6. Thermocouple Mounting on the Wire Conductor

In the temperature vs. wire current study presented in the previous section, an emissivity of 0.8 was used for the wire insulation and emissivity of 0.3 was used for the thermocouple insulation. Additional analyses were conducted in Thermal Desktop® to understand the impact of thermocouple attachment on the conductor temperature measurement in vacuum tests. In this analysis, the emissivity of insulation increased to 0.93 as reported for PFA (Perfluoroalkoxy) emissivity and low emissivity of 0.02 was used for copper where the insulation is assumed to be damaged due to the thermocouple soldering process.

Analysis was completed for 20 AWG wire at 12A current. Chromel and Constantan alloy with thermal conductivity of 19 W/m-K was used for Type E 36 AWG thermocouple conductor. As shown in Figure A-7, four configurations were modeled. The first configuration represents the conductor with insulation prior to thermocouple installation. The conductor center temperature of 181.5°C was calculated for this case. The considerable temperature decrease from 204°C reported in Figure A-5 is due to the insulation increased emissivity from 0.8 to 0.93, which enhanced the radiation loss to the cold shroud.

The second configuration includes the thermocouple attached to the conductor assuming the insulation remains undamaged. As shown in Figure A-5, the conductor center temperature was reduced to 179.6°C due to the conductive losses through the thermocouple.

In the third configuration, it was assumed that 0.05 inches (1.27 mm) of the insulation was damaged exposing the copper to the cold shroud. Since the emissivity of copper is not significant, radiation losses to the cold shroud becomes insignificant and conductor center temperature did not reduce.

In the last configuration, damaged insulation was assumed to be covered with additional FEP insulation. As the emissivity of FEP is high, radiation losses increased and reduced the conductor center temperature to 178.8°C.

Thermocouple attachment thermal analysis indicated that the temperature difference due to the presence of the thermocouple measurement could be between 1 and 3°C.

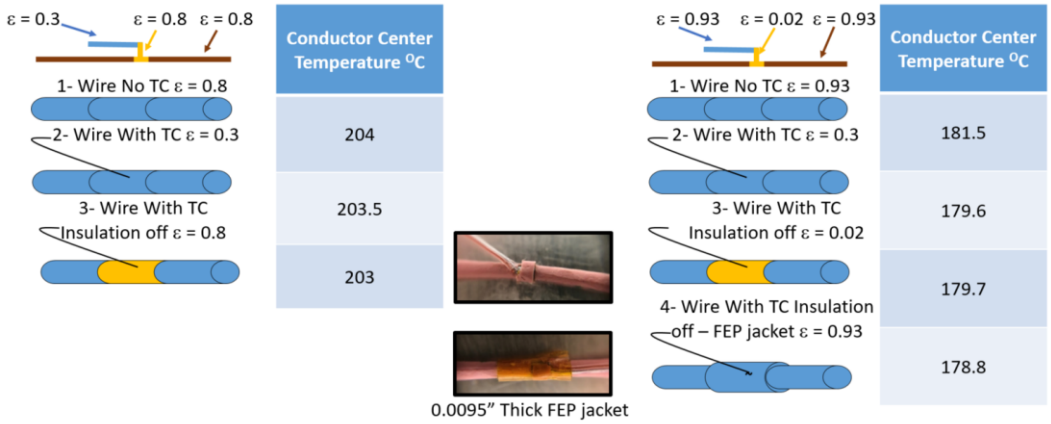

Figure A-7. Thermocouple Analysis

Appendix B. Test Article Preparation

Test article preparation is detailed in the following sections.

B.1 Single Wires

1. Obtain length of wire.

For single wire tests, a length of between 10 and 11 (3.05 m – 3.35 m) ft is cut from the wire spool using pliers.

2. Exposing the conductor for thermocouple placement.

An opening half way along the length of the wire was created to allow a thermocouple to be soldered to the conductor. The center of the wire was located and marked with a permanent marker. The center area of the wire was secured to a metal plate using Kapton® tape and a flap was made using a scalpel to expose the conductor as shown in Figure B.1-1.

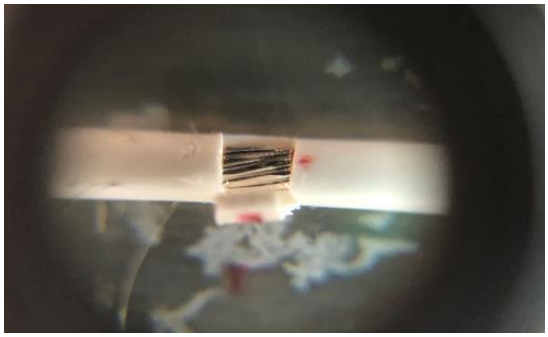

Figure B.1-1. Incision of Insulation

3. Solder thermocouple to conductor.

The plate with the wire attached was placed on a hot plate. The hot plate was set to 100°C. Once the test article has been pre-heated to 100°C flux was applied to the conductor. Using high-temperature solder, a small amount of solder was placed on the exposed conductor. While keeping the solder liquid using the soldering iron, the thermocouple was placed so the thermocouple junction is underneath the solder. Figure B.1-2 shows a thermocouple soldered to the conductor. Once the solder has solidified, remove the plate and wire from the hot plate.

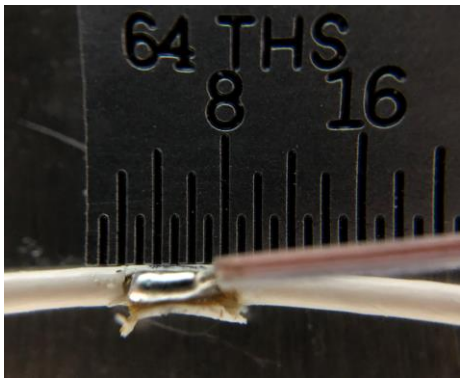

Figure B.1-2. Thermocouple Soldered to Conductor

B.2 Bundles

1. Obtain 32 segments of wire.

For the 32-wire bundle tests, 32 lengths of wire between 10 and 11 ft (3.05 m – 3.35 m) were cut from the wire spool using pliers.

2. Patterning the wire bundle.

Using four plastic 3D-printed pattern combs, each wire was inserted into the pattern and strung across a fixture (comb). The comb is shown in Figure B.2-1 with some wires running through the hole pattern. Figure B.2-4 shows the fixture that held the bundle while it was being fabricated.

Figure B.2-1. 3D Printed Pattern Comb

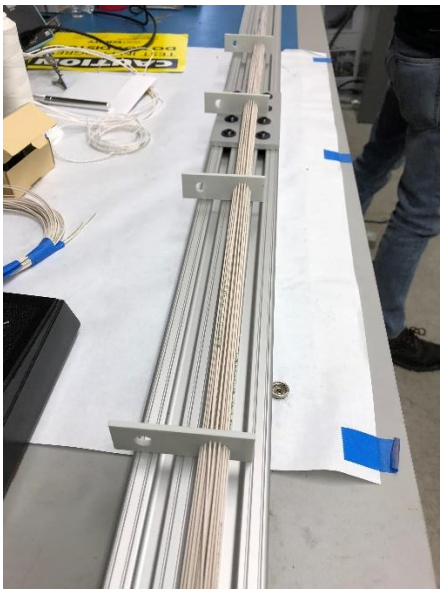

Figure B.2-2. Fixture

3. Clamp the ends of the bundle to the fixture.

The ends of the wire bundle were clamped to opposite ends of the fixture. Figure B.2-3 shows one end of the wire bundle clamped. The other end was clamped in the same way. The bundle had some slack to allow moving the wire while soldering.

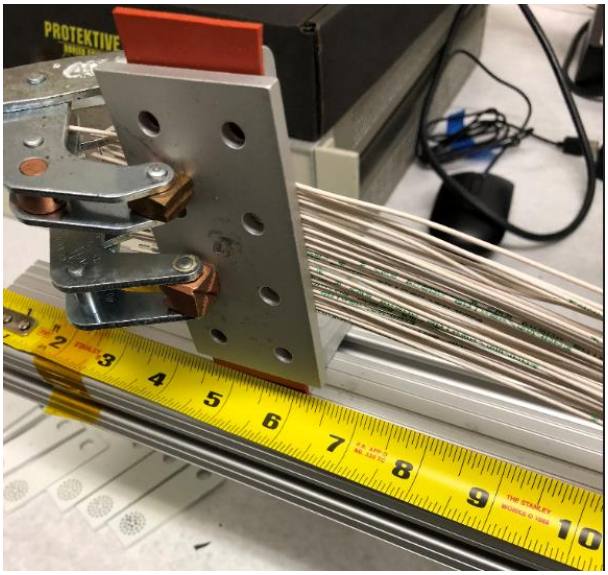

Figure B.2-3. Wire Bundle and Clamp

4. Exposing the conductor for thermocouple placement.

The center of the wire was located and marked with a permanent marker. The center area of the wire was secured to a metal plate using Kapton® tape and a flap is made using a scalpel to expose the conductor. This was done on a central wire and an exterior wire. Figure B.2-4 shows the flap made with the scalpel.

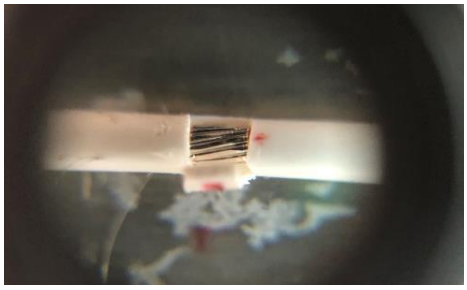

Figure B.2-4. Incision of Insulation

5. Solder thermocouple to conductor.

The plate with the wire was placed on a hot plate. The hot plate was set to 100°C. Once the test article had been pre-heated to about 100°, flux was applied to the conductor. Using high-temperature solder, a small amount of solder was placed on the exposed conductor. While keeping the solder liquid using the soldering iron, the thermocouple was placed so the thermocouple junction is underneath the solder as shown in Figure B.2-5. This was done for the central and exterior wire for the wire bundle configurations. Once the solder has solidified, remove the plate and wire from the hot plate.

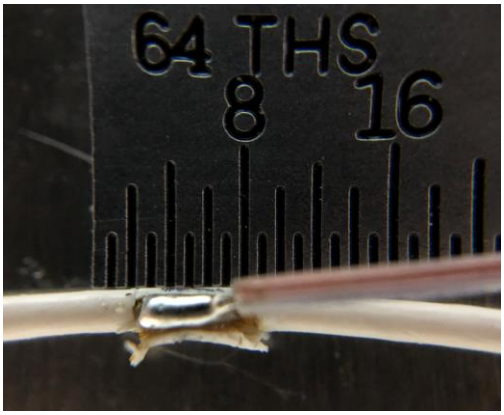

Figure B.2-6. Thermocouple Soldered to Conductor

6. Tying the bundle.

The bundle was tied together using lacing ties. Starting from the central thermocouples, a tie was placed on the central thermocouples. Figure B.2-7 shows the center of the bundle tied with lacing tape.) Working from the center outwards, about five additional ties were placed at about 0.25-inch increments on either side of the thermocouple towards each end. The remainder of the bundle was spot tied at approximately 1-inch intervals. Figure B.2-8 shows multiple ties on the bundle.

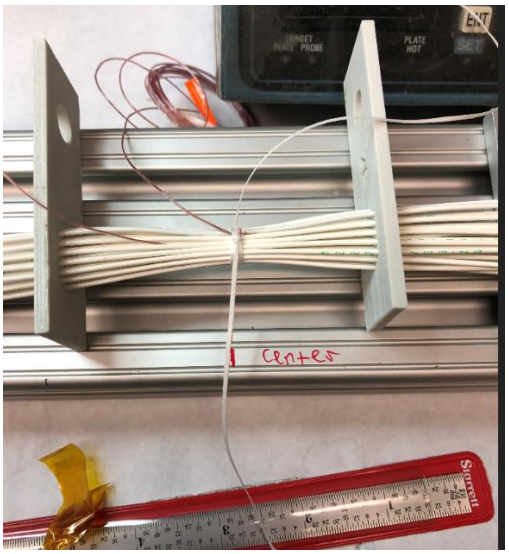

Figure B.2-7. Wire tie Placed on Center Thermocouple

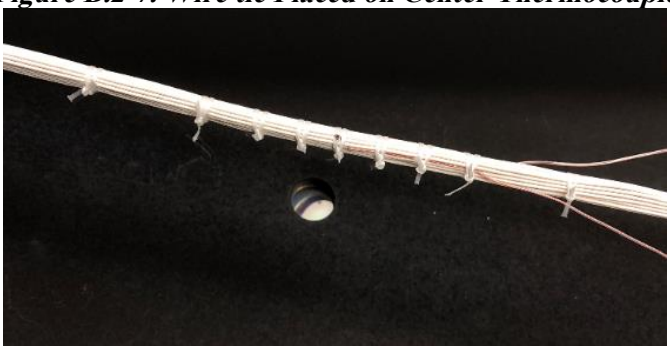

Figure B.2-8. Wire Ties at the Center of the Wire

7. Connecting ends to create one long wire.

The ends of the wire were soldered using high temperature solder (melting point 240°C). After the wire ends were soldered, Kapton® tape was used to cover the wire ends. In Figure B.2-9, the soldered ends and Kapton® tape are shown.

Figure B.2-9. Soldered Wire Ends covered in Kapton® Tape

REPORT DOCUMENTATION PAGE

Form Approved
OMB No. 0704-0188

1. REPORT DATE *(DD-MM-YYYY)*	2. REPORT TYPE	3. DATES COVERED *(From - To)*
11/15/2018	Technical Memorandum	

4. TITLE AND SUBTITLE
Re-Architecting the NASA Wire Derating Approach for Space Flight Applications

5a. CONTRACT NUMBER

5b. GRANT NUMBER

5c. PROGRAM ELEMENT NUMBER

6. AUTHOR(S)
Rickman, Steven L.; Johnson, Kenneth L.;Maghsoudi, Elham; Slenski, George A.; Furst, Benjamin I.; Wentzel, Daniel J.; Bautista, Anthony; Nelson, Emma J.

5d. PROJECT NUMBER

5e. TASK NUMBER

5f. WORK UNIT NUMBER
869021.05.05.02.20

7. PERFORMING ORGANIZATION NAME(S) AND ADDRESS(ES)
NASA Langley Research Center
Hampton, VA 23681-2199

8. PERFORMING ORGANIZATION REPORT NUMBER
L-20978 NESC-RP-17-01264

9. SPONSORING/MONITORING AGENCY NAME(S) AND ADDRESS(ES)
National Aeronautics and Space Administration
Washington, DC 20546-0001

10. SPONSOR/MONITOR'S ACRONYM(S)
NASA

11. SPONSOR/MONITOR'S REPORT NUMBER(S)
NASA/TM-2018-220114

12. DISTRIBUTION/AVAILABILITY STATEMENT
Unclassified - Unlimited
Subject Category 16 Space Transportation and Safety
Availability: NASA STI Program (757) 864-9658

13. SUPPLEMENTARY NOTES

14. ABSTRACT
Mr. Steve Rickman, NASA Technical Fellow for Passive Thermal, proposed a pathfinder study to develop an apparatus for wire and wire bundle thermal testing to measure their performance, and to support development of thermal analytical models. Development of such capability would enable wire and wire bundle amperage capacity. The goal of this study was to assess the feasibility of developing physics-based and regression thermal models of single wires and wire bundles. This report contains the outcome of the NESC assessment.

15. SUBJECT TERMS
Wire Derating; Wire Bundles; Thermal Modeling; NASA Engineering and Safety Center; Thermal Analysis

16. SECURITY CLASSIFICATION OF:			17. LIMITATION OF ABSTRACT	18. NUMBER OF PAGES	19a. NAME OF RESPONSIBLE PERSON
a. REPORT	b. ABSTRACT	c. THIS PAGE			STI Help Desk (email: help@sti.nasa.gov)
					19b. TELEPHONE NUMBER *(Include area code)*
U	U	U	UU	109	(443) 757-5802